

國立臺灣大學獸醫專業學院獸醫學研究所

博士論文

Graduate Institute of Veterinary Medicine

School of Veterinary Medicine

National Taiwan University

Doctoral Dissertation



台灣擱淺鯨豚組織銀濃度與

奈米銀對鯨豚免疫細胞影響的活體外研究

Silver Tissue Contamination in Taiwanese Stranded

Cetaceans and Effects of Silver Nanoparticles on

Cetacean Immune Cells *in Vitro*

李文達

Wen-Ta Li

指導教授：鄭謙仁 博士

共同指導教授：楊瑋誠 博士

Advisor: Chian-Ren Jeng Ph.D.

Co-advisor: Wei-Chang Yang Ph.D.

中華民國 107 年 7 月

July, 2018

國立臺灣大學博士學位論文
口試委員會審定書

台灣擱淺鯨豚組織銀濃度與奈米銀對鯨豚免疫細胞影
響的活體外研究

Sliver Tissue Concentration in Taiwanese Stranded Cetaceans
and Effects of Silver Nanoparticles on Cetacean Immune Cells
in Vitro

本論文係李文達君 (D036290024) 在國立臺灣大學獸醫
所完成之博士學位論文，於民國一百零七年六月二十五日承
下列考試委員審查通過及口試及格，特此證明

口試委員：

鄭謙仁

(指導教授)

陳孟心

張惠雯

楊清誠

楊 翔

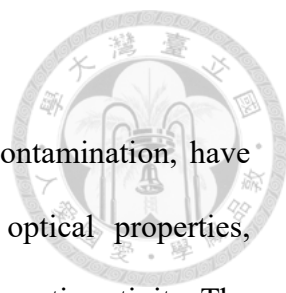
系主任、所長

鄭謙仁

摘要

奈米銀因其光學性質，電子性質，良好的抗微生物活性，催化活性和磁性活性而被廣泛應用於各類商品，也成為環境銀污染的重要來源。在齧齒類及魚類等實驗動物的研究顯示，奈米銀可由呼吸道及消化道進入血液循環並沉積在各臟器中（特別是腦組織和睪丸）。奈米銀已經被證實可以在上述這些動物模式引起細胞氧化壓力上升、去氧核苷核酸的損傷和細胞凋亡，並對藻類、海洋無脊椎動物和魚類具有毒性。鯨豚是海洋高階掠食者，也是最可能因奈米銀污染而受到影響的動物之一。但目前卻沒有任何鯨豚相關的奈米銀毒性研究被發表，因此，評估奈米銀對鯨豚的健康影響是亟需進行。本研究開發輔助方法以定位銀在次器官 (suborgan) 層級的位置 (第二章)，藉由鯨豚組織學銀濃度分析技術 (cetacean histological Ag assay; CHAA)，估算鯨豚組織的銀濃度 (第二章和第三章)，並藉上述方法進行研究，建立鯨豚可能的銀代謝途徑之假說，並證明銀可能對鯨豚健康引起系統性而非器官特定性的負面影響 (第三章)。此外，本研究也揭示奈米銀對鯨豚白血球的細胞毒性和免疫毒性 (第四章和第五章)。以上結果皆證實銀/銀化合物和奈米銀對鯨豚健康的負面影響，也顯示其在海洋環境中的潛在生態毒性。

Abstract



Silver nanoparticles (AgNPs), an important source of silver contamination, have been widely used in many commercial products due to their optical properties, electronic properties, antimicrobial activity, catalytic activity, and magnetic activity. The AgNPs are released into the environment, gradually accumulate in the ocean, and may affect the animals of high trophic level via food-web chain, such as cetaceans and humans. Several rodent and fish studies have demonstrated AgNPs can enter the blood circulation via alimentary/respiratory tracts and deposit in multiple organs especially brain and testis. AgNPs have been reported to induce cellular oxidative stress, DNA damage and apoptosis in these animal models, and cause toxic effects on algae, marine invertebrates, and fishes. Cetaceans, as the top predators of ocean, may have been negatively affected by AgNPs, but no toxicity study of AgNPs in cetaceans has been reported. Therefore, it is urgent to investigate the possible negative effects of AgNPs on the health of cetacean. The current study presented an adjuvant method to localize the Ag distribution at suborgan levels (Chapter II), estimated the Ag concentrations of various tissues by cetacean histological Ag assay (CHAA) (Chapters II and III), provided a presumptive metabolic pathway of Ag in cetaceans, demonstrated the possible systemic rather than organ-targeting negative health effects caused by Ag in cetaceans (Chapter III), and revealed the cytotoxicity and immunotoxicity caused by AgNPs on the leukocytes of cetaceans (Chapters IV and V). All the data have demonstrated the negative effects of Ag/Ag compounds and AgNPs on the health of cetaceans and their potential ecotoxicity in marine environment.



Table of Contents

摘要	i
Abstract.....	ii
Table of Contents	iii
Chapter I: General Introduction.....	1
Section 1. Nanotechnology and Silver Nanoparticles (AgNPs).....	1
Section 2. An Emerging Contaminant– AgNPs	1
Section 3. The Biodistribution and Bioavailability of AgNPs	3
Section 4. The Toxicity of AgNPs.....	4
Section 5. The Ecotoxicology of AgNPs.....	8
Section 6. Summary and Objectives.....	9
Chapter II: Use of Autometallography to Localize and Semi-quantify Silver in Cetacean Tissues (Manuscript in Submission)	12
Chapter III: Investigation of Silver (Ag) Deposition in Tissues from Stranded Cetaceans by Autometallography (AMG) Environmental Pollution, 2018, 235: 534-545	32
Chapter IV: Immunotoxicity of Silver Nanoparticles (AgNPs) on the Leukocytes of Common Bottlenose Dolphins (<i>Tursiops truncatus</i>) Scientific Reports, 2018, 8:5593 .	45
Chapter V: Th2 Cytokine Bias Induced by Silver Nanoparticles (AgNPs) in Peripheral Blood Mononuclear Cells (PBMCs) of Common Bottlenose Dolphins (<i>Tursiops truncatus</i>) (Manuscript in Submission).....	58
Chapter VI: General Discussion.....	89
References	93

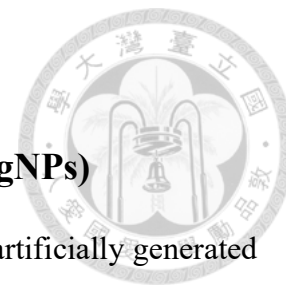
Chapter I: General Introduction

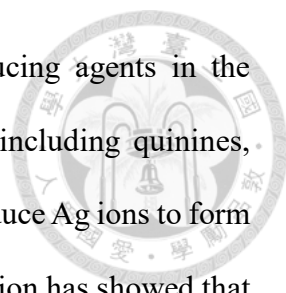
Section 1. Nanotechnology and Silver Nanoparticles (AgNPs)

Nanoparticles (NPs) are defined as a naturally, incidentally or artificially generated materials, which contain particles as individual or aggregated/agglomerated particles, and the size distribution of the particles ranges 1 to 100 nm (McGillicuddy et al., 2017). Nowadays, NPs have been widely used in biomedical products, electronic equipment, and energy production due to their special physicochemical characteristics, such as melting point, wettability, electrical/thermal conductivity, catalytic activity, and antimicrobial activity, which lead to an enhanced performance over their bulk counterparts (Jeevanandam et al., 2018; McGillicuddy et al., 2017). Although the applications of nanotechnology in different areas provide lots of business opportunities, the potential threats of NPs to humans, animals and environment should not be overlooked (Handy et al., 2008; McGillicuddy et al., 2017). Silver nanoparticles (AgNPs), different from other engineered nanomaterials, are most often used in the commercial products, such as water filters, textiles, cosmetics, food packaging and health care items, mainly due to their strong antimicrobial properties (McGillicuddy et al., 2017). Besides, its unique physicochemical properties, such as high electrical and thermal conductivities, also lead to an increased application of AgNPs in electronic devices and medical imaging (Ajmal et al., 2016; Ge et al., 2014). The production of AgNPs and the number of AgNP-containing products have dramatically increased in the past few years and are expected to increase over time (Hansen et al., 2016; Vance et al., 2015).

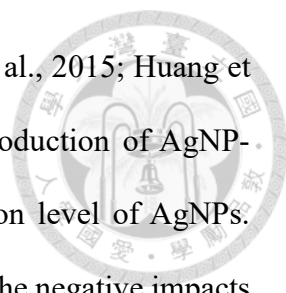
Section 2. An Emerging Contaminant– AgNPs

Previous studies have demonstrated that AgNPs in the environment are not all artificially produced (i.e. not produced by humans)(Gomez-Caballero et al., 2010; Wen





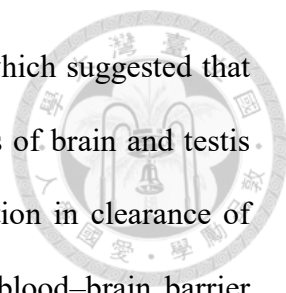
et al., 1997). Humic acids (HAs) are ubiquitous and natural reducing agents in the environment, and they are composed of many functional groups, including quinines, ketones, aldehydes, phenolic and hydroxyls, which enable them to reduce Ag ions to form AgNPs (Akaighe et al., 2011; Sal'nikov et al., 2009). Early investigation has showed that AgNPs or copper NPs can be generated from bulk objects, such as silver wire and eating utensils (Glover et al., 2011). Furthermore, some organisms such as algae, plants, and bacteria have the capability to take up Ag ions and thereby form AgNPs (Mukunthan et al., 2011; Yang et al., 2010). These findings suggest that macroscaled Ag containing objects are a potential source of AgNPs in the environment and AgNPs can be produced by natural substances or organisms. However, the increasing use of AgNPs has triggered notable interest in developing methods to produce different types of AgNPs (Yu et al., 2013). AgNPs can be released during the production, transport, decay, use, and/or disposal of AgNP-containing products, draining into the surface water, and then accumulating in the marine environment (Farre et al., 2009; Walters et al., 2014). The increased production and use of AgNPs may eventually elevate the deposition of AgNPs in the environment, and thus AgNPs have been considered as a potential source of Ag contamination (McGillicuddy et al., 2017). The fate of AgNPs in the aquatic environment is complicated and changeful. Previous studies have found that AgNPs in the aquatic environment can remain as individual particles in suspension, aggregate, dissolve, react with different chemical species, or be regenerated from Ag⁺ ions (McGillicuddy et al., 2017; Yu et al., 2013). Wang et al. (2014) have demonstrated that Ag/Ag compounds and AgNPs can precipitate in marine sediments, be ingested by benthic organisms (such as benthic invertebrate species), and thereby enter the food chain in the marine environment. Several previous studies have indicated that AgNPs can be transferred from one trophic level to the next via the food chain and cause negative effects on the animals at different



trophic levels (Buffet et al., 2014; Farre et al., 2009; Gambardella et al., 2015; Huang et al., 2016b; Wang et al., 2014). The extensive use and growing production of AgNP-containing products may aggravate the environmental contamination level of AgNPs. Therefore, aquatic animals and marine environment will suffer from the negative impacts caused by Ag/Ag compounds and AgNPs, which further raises concern about the environmental toxicity of their deposition.

Section 3. The Biodistribution and Bioavailability of AgNPs

Concerning about the environmental toxicity of Ag/Ag compounds and AgNPs, the interaction between Ag and biological systems is drawing a serious attention. There are numerous studies investigating the biodistribution and bioavailability of Ag/Ag compounds and AgNPs by using different laboratory animal models. Jung et al. (2014) demonstrated that the Japanese medaka (*Oryzias latipes*) could uptake AgNPs through gills and gastrointestinal tract, and AgNPs could enter blood circulation and mainly accumulated in the liver. When laboratory rats were exposed to 3.0×10^6 particle/cm³ AgNPs via inhalation pathway, Ag can be detected in the lung and liver tissues after 2 hours of exposure (Takenaka et al., 2001). Furthermore, central nervous system (CNS) can be targeted by airborne AgNPs, and the possible mechanism is the deposition of AgNPs compounds on the olfactory mucosa of the nasopharyngeal region of the respiratory tract and subsequent translocation via the olfactory nerve to the CNS (Ji et al., 2007; Oberdorster et al., 2004; Sung et al., 2009). On the other hand, when laboratory rats were orally exposed to AgNPs and AgNO₃ for 28 days, the results showed that Ag could be detected in the blood, feces, liver, spleen, kidney, brain, ovary and testis (Lee et al., 2013; van der Zande et al., 2012). It was also reported that 1) the highest Ag concentrations were generally found in the liver and spleen of laboratory animals after exposure, 2) the Ag concentrations of blood, feces, liver, spleen, kidney, and ovary were



significantly decreased after oral exposure of AgNPs and AgNO₃, which suggested that the Ag can be metabolized after ingestion, 3) the Ag concentrations of brain and testis were not decreased after 4 months of recovery period (an obstruction in clearance of accumulated Ag), suggesting that biological barriers, such as the blood–brain barrier (BBB) and blood-testis barrier (BTB), may play an important role in the Ag clearance from these tissues (Lee et al., 2013; van der Zande et al., 2012).

In summary, previous studies conducted in laboratory animals, including fishes, mice and rats, have demonstrated that AgNPs can enter the blood circulation through oral and inhalation exposure, accumulate in multiple organs, and be metabolized through liver and kidney. Besides, AgNPs can penetrate BBB and BTB and persistently accumulate in brain and testis.

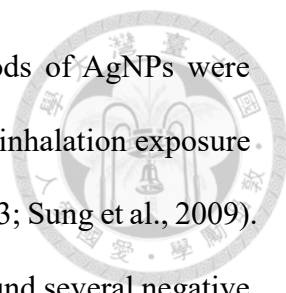
Section 4. The Toxicity of AgNPs

Since previous studies have demonstrated the biodistribution and bioavailability of AgNPs in a variety of animals, the toxicity of AgNPs is of interest.

1. *In vivo* studies

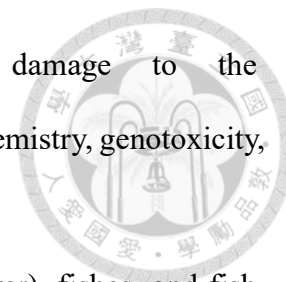
The *in vivo* studies on the toxicity of AgNPs have been conducted by using laboratory animals, including rats, mice, invertebrates, and fishes, and demonstrated that AgNPs are toxic to all tested animals in a dose-dependent manner (Buffet et al., 2014; Kim and Ryu, 2013; Myrzakhanova et al., 2013). The exposure methods in rats and mice include oral ingestion, inhalation, intraperitoneal injection, and intravenous injection; those in invertebrates (such as mussels and oyster), fishes, and fish embryos are mainly immersing (Buffet et al., 2014; Gagne et al., 2013; Kim and Ryu, 2013; Myrzakhanova et al., 2013).

For laboratory rats and mice, the concentrations and treatment time periods of AgNPs were ranged, respectively, from 1 to 1000 mg/kg and 3 to 90 days in the oral



exposure experiments; the concentrations and treatment time periods of AgNPs were ranged from 1.32 to 1.91×10^7 particles/cm³ and 14 ~ 19 days in the inhalation exposure experiments, respectively (Hadrup and Lam, 2014; Kim and Ryu, 2013; Sung et al., 2009). Previous studies of inhalation toxicity of AgNPs in laboratory rats found several negative health effects, including 1) significantly increased numbers of goblet cells and the amount of mucin of respiratory tract (1.32×10^6 particles/cm³, 1.98 to 64.9 nm AgNPs; 6 hours/day, 5 times a week for 4 weeks)(Hyun et al., 2008), 2) pulmonary inflammation, decreased pulmonary function, and bile duct hyperplasia (2.9×10^6 particles/cm³, 2 to 65 nm AgNPs; 6 hours/day, 5 times a week for 13 weeks)(Sung et al., 2009), 3) alteration of gene expression in the brain with motor neuron disorders, neurodegenerative disease, and altered immune cell function (1.91×10^7 particles/cm³, 22.18 ± 1.72 nm AgNPs; 6 hours/day, 5 times a week for 2 weeks)(Lee et al., 2010). On the other hand, early studies of oral toxicity of AgNPs in laboratory rats found several negative health effects, including 1) weight loss (5 mg/kg) and damage to intestinal epithelial cells (20 mg/kg) (3 to 20 nm AgNPs for 21 days) (Shahare and Yashpal, 2013), 2) weight loss, pigmentation in ileum, increases in alkaline phosphatase (ALKP) activity and serum cholesterol level, and bile duct hyperplasia (56 ± 1.46 nm AgNPs for 90 days) (Kim et al., 2008; Kim et al., 2010). Apart from previous studies with high concentrations of AgNPs exposure, there were some studies conducted of relatively low concentrations of AgNPs. Sardari et al. (2012) had found that rats orally exposed to 1 to 2 mg/kg/days of 70 nm AgNPs for 30 days could induce hepatitis, necrosis of glomerular cells/proximal tubular epithelial cells, changes in normal splenic architecture. In addition, significantly increased ALKP and aspartate transaminase (AST) activities and changes in the levels of cytokines, and mild inflammation of renal cortex in the mice exposed to 1 mg/kg/days of 42 nm AgNPs for 28 days by oral administration (Park et al., 2010a). As above, the toxicity caused by

AgNPs in laboratory animals included weight loss, damage to the alimentary/hepatobiliary system, abnormalities in hematology/biochemistry, genotoxicity, neurotoxicity, and immunotoxicity.

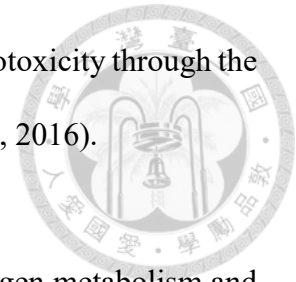


In previous studies of invertebrates (such as mussels and oyster), fishes, and fish embryos, the exposure concentrations and exposure time periods of AgNPs were ranged, respectively, from 0.0008 to 50 mg/L and 1 to 14 days. These studies demonstrated that AgNPs could cause disruption of the ionic regulation/steroidogenesis, histological alterations of gills (telangiectasia, circulatory disturbances, epithelial lifting, epithelial desquamation, deformed lamellae, and epithelial hyperplasia), neurotoxicity, immunotoxicity, cytotoxicity, and genotoxicity (Degger et al., 2015; Gagne et al., 2013; Hawkins et al., 2015; Kim and Ryu, 2013; Kwok et al., 2016; Thummabancha et al., 2016; Wu and Zhou, 2013).

2. *In vitro* studies

Numerous studies of *in vitro* toxicity of AgNPs have been published, which include human cancer cell lines (such as skin carcinoma cells [A431], human lung adenocarcinoma cells [A549], human hepatoma cells [HepG2]), rainbow trout hepatocyte, rainbow trout gill cells, and Japanese medaka fibroblast cells (OLHNI2) (Kim and Ryu, 2013; Zhang et al., 2014; Zhang et al., 2016). Although the possible mechanisms of toxic effects caused by AgNPs are not fully understood, previous studies have suggested that the AgNPs can cause cytotoxicity (i.e. mitochondrial dysfunction and apoptosis) and genotoxicity (i.e. DNA damage, formation of micronuclei, cell cycle arrest) via reactive oxygen species (ROS)-dependent pathway and ROS-independent pathway (Kim and Ryu, 2013; Zhang et al., 2014; Zhang et al., 2016). An early study has found that AgNPs can penetrate through the cell membrane, be ionized in the cytoplasm, and then induce negative effects, which is considered a Trojan-horse type mechanism (Park et al., 2010b).

Furthermore, recent studies have demonstrated that AgNPs cause cytotoxicity through the disruption of normal autophagic flux (Mao et al., 2016; Mishra et al., 2016).



2.1 ROS-dependent pathway

Reactive oxygen species (ROS) are by-products of cellular oxygen metabolism and mainly produced during mitochondrial respiration in eukaryotic cells. When there are increased amounts of ROS accumulating in cells, this condition is known as oxidative stress (Kim and Ryu, 2013). It is reported that the AgNPs can induce oxidative stress by increasing the amount of intracellular ROS with glutathione depletion, lipid peroxidation enhancement, DNA damage, cell cycle alteration, and cell proliferation inhibition, and these changes ultimately lead to cell death (Kim and Ryu, 2013; Zhang et al., 2014).

2.2 ROS-independent pathway

A previous study using HepG2 and Caco2 cell lines showed that AgNPs could cause damages to the DNA and mitochondria without increasing oxidative stress (Sahu et al., 2014). Farkas et al. (2010) demonstrated that the integrity of cell membrane and the metabolic activity of rainbow trout hepatocytes were significantly decreased without increased oxidative stress. These findings suggest that the cytotoxicity caused by AgNPs may not be associated with a ROS-dependent pathway.

3. AgNPs and Ag ion

Because Ag ions are consistently dissolved from AgNPs, the toxicity of AgNPs is actually due to the dissolved Ag ions and/or AgNPs is still controversial. Some studies suggested that the dissolved Ag ions are the cause of toxicity induced by AgNPs (Lubick, 2008) or AgNPs may act as the Trojan-horse to bring Ag ions into the cells and induce toxic effects (Farkas et al., 2010). However, there were several studies indicating that 1) the toxicity of AgNPs was higher than that of pure Ag ions, 2) only AgNPs could cause formation of micronuclei, and 3) the alteration on gene expression induced by AgNPs was

different from that by pure Ag ions (Kim et al., 2009a; Piao et al., 2011; Sahu et al., 2014). Therefore, the toxic mechanisms of AgNPs and Ag ions may be different.

4. Factors Affecting the Toxicity of AgNPs

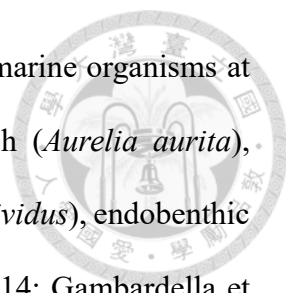
The toxicity of AgNPs is influenced by not only cell type and exposure time/concentration, but also the different coatings and sizes of AgNPs (Kim and Ryu, 2013; Riaz Ahmed et al., 2017; Zhang et al., 2014; Zhang et al., 2016)

5. The effect of AgNPs on immune system

According to the previous *in vivo* studies, AgNPs would enter the blood circulation through alimentary/respiratory administrations, and thus the negative effects caused by AgNPs to the leukocytes should be of concern. Several studies on the negative effects of AgNPs on human leukocytes have demonstrated that AgNPs could cause several effects in human neutrophils, including morphological alterations, cytotoxicity, atypical cell death, inhibition of de novo protein synthesis, increased production of the CXCL8 chemokine (IL-8), and impaired lysosomal activity (Liz et al., 2015; Poirier et al., 2014; Poirier et al., 2016; Soares et al., 2016). Cytotoxicity and inhibition of lymphocyte proliferation in lymphocytes and macrophages were also revealed (Huang et al., 2016a; Shin et al., 2007). However, the effects of AgNPs on the functional activities of human neutrophils and lymphocytes are still poorly understood.

Section 5. The Ecotoxicology of AgNPs

Due to the extensive use of AgNP-containing product and increased production of AgNPs, AgNPs have been considered as potential sources of Ag contamination. The environmental contamination level of Ag (including Ag, Ag compounds, and AgNPs) have dramatically increased in the past few years and are expected to increase over time. Therefore, it raises the public concern about the environmental toxicity of Ag. The current knowledge regarding ecotoxicological data of AgNPs in the marine ecosystem is still



scarce, and only limited data on the potential toxicity of AgNPs to marine organisms at different trophic levels has been reported, including alga, jellyfish (*Aurelia aurita*), arthropod, oyster (*Crassostrea virginica*), sea urchin (*Paracentrotus lividus*), endobenthic species, and marine medaka (*Oryzias melastigma*) (Buffet et al., 2014; Gambardella et al., 2015; Garcia-Alonso et al., 2014; Huang et al., 2016b; Moreno-Garrido et al., 2015; Ringwood et al., 2010; Wang et al., 2014). The results have demonstrated that AgNPs are toxic to all the tested marine organisms and suggested that the AgNPs may cause negative effects on the marine organisms at different trophic levels. Recent study has indicated that the AgNPs in marine environment will aggregate/precipitate into the sediments, be ingested by filter feeders and sediment-dwelling organisms, and transferred from one trophic level to the next level via the food chain (Buffet et al., 2014; Farre et al., 2009; Wang et al., 2014). The environmental contamination level of Ag is expected to increase greatly in the near future, and cetaceans as the top predators in the ocean may suffer from the negative health effects caused by Ag/Ag compounds and AgNPs.

Section 6. Summary and Objectives

Silver nanoparticles (AgNPs) have been extensively used in numerous commercial products, including textiles, cosmetics, health care items, and electronic devices/medical images. AgNPs can be released during the production, transport, erosion, washing, and/or disposal of AgNP-containing products, subsequently draining into the aquatic environment, and ultimately accumulating in the ocean. Therefore, AgNPs have been considered as potential sources of Ag contamination, which has raised the public concern about the environmental toxicity of Ag. Ag can be transferred from one trophic level to the next via the food chain and may cause negative effects on the animals at higher trophic levels. The environmental contamination level of Ag is expected to increase greatly in the near future, and aquatic animals and marine environment may suffer the potentially

negative impacts caused by Ag. However, the ecotoxicological studies on AgNPs and Ag are still sparse. Cetaceans, as the top predators in the ocean, may endure the negative health impact by long-term exposure to and accumulation of Ag/Ag compounds in their bodies.

Although the concentrations of Ag/Ag compounds in cetacean tissues can be measured by inductively coupled plasma mass spectroscopy (ICP-MS), the use of ICP-MS is limited by its high capital cost (instrument and maintenance) and the requirement for tissue storage/preparation. Considering the difficulties in measuring Ag concentrations by ICP-MS in most stranded cetaceans, it is valuable to develop a histological method using formalin-fixed and paraffin-embedded (FFPE) tissue samples to localize Ag and estimate the Ag concentrations in the cetacean liver and kidney tissues. On the other hand, the toxic effects caused by AgNPs may be different from those caused by Ag/Ag compounds, and AgNPs can enter blood circulation after alimentary exposure. Therefore, it is necessary to investigate the negative effects caused by AgNPs by using the cetacean leukocytes (consistent exposure). Most importantly, cetaceans as well as humans are mammals; and the negative health impact caused by Ag/Ag compounds and AgNPs in cetaceans may also occur in humans. In other words, cetaceans are good sentinel animals for the condition of marine environment and human health.

As above, the current study aimed to 1) develop a histological method to evaluate the tissue distribution of Ag and to estimate the Ag concentrations in the liver and kidney of cetaceans (**Chapter II**); 2) determine the metabolic pathway of Ag, estimate Ag concentrations of cetacean liver and kidney tissues by CHAA, and investigate the histopathological lesions possibly caused by Ag in cetaceans (**Chapter III**); 3) investigate the immunotoxicity of AgNPs on the leukocytes of cetaceans (**Chapter IV**); and 4) evaluate the changes in *in vitro* cytokine profile of cetacean peripheral blood mononuclear

cells (cPBMCs) exposed to AgNPs (**Chapter V**).



Chapter II: Use of Autometallography to Localize and Semi-quantify Silver in Cetacean Tissues (Manuscript in Submission)



AUTHORS & AFFILIATIONS:

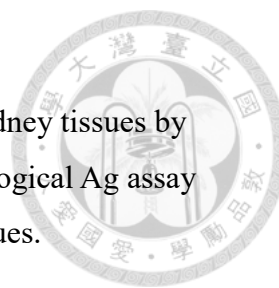
Wen-Ta Li^a, Bang Yeh Liou^a, Wei-Cheng Yang^b, Meng-Hsien Chen^c, Hui-Wen Chang^a, Hue-Ying Chiou^d, Victor Fei Pang^a, and Chian-Ren Jeng^{a*}

^aGraduate Institute of Molecular and Comparative Pathobiology, National Taiwan University, Taipei, Taiwan; ^bCollege of Veterinary Medicine, National Chiayi University, Chiayi, Taiwan; ^cDepartment of Oceanography and Asia-Pacific Ocean Research Center, National Sun Yat-sen University, Kaohsiung, Taiwan; ^dGraduate Institute of Veterinary Pathobiology, National Chung Hsing University, Taichung, Taiwan

CORRESPONDING AUTHOR: Chian-Ren Jeng

KEYWORDS:

Autometallography (AMG); Cetacean; Cetacean Histological Ag Assay (CHAA); ImageJ; Inductively Coupled Plasma Mass Spectroscopy (ICP-MS); Silver (Ag); Quantitative Analysis



SHORT ABSTRACT:

A protocol is presented to localize Ag in cetacean liver and kidney tissues by autometallography. Furthermore, a new assay, named cetacean histological Ag assay (CHAA) is developed to estimate the Ag concentrations in those tissues.

LONG ABSTRACT:

Silver nanoparticles (AgNPs) have been extensively used in commercial products, including textiles, cosmetics, and health care items, due to their strong antimicrobial effects. They also may be released into the environment and accumulate in the ocean. Therefore, AgNPs are the major source of Ag contamination, and public awareness of the environmental toxicity of Ag is increasing. Previous studies have demonstrated the bioaccumulation (in producers) and magnification (in consumers/predators) of Ag. Cetaceans, as the apex predators of ocean, may have been negatively affected by the Ag/Ag compounds. Although the concentrations of Ag/Ag compounds in cetacean tissues can be measured by inductively coupled plasma mass spectroscopy (ICP-MS), the use of ICP-MS is limited by its high capital cost and the requirement for tissue storage/preparation. Therefore, an autometallography (AMG) method with image quantitative analysis by using formalin-fixed, paraffin-embedded (FFPE) tissue may be an adjuvant method to localize Ag distribution at the suborgan level and estimate the Ag concentration in cetacean tissues. The AMG positive signals are mainly brown to black granules of various sizes in the cytoplasm of proximal renal tubular epithelium, hepatocytes, and Kupffer cells. Occasionally, some amorphous golden yellow to brown AMG positive signals are noted in the lumen and basement membrane of some proximal renal tubules. The assay for estimating the Ag concentration is named Cetacean Histological Ag Assay (CHAA), which is a regression model established by the data from image quantitative analysis of the AMG method and ICP-MS. The use of AMG with CHAA to localize and semi-quantify heavy metals provides a convenient methodology for spatio-temporal and cross-species studies.

INTRODUCTION:

Silver nanoparticles (AgNPs) have been extensively used in commercial products, including textiles, cosmetics, and health care items, due to their great antimicrobial effects^{1,2}. Therefore, the production of AgNPs and the number of AgNP-containing products are increased over time^{3,4}. However, AgNPs may be released into the environment and accumulate in the ocean^{5,6}. They have become the major source of Ag

contamination, and the public awareness of the environmental toxicity of Ag is increasing.

The status of AgNPs and Ag in the marine environment is complicated and constantly changing. Previous studies have indicated that AgNPs can remain as particles, aggregate, dissolve, react with different chemical species, or be regenerated from Ag⁺ ions^{7,8}. Several types of Ag compounds, such as AgCl, have been found in marine sediments, where they can be ingested by benthic organisms and enter the food chain^{9,10}. According to a previous study conducted in the Chi-ku Lagoon area along the southwestern coast of Taiwan, the Ag concentrations of marine sediments are extremely low and similar to the crustal abundance, and those of fish liver tissue are usually below the detection limit (< 0.025 µg/g wet/wet)¹¹. However, previous studies conducted in different countries have demonstrated relatively high Ag concentrations in the livers of cetaceans^{12,13}. The Ag concentration in the livers of cetaceans is age-dependent, suggesting that the source of Ag in their bodies is most likely their prey¹². These findings further suggest the biomagnification of Ag in animals at higher trophic levels. Cetaceans, as the apex predators in the ocean, may have suffered negative health impacts caused by Ag/Ag compounds¹²⁻¹⁴. Most importantly, like cetaceans, humans are mammals, and the negative health impacts caused by Ag/Ag compounds in cetaceans may also occur in humans. In other words, cetaceans could be sentinel animals for the health of marine environment and humans. Therefore, the health effects, the tissue distribution, and concentration of Ag in cetaceans are of great concern.

Although the concentrations of Ag/Ag compounds in cetacean tissues can be measured by inductively coupled plasma mass spectroscopy (ICP-MS), the use of ICP-MS is limited by its high capital cost (instrument and maintenance) and the requirements for tissue storage/preparation^{12,15}. In addition, it is usually difficult to collect comprehensive tissue samples in all investigations of stranded cetacean cases due to logistical difficulties, a shortage of manpower, and a lack of related resources¹². The frozen tissue samples for ICP-MS analysis are not easily stored because of limited refrigeration space, and frozen tissue samples may be discarded due to broken refrigeration equipment¹². These aforementioned obstacles hamper investigations of contamination levels in cetacean tissues by ICP-MS analysis using frozen tissue samples. In contrast, formalin fixed tissue samples are relatively easy to collect during the necropsy of dead-stranded cetaceans. Therefore, it is necessary to develop an easy to

use and inexpensive method to detect/measure the heavy metals in cetacean tissues by using formalin fixed tissue samples.

Although the suborgan distributions and concentrations of alkali and alkaline earth metals may be altered during the formalin-fixed, paraffin-embedded (FFPE) process, only lesser effects on transition metals, such as Ag, have been noted¹⁶. Hence, FFPE tissue has been considered as an ideal sample resource for metal localization and measurements^{16,17}. Autometallography (AMG), a histochemical process, can amplify heavy metals as variably sized golden yellow to black AMG positive signals on FFPE tissue sections, and these amplified heavy metals can be visualized under light microscopy¹⁸⁻²¹. Hence, the AMG method provides information on the suborgan distributions of heavy metals. It can provide important additional information for studying the metabolic pathways of heavy metals in biological systems because ICP-MS can only measure the concentration of heavy metals at the organ level¹⁸. Furthermore, digital image analysis software, such as ImageJ, has been applied to the quantitative analysis of histological tissue sections^{22,23}. The variably-sized golden yellow to black AMG positive signals of FFPE tissue sections can be quantified and used to estimate the concentrations of heavy metals. Although the absolute Ag concentration cannot be directly determined by the AMG method with image quantitative analysis, it can be estimated by a regression model based on the data obtained from the image quantitative analysis and ICP-MS, which is named cetacean histological Ag assay (CHAA). Considering the difficulties in measuring Ag concentrations by ICP-MS analysis in most stranded cetaceans, CHAA is a valuable adjuvant method to estimate Ag concentrations in cetacean tissues, which cannot be determined by ICP-MS analysis due to the lack of frozen tissue samples. This paper describes the protocol of a histochemical technique (AMG method) for localizing Ag at the suborgan level and an assay named CHAA to estimate the Ag concentrations in the liver and kidney tissues of cetaceans.

[Place **Figure 1** here]

PROTOCOL:

The study was performed in accordance with international guidelines, and the use of cetacean tissue samples was permitted by the Council of Agriculture of Taiwan (Research Permit 104-07.1-SB-62).

1. Tissue Sample Preparation for ICP-MS Analysis

Note: The liver and kidney tissues were collected from freshly dead and moderately autolyzed stranded cetaceans²⁴, including 6 stranded cetaceans of 4 different species, 1 *Grampus griseus* (Gg), 2 *Kogia* spp. (Ko), 2 *Lagenodelphis hosei* (Lh), 1 *Stenella attenuata* (Sa). Each stranded cetacean had a field number for individual identification. The tissue sample preparation for ICP-MS analysis followed the method established in M.H. Chen's lab, and M.H. Chen's lab conducted the ICP-MS analysis^{11,13,25}.

1.1. Collect liver and kidney tissues for ICP-MS analysis from stranded cetaceans and store them at $-20\text{ }^{\circ}\text{C}$ until use.

1.2. Collect pair-matched liver and kidney tissues from the same stranded cetaceans for AMG analysis (please see step 2).

1.3. Trim the outer layer of the tissue samples collected for ICP-MS analysis with a stainless-steel scalpel. Cut the inner part of the tissue samples into small cubes (about 1 cm^3) and place them in zip lock plastic bags. Normally, each bag contains 10 g of the tissues.

1.4. Store the plastic bags containing tissue samples at $-20\text{ }^{\circ}\text{C}$ for subsequent procedures.

1.5. Put the 1 cm^3 cubes samples in a freeze dry system (-50°C , Vacuum pump with a displacement of at least 98 L/min, 0.002 mBar) for at least 72 h till completely dried by weighting to the constant.

1.6. Homogenize the dried cubes into powder by homogenizer for subsequent tissue digestion.

1.7. Weigh 0.3 g of homogenized freeze-dried samples in 30 mL polytetrafluoroethylene (PTFE) bottles and mix them with 10 mL of 65% w/w nitric acid.

1.8. Put closures on the PTFE bottles, but leave the closures untightened.

Note: it allows the brown fume to be formed in the PTFE bottles and reflux inside the bottle for digestion till the brown fume disappear and turn clear.

1.9. Heat the digested samples with a hot plate, from $30\text{ }^{\circ}\text{C}$ to $110/120\text{ }^{\circ}\text{C}$ (according to the brown fume forming condition) in the PTFE bottles for 2 to 3 weeks until the brownish gas in the PTFE bottles becomes colorless and the liquid in the PTFE bottles becomes translucent greenish pale yellow or completely clear.

Note: Perform the heating process in chemical fume hood.

1.10. Heat the digested samples at $120\text{ }^{\circ}\text{C}$ to evaporate the nitric acid in the PTFE bottles until only 0.5 to 1 mL remains.

Note: Perform the heating process in a chemical fume hood, and always monitor the temperature increase to ensure that no brownish gas leaks from the PTFE bottles' closures.

1.11. Tighten the closures and cool them at room temperature for about one hour.

1.12. Place the funnels with filter papers on 25 mL volumetric flasks and wash the remaining liquid with 1 M HNO₃ to a final volume of 25 mL.

Note: Wash the bottle for at least three times and the closure twice.

1.13. Validate the analytical quality of ICP-MS analysis by using the standard reference materials, including DOLT-2 (dogfish liver) and DORM-2 (dogfish muscle).

1.14. Use duplicates of each analytical sample and triplicates of standard reference materials for ICP-MS analysis.

1.15. Average the Ag concentrations of each analytic samples and present the data as dry weight basis concentration (µg/g dry weight).

2. Tissue Sample Preparation for AMG Analysis

2.1. Collect pair-matched liver and kidney tissues for AMG analysis from a stranded cetacean and fix them in 10% neutral buffered formalin until use.

Note: Store the tissue samples in plastic bottles in 10% neutral buffered formalin (NBF, pH 7.0) for 24 to 48 hours. The volume of NBF should be at least 10 times greater than the tissue volume.

2.2. Trim the formalin fixed liver and kidney tissues with stainless steel disposable microtome blades and put the trimmed tissue sections in cassettes with labels.

Note: The size of each tissue sections should be approximately 2 x 1 cm and the thickness of each tissue section should not exceed 3 mm. Put the liver and kidney tissues from the same individual in the same cassette.

2.3. Dehydrate the trimmed tissue sections with a tissue processor through a series of graded ethanol (70% for 1 h, 80% for 1 h, 95% for 1 h, 95% for 2 h, 100% for 1 h x 2 staining dishes, and 100% for 2 h), non-xylene (for 1 h and 2 h in different staining dishes), and immerse the dehydrated tissue samples in paraffin (for 1 h and 2 h in different staining dishes).

2.4. Place the dehydrated tissue samples in the bottoms of steel histology molds and embed the dehydrated tissue samples with paraffin.

2.5. Chill the formalin fixed paraffin-embedded (FFPE) tissue blocks at -20 °C. Trim the FFPE blocks with the microtome until the tissue surface is exposed.

2.6. Chill the FFPE blocks at $-20\text{ }^{\circ}\text{C}$ again. Section the FFPE blocks at $5\text{ }\mu\text{m}$ by microtome.

2.7. Fill a water bath with double-distilled water at $45\text{ }^{\circ}\text{C}$. Lift the ribbons of tissue sections and make them float on the surface of the warm water by using tweezers and brushes.

2.8. Separate the ribbons of tissue sections with tweezers. Place a section onto a microscope slide.

2.9. Place the microscope slides on a slide warmer and allow sections to dry overnight at $37\text{ }^{\circ}\text{C}$.

2.10. Put the microscope slides in slide racks and deparaffinize them by soaking them in 3 different staining dishes of pure non-xylene (approximately 200 to 250 mL) for 8, 5, and 3 min.

2.11. Hydrate the tissue sections in slide racks by soaking them in different staining dishes of graded ethanol solutions (100% ethanol twice, 90% ethanol once and 80% ethanol once [1 min each]), and rinse them in double-distilled water.

Note: These solutions are approximately 200 to 250 mL in different staining dishes.

2.12. Rinse the tissue sections in phosphate-buffered saline (PBS) with 0.5% Triton X-100, wash them with PBS for several times, and then rinse them in double-distilled water.

Note: These solutions are approximately 200 to 250 mL in different staining dishes.

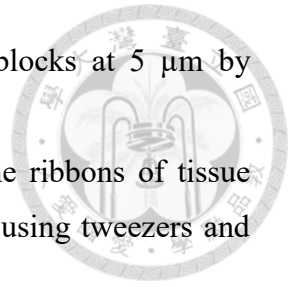
2.13. Prepare equal amounts of the three components (initiator, moderator, and activator) provided by silver enhancement kit in dark and mix them thoroughly.

Note: The solutions of moderator and activator are sticky, so please use pipette with wide tip openings (or cut the tips to create wider openings). For each slide, 300 μL of the mixed solution (depending on the size of the tissue section) is usually enough.

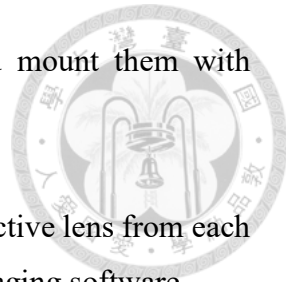
Therefore, if 10 slides are used, the amount of each component (initiator, moderator, and activator) is 1000 μL (the mixed solution is 3000 μL for 10 slides).

2.14. Incubate the tissue sections in the mixed solution for 15 min in dark at room temperature. Fully cover the tissue sections on the slides with the mixed solution. A longer incubation time may lead to false-positive AMG signals.

2.15. Wash the slides with double-distilled water and stain them in hematoxylin for 10 s as a counterstain.



- 2.16. Wash the slides with running tap water, dry them, and mount them with mounting medium.
- 2.17. Examine the slides under a light microscope.
- 2.18. Randomly capture ten histological images with a 40X objective lens from each tissue section by using a connected digital camera with computer imaging software.



3. Semi-Quantitative Analysis for AMG Positive Values of Histological Images

Note: AMG positive value means the percentage of the area with AMG positive signals.

- 3.1. Use image analysis software (ImageJ) to analyze the histological images.
- 3.2. Open the histological image by pressing **File | Open**.
- 3.3. Split the chosen picture into three color channels (red, blue, and green) by pressing **Image | Type | RGB Stack**.
- 3.4. Quantify the AMG positive signals by using the blue channel. Nuclear false positive signals are usually decreased under the blue channel when hematoxylin stain is applied for nuclear counterstain (**Figure 2**).
- 3.5. Measure the percentage of the area with AMG positive signals in each histological image with the threshold tool (**Image | Adjust | Threshold**).
- 3.6. Manually adjust the cut-off value of the threshold for each histological image (from 90 to 110) based on the presences of false positive areas in nuclei and/or red blood cells.
Note: In default setting, the AMG positive signals should be highlighted in red.
- 3.7. Press **Analyze | Set Measurements**, and check the box of **Area Fraction** to specify that the area fraction is recorded.
- 3.8. Press **Analyze | Measure**. The positive percent area of each histological image is displayed in the column of **%Area** of the **Result** window.
- 3.9. Average the positive percent areas of 10 histological images from each tissue section and define the result as the AMG positive value for each tissue section.

[Place **Figure 2** here]

4. Establishment of the Cetacean Histological Ag Assay (CHAA) by Regression Model

Note: The following analysis is performed in Prism 6.01 for Windows.

- 4.1. Evaluate the correlation between the results of ICP-MS and AMG positive values.
- 4.2. Open the Prism software, create a new prism project file, and choose **XY and Correlation**.
- 4.3. Input data including the results of ICP-MS and AMG positive values.

4.4. Press **Analysis** and choose **Correlation** under the category **XY Analysis** to analyze the strength of association between the results of the ICP-MS and AMG positive values by Pearson correlation analysis.

Note: The results of the ICP-MS and AMG positive values have to be positively correlated with each other; otherwise, the subsequent regression model should not be developed.

4.5. Statistically compare the regression models, including linear regression, quadratic regression, cubic regression, and linear regression through origin, through statistics software^{12,26,27}.

Note: If the regression model generates an unrealistic Ag concentration, the regression model should be abandoned¹².

4.6. Go back to the Data Table (left panel) and press **Analysis | Nonlinear regression (curve fit)** under the category **XY Analysis | OK**.

4.7. In the window **Parameters: Nonlinear regression**, choose different regression model in the page **Fit** and then compare different regression models in the page **Compare**.

4.8. In the page **Compare**, choose the comparison methods, including the extra sum-of-squares F test and Akaike's information criterion (AIC). According to the results of the comparison methods, use a relatively appropriate regression model in the CHAA.

4.9. Estimate Ag concentrations of the cetacean liver and kidney tissues with unknown Ag concentrations by using the CHAA.

4.10. Evaluate the accuracy and precision of the CHAA for liver and kidney tissues. The difference between precision and accuracy is illustrated in **Figure 3**.

4.11. Accuracy: Calculate the mean standard deviation (SD) from differences between known and estimated Ag concentrations.

4.12. Precision: Perform repeated measurement (at least triplicate) of AMG positive values of serial sections from the same FFPE tissues. Calculate the mean SD of measurements from liver or kidney tissues from differences between known and estimated Ag concentrations

Note: The methods of evaluating the accuracy and precision are depicted in **Figure 4**.

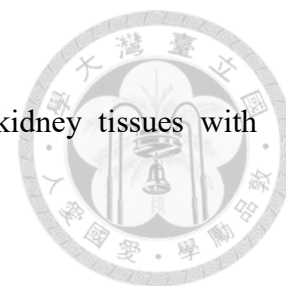
[Place Figures 3 and 4 here]

5. Estimation of Ag Concentrations by CHAA.

5.1. Collect the liver and kidney tissues from stranded cetaceans and fix them in 10% neutral buffered formalin.

5.2. Process the formalin-fixed tissues routinely (please see step 2).

5.3. Estimate the Ag concentrations of the cetacean liver and kidney tissues with unknown Ag concentrations by CHAA (please see steps 3 and 4).



REPRESENTATIVE RESULTS:

Representative images of the AMG positive signals in the cetacean liver and kidney tissues are shown in **Figure 5**. The AMG positive signals include variably-sized brown to black granules of various sizes in the cytoplasm of proximal renal tubular epithelium, hepatocytes, and Kupffer cells. Occasionally, amorphous golden yellow to brown AMG positive signals are noted in the lumen and basement membrane of some proximal renal tubules. There is a positive correlation between the results of ICP-MS and AMG positivity values in liver and kidney tissues, and linear regression through origin is preferred according to the extra sum-of-squares F test and AIC^{12,26,27}. In the accuracy test, the mean SDs of the CHAA for liver and kidney are 3.24 and 0.16, respectively. In the precision test, the mean SDs of the CHAA for liver and kidney are 2.8 and 0.35, respectively. The raw data of the accuracy and precision tests are summarized in **Table 1**. The AMG positive values, Ag concentrations estimated by CHAA, and Ag concentrations measured by ICP-MS from the liver and kidney tissues of these six stranded cetaceans are summarized in **Table 2**.

FIGURE AND TABLE LEGENDS:

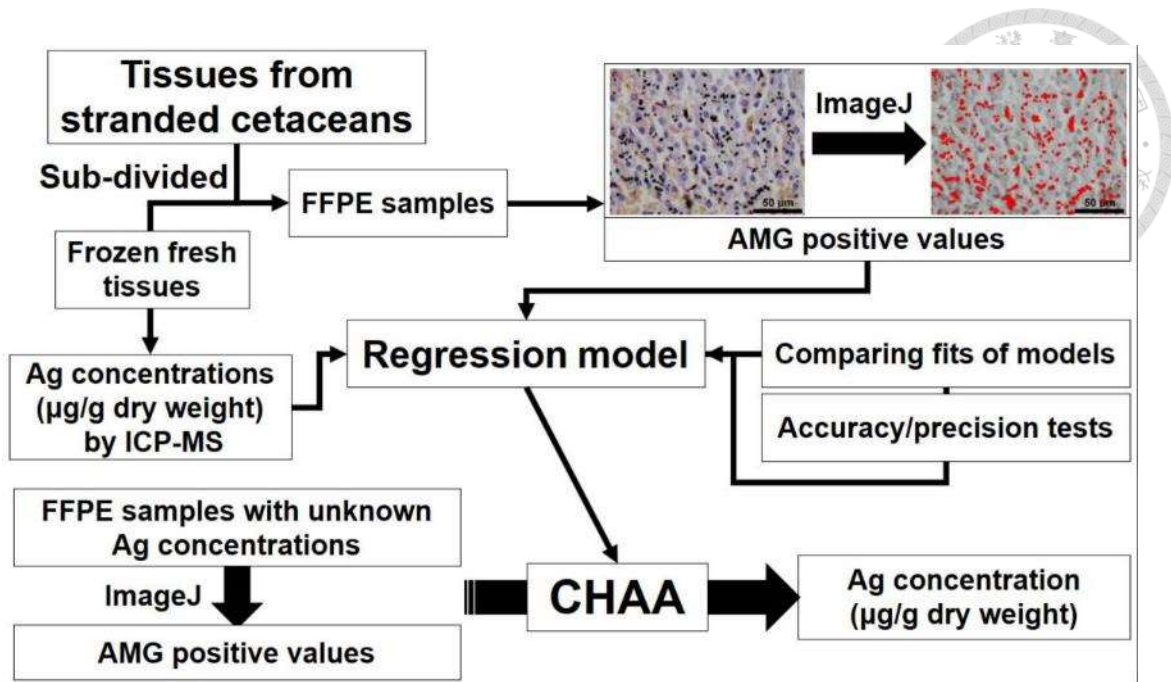


Figure 1: Flowchart depicting the establishment and application of cetacean histological Ag assay (CHAA) for estimating Ag concentrations. CHAA = cetacean histological Ag assay, FFPE = Formalin-fixed, paraffin-embedded, ICP-MS = inductively coupled plasma mass spectroscopy.

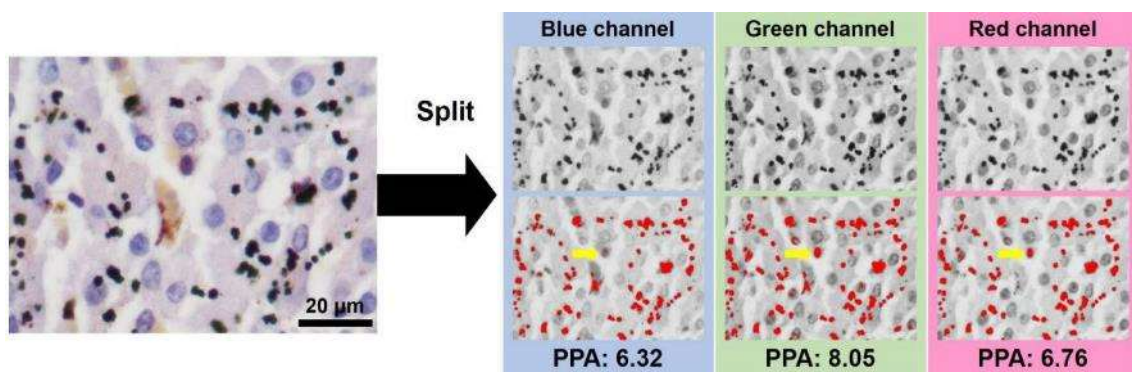


Figure 2: The presence of nuclear false positive signals under different color channels (counterstain: hematoxylin stain). Representative nuclear false positive signals are indicated by yellow arrows. PPA = positive percentage of areas.

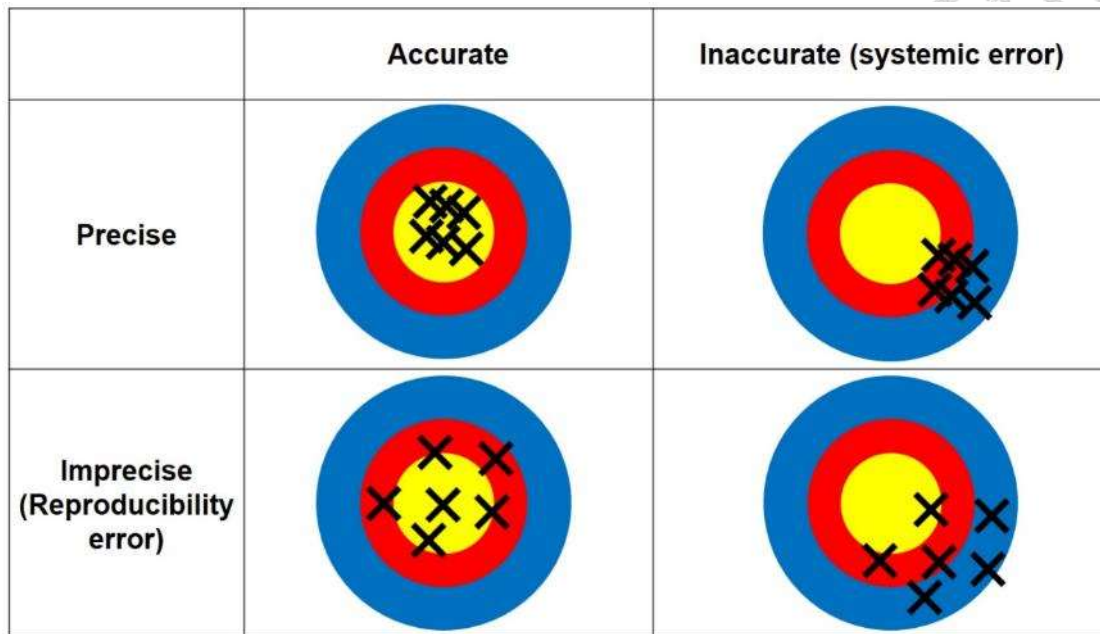


Figure 3: The difference between accuracy and precision. Accuracy means how close the measurement is to the true value (*i.e.*, Ag concentration determined by ICP-MS); precision means the repeatability of the measurement (*i.e.*, the consistency among the repeated measurements of AMG positive values from the triplicate tissue sections).

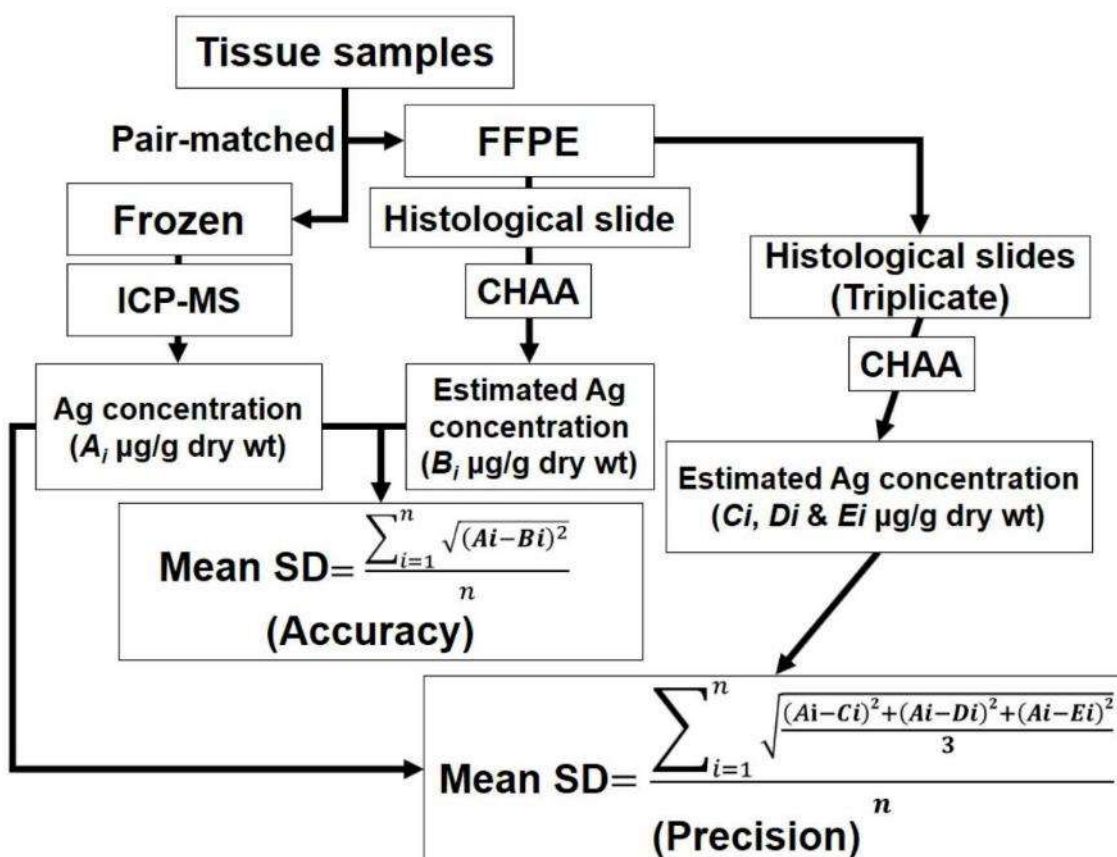


Figure 4: The scheme depicting the methods of evaluating the accuracy and precision. CHAA = cetacean histological Ag assay; FFPE = Formalin-fixed, paraffin-embedded; ICP-MS = inductively coupled plasma mass spectroscopy; A_i = Each of the Ag concentrations determined by ICP-MS of each pair-matched tissue sample; B_i = Each of the Ag concentrations estimated by CHAA of each pair-matched tissue sample; C_i , D_i , and E_i = Each of The Ag concentrations estimated by CHAA of triplicate samples from each pair-matched tissue sample; $i = 1$ to n . Please see raw data of the accuracy and precision tests in the section of representative results.

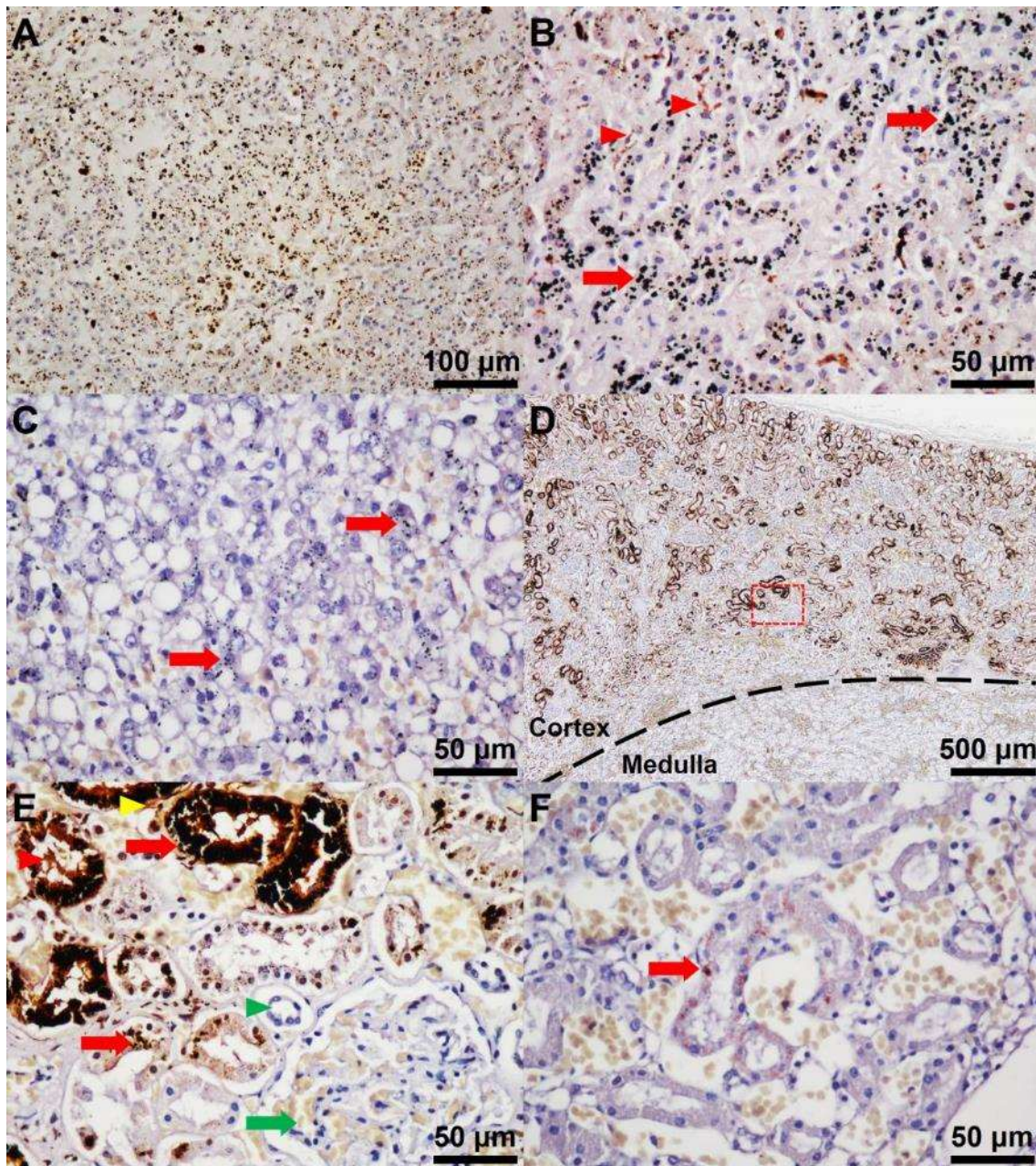


Figure 5: Representative histological images of the AMG positive signals in the liver and kidney tissues of cetaceans (counterstain: hematoxylin stain). (A) The

AMG positive signals in cetacean liver tissue are evenly distributed (*Grampus griseus* (Gg); field code: TP20111116; Ag concentration measured by inductively coupled plasma mass spectroscopy (ICP-MS): 21.82 µg/g dry weight). **(B)** The AMG positive signals are brown to black granules of various sizes in the cytoplasm of hepatocytes (red arrows) and Kupffer cells (red arrow heads) (Gg; field code: TP20111116). **(C)** A few AMG positive signals of brown to black granules are shown in the cytoplasm of hepatocytes (red arrows) (*Kogia* spp. (Ko); field code: TC20110722; Ag concentration measured by ICP-MS: 3.86 µg/g dry weight). **(D)** The AMG positive signals in cetacean kidney tissue are mainly located in the renal cortex (Gg; field code: TP20111116; Ag concentration measured by ICP-MS: 0.42 µg/g dry weight). The black dashed line is placed on the junction between the renal cortex and medulla. **(E)** Higher magnification of **Figure 5D** (red dashed rectangle). The AMG positive signals in the renal cortex are brown to black granules of various sizes in the cytoplasm of the proximal renal tubular epithelium (red arrows). Amorphous golden yellow to brown AMG positive signals are shown in the lumens (red arrow head) and basement membrane (yellow arrow head) of some proximal renal tubules. No to minimal AMG positive signals are shown in the glomeruli (green arrow) and distal renal tubules (green arrow head)(Gg; field code: TP20111116). **(F)** Scattered brown granules of various sizes are shown in the cytoplasm of the proximal renal tubular epithelium (red arrows) (Ko; field code: TC20110722; Ag concentration measured by ICP-MS: 0.05 µg/g dry weight).

Table 1: The representative results of the accuracy and precision tests for cetacean histological Ag assay (CHAA). CHAA = cetacean histological Ag assay, ICP-MS = inductively coupled plasma mass spectroscopy, SD = standard deviation.

Accuracy test

Field number	Liver			Kidney		
	CHAA*	ICP-MS	SD	CHAA*	ICP-MS	SD
TP20111116	16.82	21.82	4.99	0.64	0.42	0.22
TC20110611	10.12	2.77	0.96	0.11	0.05	0.35
TC20110722	2.70	3.86	1.15	0.01	0.05	0.04
TD20110608	0.76	0.06	7.35	0.02	0.05	0.06
TP20110830	13.97	14.93	4.28	0.69	1.04	0.24
IL20110101	6.00	1.73	0.72	0.38	0.14	0.03

		Mean	SD	Mean	SD		
		3.24		0.16			
Precision test							
Field number	Liver			Kidney			
	CHAA*	ICP-MS	SD	CHAA*	ICP-MS	SD	
TP20111116	20.90			0.21			
	16.11	21.82	4.08	0.22	0.42	0.44	
	17.75			0.14			
TD20110608	1.52			0.00			
	2.40	0.06	1.71	0.00	0.05	0.02	
	1.12			0.00			
TP20110830	13.12			0.45			
	12.50	14.93	2.70	0.26	1.04	0.59	
	11.35			0.33			
		Mean SD	2.83	Mean SD	0.35		

Table 2: The AMG positive values, Ag concentrations ($\mu\text{g/g}$, dry weight) estimated by cetacean histological Ag assay (CHAA), and Ag concentrations ($\mu\text{g/g}$, dry weight) measured by ICP-MS from the liver and kidney tissues of six stranded cetaceans. Gg = *Grampus griseus*, Ko = *Kogia* spp., Lh = *Lagenodelphis hosei*, Sa = *Stenella attenuata*.

Field number	Species	Liver			Kidney		
		AMG	CHAA*	ICP-MS	AMG	CHAA*	ICP-MS
TP20111116	Gg	7.48	16.82	21.82	8.82	0.64	0.42
TC20110611	Ko	4.50	10.12	2.77	1.52	0.11	0.05
TC20110722	Ko	1.20	2.70	3.86	0.11	0.01	0.05
TD20110608	Lh	0.34	0.76	0.06	0.21	0.02	0.05
TP20110830	Lh	6.21	13.97	14.93	9.43	0.69	1.04
IL20110101	Sa	2.67	6.00	1.73	5.26	0.38	0.14

DISCUSSION:

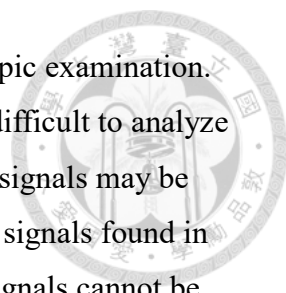
The purpose of the article study is to establish an adjuvant method to evaluate the Ag distribution at suborgan levels and to estimate Ag concentrations in cetacean tissues. The current protocols include 1) determination of Ag concentrations in cetacean tissues

by ICP-MS, 2) AMG analysis of pair-matched tissue samples with known Ag concentrations, 3) establishment of the regression model (CHAA) for estimating the Ag concentrations by AMG positive values, 4) evaluation of the accuracy and precision of CHAA, and 5) estimation of Ag concentrations by CHAA.

In this study, the data of ICP-MS were significantly and positively correlated with those of AMG positive values, suggesting that the Ag concentration in cetacean tissues can be estimated by the AMG positive value. Therefore, the CHAA, which is based on the AMG positive value and regression model, has been developed for estimating the Ag concentrations in the liver and kidney tissues of cetaceans. Generally, a regression model with more parameters (*i.e.*, a more complex regression model) fits well into the data, but it is undetermined that the more complex one is actually better than the simpler one. Therefore, the best regression model must be chosen by statistical analysis^{26,27}. The results of the statistical analysis indicate that the linear regression model is sufficient to estimate the Ag concentration based on the AMG positive value¹².

In CHAA for kidney tissue, the mean SD (0.35) of the precision test was larger than that of the accuracy test (0.16). Conversely, in CHAA for liver tissue, the mean SD (2.8) of the precision test was smaller than that of the accuracy test (3.24). Based on this result, it is suggested that the uneven distribution of the AMG positive signals and the relatively low Ag concentrations in cetacean kidney tissue interfere negatively with the precision of CHAA for kidney tissue. Therefore, the CHAA for kidney tissue may be accurate but imprecise. However, the even distribution of the AMG positive signals and the relatively high Ag concentrations in cetacean liver tissues suggest that the CHAA for liver tissue is a reliable method to estimate the Ag concentrations in cetacean liver tissues. Furthermore, if more tissues with known Ag concentrations determined by ICP-MS are available, a more accurate and precise regression model can be developed to estimate the Ag concentration.

Although the current protocols provide an adjuvant method to investigate Ag in animal tissues, some limitations on the AMG method should be noted. First, false-positive AMG signals may present due to interference from other heavy metals, such as mercury, bismuth and zinc²⁸. Therefore, the results of the AMG method have to be interpreted with other specific methods, such as ICP-MS, to monitor the actual composition of heavy metals²⁸. Second, it is difficult to detect a homogeneously distributed heavy metal because it may generate brighter amorphous AMG positive



signals, which may not be identified by visualization under microscopic examination. Furthermore, the amorphous and brighter AMG positive signals are difficult to analyze with image analysis software because the color of the AMG positive signals may be similar to that of the background (e.g., the amorphous AMG positive signals found in the lumen of proximal renal tubules). Therefore, the AMG positive signals cannot be highlighted after the adjustment of the cut-off value of the threshold in the image analysis software. Third, because the AMG positive values are based on the percentage of the area of AMG positive signals, it is possible that the values of highly concentrated heavy metals may be underestimated.

FFPE samples are relatively easy to collect and store, and our previous study has demonstrated that the current AMG method can successfully amplify FFPE samples stored for over 15 years¹². The mechanism of AMG is not affected by different animal species, for it has been widely used in various animal species^{20,29-31}. Although the current article is focused on the cetaceans, the protocols described here may also be used in different animal species. In addition, the cost of the AMG method with ICP-MS is relatively low (as compared to laser ablation-ICP-MS), and thus the current protocols are valuable for researchers or countries lacking sufficient research funding to investigate the distribution and concentration of heavy metals in animal tissues. In conclusion, the use of AMG with quantitative analysis to localize and semi-quantify heavy metals provides a convenient methodology for spatio-temporal and cross-species studies.

ACKNOWLEDGMENTS:

We thank the Taiwan Cetacean Stranding Network for sample collection and storage, including the Taiwan Cetacean Society, Taipei; the Cetacean Research Laboratory (Prof. Lien-Siang Chou), the Institute of Ecology and Evolutionary Biology, National Taiwan University, Taipei; the National Museum of Natural Science (Dr. Chiou-Ju Yao), Taichung; and the Marine Biology & Cetacean Research Center, National Cheng-Kung University. We also thank Forestry Bureau, Council of Agriculture, Executive Yuan for their permit. This study is partially supported by the Ministry of Science & Technology, Taiwan under Grant MOST 106-2313-B-002-054-.

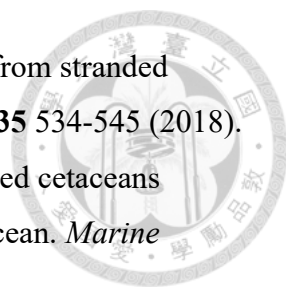
DISCLOSURES:

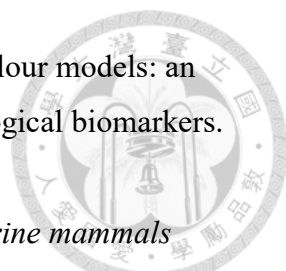
The authors have nothing to disclose.



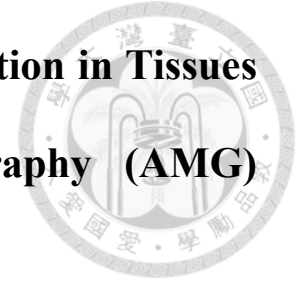
REFERENCES:

- 1 McGillicuddy, E. *et al.* Silver nanoparticles in the environment: Sources, detection and ecotoxicology. *Science Total Environment*. **575**, 231-246 (2017).
- 2 Yu, S.J., Yin, Y.G., Liu, J.F. Silver nanoparticles in the environment. *Environmental Science: Processes and Impacts*. **15** (1), 78-92 (2013).
- 3 Hansen, S.F. *et al.* Nanoproducts- what is actually available to European consumers? *Environmental Science: Nano*. **3** (1), 169-180 (2016).
- 4 Vance, M.E. *et al.* Nanotechnology in the real world: Redeveloping the nanomaterial consumer products inventory. *Beilstein Journal of Nanotechnology*. **6** 1769-1780 (2015).
- 5 Farre, M., Gajda-Schranz, K., Kantiani, L., Barcelo, D. Ecotoxicity and analysis of nanomaterials in the aquatic environment. *Analytical and Bioanalytical Chemistry*. **393** (1), 81-95 (2009).
- 6 Walters, C.R., Pool, E.J., Somerset, V.S. Ecotoxicity of silver nanomaterials in the aquatic environment: a review of literature and gaps in nano-toxicological research. *Journal of Environmental Science and Health. Part A, Toxic/hazardous Substances & Environmental Engineering*. **49** (13), 1588-1601 (2014).
- 7 Levard, C., Hotze, E.M., Lowry, G.V., Brown, G.E., Jr. Environmental transformations of silver nanoparticles: impact on stability and toxicity. *Environmental Science & Technology*. **46** (13), 6900-6914 (2012).
- 8 Massarsky, A., Trudeau, V.L., Moon, T.W. Predicting the environmental impact of nanosilver. *Environmental Toxicology and Pharmacology*. **38** (3), 861-873 (2014).
- 9 Wang, H. *et al.* Toxicity, bioaccumulation, and biotransformation of silver nanoparticles in marine organisms. *Environmental Science and Technology*. **48** (23), 13711-13717 (2014).
- 10 Buffet, P.E. *et al.* A marine mesocosm study on the environmental fate of silver nanoparticles and toxicity effects on two endobenthic species: the ragworm *Hediste diversicolor* and the bivalve mollusc *Scrobicularia plana*. *Science of the Total Environment*. **470-471** 1151-1159 (2014).
- 11 Chen, M.H. Baseline metal concentrations in sediments and fish, and the determination of bioindicators in the subtropical Chi-ku Lagoon, S W Taiwan. *Marine Pollution Bulletin*. **44** (7), 703-714 (2002).

- 
- 12 Li, W.T. *et al.* Investigation of silver (Ag) deposition in tissues from stranded cetaceans by autometallography (AMG). *Environmental Pollution*. **235** 534-545 (2018).
- 13 Chen, M.H. *et al.* Tissue concentrations of four Taiwanese toothed cetaceans indicating the silver and cadmium pollution in the western Pacific Ocean. *Marine Pollution Bulletin*. **124** (2), 993-1000 (2017).
- 14 Li, W.T. *et al.* Immunotoxicity of silver nanoparticles (AgNPs) on the leukocytes of common bottlenose dolphins (*Tursiops truncatus*). *Scientific Reports*. “In Press” (2018).
- 15 Bornhorst, J.A., Hunt, J.W., Urry, F.M., McMillin, G.A. Comparison of sample preservation methods for clinical trace element analysis by inductively coupled plasma mass spectrometry. *American Journal of Clinical Pathology*. **123** (4), 578-583 (2005).
- 16 Bonta, M., Torok, S., Hegedus, B., Dome, B., Limbeck, A. A comparison of sample preparation strategies for biological tissues and subsequent trace element analysis using LA-ICP-MS. *Analytical and Bioanalytical Chemistry*. **409** (7), 1805-1814 (2017).
- 17 Bischoff, K., Lamm, C., Erb, H.N., Hillebrandt, J.R. The effects of formalin fixation and tissue embedding of bovine liver on copper, iron, and zinc analysis. *Journal of Veterinary Diagnostic Investigation*. **20** (2), 220-224 (2008).
- 18 Miller, D.L., Yu, I.J., Genter, M.B. Use of Autometallography in Studies of Nanosilver Distribution and Toxicity. *International Journal of Toxicology*. **35** (1), 47-51 (2016).
- 19 Anderson, D.S. *et al.* Influence of particle size on persistence and clearance of aerosolized silver nanoparticles in the rat lung. *Toxicological Sciences*. **144** (2), 366-381 (2015).
- 20 Kim, W.Y., Kim, J., Park, J.D., Ryu, H.Y., Yu, I.J. Histological study of gender differences in accumulation of silver nanoparticles in kidneys of Fischer 344 rats. *Journal of Toxicology and Environmental Health, Part A*. **72** (21-22), 1279-1284 (2009).
- 21 Danscher, G. Applications of autometallography to heavy metal toxicology. *Pharmacology Toxicology*. **68** (6), 414-423 (1991).
- 22 Deroulers, C. *et al.* Analyzing huge pathology images with open source software. *Diagnostic Pathology*. **8**, 92 (2013).

- 
- 23 Shu, J., Dolman, G.E., Duan, J., Qiu, G., Ilyas, M. Statistical colour models: an automated digital image analysis method for quantification of histological biomarkers. *BioMedical Engineering Online*. **15**, 46 (2016).
- 24 Geraci, J.R., Lounsbury, V.J. Specimen and data collection. *Marine mammals ashore: a field guide for strandings*. National Aquarium. Baltimore. 167-230 (2005)
- 25 Shih, C.-C., Liu, L.-L., Chen, M.-H., Wang, W.-H. Investigation of heavy metal bioaccumulation in dolphins from the coastal waters off Taiwan. National Sun Yat-sen University. Kaohsiung (2001).
- 26 Liang, C.S. *et al.* The relationship between the striatal dopamine transporter and novelty seeking and cognitive flexibility in opioid dependence. *Progress in Neuro-Psychopharmacology and Biological Psychiatry*. **74**, 36-42 (2017).
- 27 Spiess, A.N., Neumeyer, N. An evaluation of R^2 as an inadequate measure for nonlinear models in pharmacological and biochemical research: a Monte Carlo approach. *BMC Pharmacology*. **10**, 6 (2010).
- 28 Stoltenberg, M., Danscher, G. Histochemical differentiation of autometallographically traceable metals (Au, Ag, Hg, Bi, Zn): protocols for chemical removal of separate autometallographic metal clusters in Epon sections. *Histochemical Journal*. **32** (11), 645-652 (2000).
- 29 Dimitriadis, V.K., Domouhtsidou, G.P., Raftopoulou, E. Localization of Hg and Pb in the palps, the digestive gland and the gills in *Mytilus galloprovincialis* (L.) using autometallography and X-ray microanalysis. *Environmental Pollution*. **125** (3), 345-353 (2003).
- 30 Loumbourdis, N.S., Danscher, G. Autometallographic tracing of mercury in frog liver. *Environmental Pollution*. **129** (2), 299-304 (2004).
- 31 Stoltenberg, M., Larsen, A., Kemp, K., Bloch, D., Weihe, P. Autometallographic tracing of mercury in pilot whale tissues in the Faroe Islands. *International Journal of Circumpolar Health*. **62** (2), 182-189 (2003).

**Chapter III: Investigation of Silver (Ag) Deposition in Tissues
from Stranded Cetaceans by Autometallography (AMG)
Environmental Pollution, 2018, 235: 534-545**



Wen-Ta Li^a, Hui-Wen Chang^a, Meng-Hsien Chen^b, Hue-Ying Chiou^c, Bang Yeh Liou^a,
Victor Fei Pang^a, Wei-Cheng Yang^{d*} and Chian-Ren Jeng^{a*}

^aGraduate Institute of Molecular and Comparative Pathobiology, National Taiwan University, Taipei, Taiwan; ^bDepartment of Oceanography and Asia-Pacific Ocean Research Center, National Sun Yat-sen University, Kaohsiung, Taiwan; ^cGraduate Institute of Veterinary Pathobiology, National Chung Hsing University, Taichung, Taiwan; ^dCollege of Veterinary Medicine, National Chiayi University, Chiayi, Taiwan

*Correspondence: Wei-Cheng Yang. Email: jackywc@gmail.com; Chian-Ren Jeng.
Email: crjeng@ntu.edu.tw



Investigation of silver (Ag) deposition in tissues from stranded cetaceans by autometallography (AMG)[☆]

Wen-Ta Li^a, Hui-Wen Chang^a, Meng-Hsien Chen^b, Hue-Ying Chiou^c, Bang-Yeh Liou^a, Victor Fei Pang^a, Wei-Cheng Yang^{d, **}, Chian-Ren Jeng^{a, *}

^a Graduate Institute of Molecular and Comparative Pathobiology, National Taiwan University, Taipei, Taiwan, ROC

^b Department of Oceanography and Asia-Pacific Ocean Research Center, National Sun Yat-sen University, Kaohsiung, Taiwan, ROC

^c Graduate Institute of Veterinary Pathobiology, National Chung Hsing University, Taichung, Taiwan, ROC

^d College of Veterinary Medicine, National Chiayi University, Chiayi, Taiwan, ROC



ARTICLE INFO

Article history:

Received 28 October 2017

Received in revised form

2 January 2018

Accepted 4 January 2018

Keywords:

Autometallography

Cetacean

Inductively coupled plasma mass spectrometry (ICP-MS)

Silver (Ag)

ABSTRACT

Silver, such as silver nanoparticles (AgNPs), has been widely used in commercial products and may be released into the environment. The interaction between Ag deposition and biological systems is raising serious concerns because of one health consideration. Cetaceans, as the top predators of the oceans, may be exposed to Ag/Ag compounds and suffer negative health impacts from the deposition of these compounds in their bodies. In the present study, we utilized autometallography (AMG) to localize the Ag in the liver and kidney tissues of cetaceans and developed a model called the cetacean histological Ag assay (CHAA) to estimate the Ag concentrations in the liver and kidney tissues of cetaceans. Our results revealed that Ag was mainly located in hepatocytes, Kupffer cells and the epithelial cells of some proximal renal tubules. The tissue pattern of Ag/Ag compounds deposition in cetaceans was different from those in previous studies conducted on laboratory rats. This difference may suggest that cetaceans have a different metabolic profile of Ag, so a presumptive metabolic pathway of Ag in cetaceans is advanced. Furthermore, our results suggest that the Ag contamination in cetaceans living in the North-western Pacific Ocean is more severe than that in cetaceans living in other marine regions of the world. The level of Ag deposition in cetaceans living in the former area may have caused negative impacts on their health condition. Further investigations are warranted to study the systemic Ag distribution, the cause of death/stranding, and the infectious diseases in stranded cetaceans with different Ag concentrations for comprehensively evaluating the negative health effects caused by Ag in cetaceans.

© 2018 Elsevier Ltd. All rights reserved.

1. Introduction

Commercial products containing silver (Ag) have been used for over 100 years, and awareness of Ag contamination in the environment has markedly increased due to the extensive use of silver nanoparticles (AgNPs) (Nowack et al., 2011). AgNPs have been used in numerous commercial products, such as water filters, textiles, cosmetics, food packaging and medical items, mainly due to their strong antimicrobial properties (Yu et al., 2013). AgNPs also have unique physicochemical properties, such as high electrical and

thermal conductivities, so they are increasingly applied in electronic devices and medical imaging (Ajmal et al., 2016; Ge et al., 2014). The production of AgNPs and the number of AgNP-containing products has dramatically increased in the last decade and is expected to increase over time (Hansen et al., 2016; Vance et al., 2015). AgNPs can be released during the production, transport, erosion, washing, and/or disposal of AgNP-containing products, subsequently draining into the aquatic environment and ultimately accumulating in the ocean (Farre et al., 2009; Walters et al., 2014). The fate of AgNPs in the aquatic environment is complicated and variable. Previous studies indicated that AgNPs in the aquatic environment can remain as individual particles in suspension, aggregate, dissolve, react with different species in the environment, or be regenerated from silver ions (Levard et al., 2012; Massarsky et al., 2014). Furthermore, different types of Ag speciation, such as AgCl, Ag₂S, and Ag₀, can be found in marine

[☆] This paper has been recommended for acceptance by Maria Cristina Fossi.

* Corresponding author.

** Corresponding author.

E-mail addresses: jackywc@gmail.com (W.-C. Yang), crjeng@ntu.edu.tw (C.-R. Jeng).

sediments contaminated with AgNPs, where they are ingested by benthic organisms and subsequently enter the food chain in marine environments (Wang et al., 2014). The increasing use and growing production of AgNPs, as potential sources of Ag contamination, raise public concern about the environmental toxicity of Ag.

Ag can be transferred from one trophic level to the next via the food chain and may cause negative effects on the animals at higher trophic levels, such as cetaceans (Buffet et al., 2014; Farre et al., 2009; Wang et al., 2014), and cetaceans have been thought to suffer potentially detrimental impacts from excessive silver exposure (Chen et al., 2017). The Ag concentrations in cetaceans have been investigated by several studies in different countries, and their results have varied among different organs, age classes, animal species, and habitats (Dehn et al., 2006; Reed et al., 2015; Romero et al., 2017; Seixas et al., 2009). The levels of unhealthy and critically dangerous concentrations of Ag in small cetaceans of the North Pacific Ocean have been established, and the suggested threshold concentrations of Ag are 0.43 ± 0.28 and 0.08 ± 0.03 $\mu\text{g/g}$ dry weight for liver and kidney tissues, respectively (Chen et al., 2017). A recent study conducted in Taiwan found an extremely high Ag concentration (726.11 $\mu\text{g/g}$ dry weight) in the liver tissue of a stranded Fraser's dolphin (*Lagenodelphis hosei*), which implies that dolphins in the marine environment of the North-western Pacific Ocean may have severe Ag contamination (Chen et al., 2017). Cetaceans are longevous, and being at the highest trophic levels of marine ecosystem, and they share common food resources with humans. The bioaccumulation effect of anthropogenic contaminants in cetaceans may eventually occur in humans (Bossart, 2011). These reasons further support that cetaceans are ideal sentinel animals for evaluating the health of marine environments and humans. Hence, it is crucial to determine the contamination status (e.g., tissue concentrations and distribution) of Ag in cetaceans.

Generally, the concentrations of trace metals in cetacean tissues are determined by inductively coupled plasma mass spectroscopy (ICP-MS) (Caceres-Saez et al., 2013; Chen et al., 2017; Mendez-Fernandez et al., 2014; Romero et al., 2017). The advantages of using ICP-MS include the provision of quantitative data with favourable detection limits (0.01–0.1 $\mu\text{g/L}$), simple specimen preparation, and the capability of simultaneous measurement of several elements (Nuttall et al., 1995). However, ICP-MS still has some disadvantages. The capital cost for establishing the ICP-MS and sample storage (including instruments, electricity charges and consumables) are relatively high (Bornhorst et al., 2005; Nuttall et al., 1995). In addition, ICP-MS detects target contaminants only on the organ level, and not the histological location or cell level (Miller et al., 2016). The standard procedure of tissue samples collection from stranded cetacean for ICP-MS analysis usually requires a relatively large sized frozen tissue sample ($6 \times 6 \times 6$ cm, approximately 200 g) due to the possibility of contamination during sample collection in the field environment (Geraci and Lounsbury, 2005), and these frozen samples may not be easy to store in limited refrigeration space. Furthermore, complete sample collection from the stranded cetaceans were seriously limited by several factors including difficulties of logistics and shortage of manpower. Therefore, the samples can be collected are usually the formalin fixed samples. If a relatively rapid, easy to use and inexpensive methodology by using the formalin fixed samples is developed, it will facilitate investigation of the suborgan distribution and concentration of target contaminants in cetaceans.

Formalin-fixed, paraffin-embedded (FFPE) tissues can be a sample resource for molecular analysis (such as polymerase chain reaction) and metal measurements (Bischoff et al., 2008; Bonta et al., 2017; Kokkat et al., 2013; Tran et al., 2014). Bonta et al. (2017) found that the FFPE process caused severe alteration in the

suborgan distributions and concentrations of alkali and alkaline earth metals but led to lesser effects on those of transition metals. In addition, previous studies have indicated that heavy metals can be amplified in FFPE tissue sections by autometallography (AMG), which is a histochemical process, and thereby can be visualized under light microscopy (Anderson et al., 2015; Danscher, 1991; Kim et al., 2009; Miller et al., 2016). Although the AMG method may have a relatively low sensitivity (comparing to ICP-MS), difficulty to unveil a homogeneously diffused material, underestimation of the content in case of a great concentration of heavy metals in a narrowed surface, it is still a valuable method to study the suborgan distribution of heavy metals. Furthermore, AMG method may amplified a group of trace metals, including gold, silver, mercury, bismuth and zinc, and thus the results of AMG method may be interfered by other trace metals (Stoltenberg and Danscher, 2000). Therefore, the interpretation of AMG positivity signals in the tissue from wild animals (which are not an intentional and well-controlled exposure to a single product) should be incorporated with other specific methods to monitor the actual composition of heavy metals, such as ICP-MS (Stoltenberg and Danscher, 2000). The quantitative analysis of histological tissue sections with histochemical staining has been developed by the use of digital image analysis software, such as imageJ (Deroulers et al., 2013; Jensen, 2013; Parlee et al., 2014; Shu et al., 2016). The present study utilized the histochemical technique (autometallography; AMG) to localize Ag in cetacean tissues, investigated the histopathological lesions possibly caused by the Ag, and developed an assay to estimate the Ag concentration in the liver and kidney tissues of cetaceans by a regression model based on the data from image quantitative analysis and ICP-MS.

2. Materials and methods

2.1. Sample source

The research permit (104-071-SB-62) for the cetacean sample collection was provided by Council of Agriculture of Taiwan. From 1999 to 2016, liver and kidney tissues from 110 stranded cetaceans of 7 different species, including 22 *Feresa attenuata* (Fa), 5 *Grampus griseus* (Gg), 38 *Kogia* spp. (Ko), 13 *Lagenodelphis hosei* (Lh), 13 *Stenella attenuata* (Sa), 8 *Steno bredanensis* (Sb), and 11 *Tursiops truncatus* (Tt), were collected. A field number was given to each cetacean for individual identification. The liver and kidney tissues used in the present study were from freshly dead and moderately autolysed stranded cetaceans (Geraci and Lounsbury, 2005). Some liver and kidney tissues were collected from live stranded cetaceans after they died during rescue or rehabilitation efforts. Each individual was classified into 1 of 2 age classes (young or adult) by relative measures of age, such as body length, tooth wear, the presence of hair follicles on rostrum and lingual marginal papillae, skin colour, the status of reproductive organs, and/or fusion of cranial sutures (Hohn, 2009), since age determination by the growth layers of teeth was not done in all individuals. The biological characteristics of each cetacean species are summarized in Table 1.

In total, 220 formalin fixed tissue samples (110 from liver and 110 from kidney) were collected for subsequent histological analysis. Among these 110 stranded cetaceans, only 12 frozen tissue samples (6 from liver and 6 from kidney) were collected, put into zip-lock plastic bags, and stored at -20°C for determination of Ag concentrations by ICP-MS.

2.2. AMG reactivity of formalin-fixed tissues

The representative formalin-fixed tissues of liver and kidney

Table 1
Biological characteristics and estimated Ag concentrations (mean \pm SD, $\mu\text{g/g}$) in the liver and kidney tissues of *Feresa attenuata*, *Grampus griseus*, *Kogia* spp., *Lagenodelphis hosei*, *Stenella attenuata*, and *Steno bredanensis*, *Tursiops truncatus* from Taiwan. N: sample size; U: unknown sex.

	All species				<i>Feresa attenuata</i>				<i>Grampus griseus</i>				<i>Kogia</i> spp.							
	N	Liver		Kidney		N	Liver		Kidney		N	Liver		Kidney		N	Liver		Kidney	
		Mean	SD	Mean	SD		Mean	SD	Mean	SD		Mean	SD	Mean	SD		Mean	SD	Mean	SD
All	110	10.49	6.48	0.50	0.45	22	12.95	6.64	0.91	0.43	5	12.67	7.09	0.43	0.36	38	9.32	6.08	0.38	0.36
Adult	84	12.82	5.32	0.63	0.43	19	14.74	5.17	1.04	0.28	4	15.14	5.13	0.54	0.32	28	11.61	5.36	0.49	0.35
Young	26	2.97	3.42	0.08	0.10	3	1.68	1.51	0.07	0.06	1	2.79	–	0.02	–	10	2.92	1.96	0.08	0.14
Female	36	9.55	5.69	0.58	0.51	8	12.43	6.05	0.96	0.43	1	12.03	–	0.35	–	12	8.53	6.04	0.50	0.52
Male	59	10.88	7.05	0.41	0.38	7	11.94	8.82	0.76	0.55	3	11.64	9.58	0.27	0.22	25	9.74	6.30	0.32	0.25
U	15	11.24	6.03	0.70	0.48	7	14.56	5.42	0.99	0.29	1	16.37	–	1.01	–	1	8.43	–	0.54	–

	<i>Lagenodelphis hosei</i>				<i>Stenella attenuata</i>				<i>Steno bredanensis</i>				<i>Tursiops truncatus</i>							
	N	Liver		Kidney		N	Liver		Kidney		N	Liver		Kidney		N	Liver		Kidney	
		Mean	SD	Mean	SD		Mean	SD	Mean	SD		Mean	SD	Mean	SD		Mean	SD	Mean	SD
All	13	6.96	6.87	0.44	0.46	13	12.65	6.28	0.63	0.44	8	11.89	6.13	0.14	0.13	11	9.27	5.60	0.33	0.42
Adult	6	13.43	4.32	0.85	0.35	10	13.62	6.15	0.77	0.40	7	13.42	4.67	0.16	0.12	10	10.11	5.11	0.36	0.43
Young	7	1.41	0.99	0.08	0.07	3	9.43	6.76	0.18	0.06	1	1.15	–	0.01	–	1	0.83	–	0.01	–
Male	4	8.69	5.51	0.56	0.42	3	5.85	3.59	0.67	0.46	4	9.57	6.45	0.09	0.08	4	9.86	5.85	0.53	0.69
Female	8	6.75	7.88	0.42	0.52	8	15.51	5.83	0.58	0.42	4	14.21	5.64	0.19	0.15	4	11.29	6.28	0.28	0.07
U	1	1.66	–	0.09	–	2	11.43	1.08	0.78	0.76	0	–	–	–	–	3	5.77	4.36	0.12	0.10

from each individual were selected (random or the regions with significant lesions), trimmed, dehydrated through a series of graded ethanol, and then infiltrated with paraffin. The FFPE tissues were sectioned at 5 μm , deparaffinised with xylene, treated with 0.5% Triton X-100 in phosphate-buffered saline (PBS), and washed several times with PBS and double-distilled water. The tissue sections were stained by silver enhancement method (Kim et al., 2009; Miller et al., 2016) and counterstained with hematoxylin for 10 s. The tissue sections were air dried, mounted with Canada balsam, and examined under a light microscope (Nikon ECLIPSE Ni-U, Nikon Corporation, Japan). The AMG positive signals were golden yellow to black dots or amorphous golden yellow substances. Images were captured using a Nikon ECLIPSE Ni-U microscope connected to a digital camera (Nikon DS-Fi2, Nikon Corporation) and computer imaging software (NIS-Elements D, Nikon Corporation). Ten histological images were randomly captured with a 40X objective lens from each tissue section and used in semi-quantitative analysis.

2.3. Semi-quantitative analysis for AMG positivity of histological images

Semi-quantitative analysis on these histological images was performed using ImageJ (National Institutes of Health, Bethesda, MD). Briefly, the histological images were split into three colour channels (red, blue, and green), and the blue channel was used for quantifying the AMG positive signals. The cut-off values of the threshold levels for each histological image were manually adjusted (from 90 to 110) due to the presence of false positive areas in nuclei and/or red blood cells, and the positive percent area of each histological image was displayed in the “Result” window. The positive percent areas of 10 histological images from each tissue section were averaged and defined as the AMG positivity value for each tissue section. However, the distribution pattern of the AMG positive signals (such as high concentration of AMG positive signals in a single region rather than a homogenous ground of AMG positive signals in the whole section) may affect the results of semi-quantitative analysis, the reliability of the semi-quantitative analysis should be seriously evaluated with the pattern of the AMG positive signals.

2.4. The correlation between the results of ICP-MS and AMG positivity values

The Ag concentrations of the liver and kidney tissues were determined using ICP-MS according to previously published methods (Chen et al., 2002, 2017). In total, 6 liver and 6 kidney tissues from 6 cetaceans, including 2 Ko, 1 Gg, 2 Lh, and 1 Sa, were investigated. Data from the liver and kidney tissues were analysed separately. The strength of association between the results of ICP-MS and AMG positivity values from the same liver and kidney tissues were analysed by Pearson correlation analysis.

2.5. Establishment of the Cetacean Histological Ag Assay (CHAA)

The Ag concentrations of the liver and kidney tissues with unknown Ag concentrations were estimated by regression models based on AMG positivity values from cetacean tissues with known Ag concentration, hereafter referred to as the Cetacean Histological Ag Assay (CHAA) for livers and kidneys. The flowchart of the strategy to estimate the concentration of Ag by AMG through CHAA was illustrated (Fig. 1). The regression models were compared using the extra sum-of-squares F test and Akaike's information criterion (AIC) (Liang et al., 2017; Spiess and Neumeier, 2010). Most importantly, the selected model had to generate scientifically valid results. For instance, if one of the regression models estimated unrealistic Ag concentrations, the regression model was abandoned. The effect size for the selected regression model was reported by adjusted R^2 .

The accuracy of the CHAA for livers and kidneys was evaluated by the mean standard deviation (SD) calculated from differences between known and estimated Ag concentrations (Polanowski et al., 2014). The precision of the semi-quantitative analysis by ImageJ in the liver and kidney tissues of cetaceans was evaluated by repeated measurement of AMG positivity values of serial sections from the same FFPE tissues. Three liver and 3 kidney tissues with known Ag concentrations of 0.06, 14.93, 21.82, 0.05, 1.04 and 0.42 $\mu\text{g/g}$ were analysed 3 times each. The mean SDs for 9 measurements from liver and kidney tissues were calculated from differences between known and estimated Ag concentrations and used to evaluate the precision of the semi-quantitative analysis for AMG positivity (Polanowski et al., 2014).

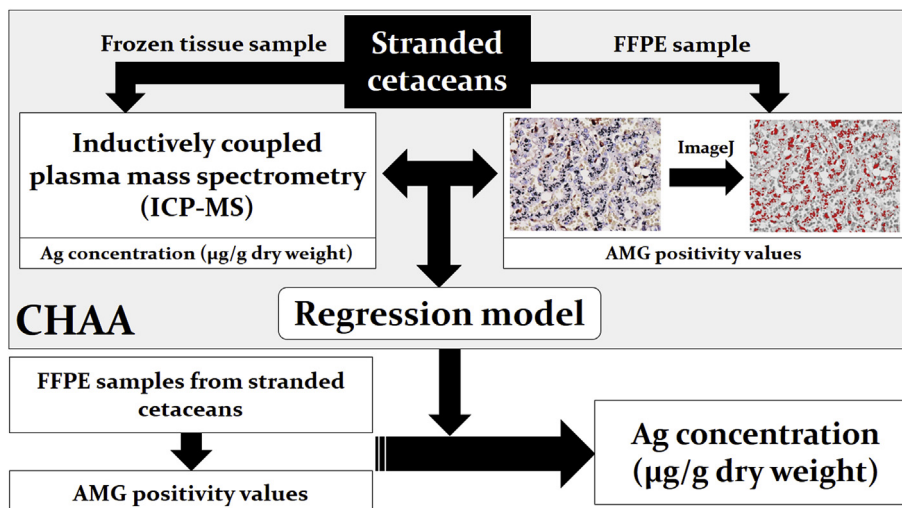


Fig. 1. Flowchart of the strategy to estimate the concentration of Ag by autometallography (AMG) through cetacean histological Ag assay (CHAA).

2.6. Estimation of Ag concentrations in FFPE tissue sections

The Ag concentrations of the liver and kidney tissues of cetaceans not investigated by ICP-MS were estimated by CHAA. The estimated Ag concentrations of liver and kidney tissues were first checked by D'Agostino-Pearson normality test, and the data were not normally distributed. Therefore, the Kruskal-Wallis Test (post hoc test: Dunn's multiple comparison test) and Mann-Whitney *U* test were used for further analysis. Three parameters—age class, sexuality, and species—were analysed. All data were plotted on box-plot graphics. The bar in the middle of the box represented the second quartile (median), and the bottom and top of the box described the first and third quartiles. The whiskers showed the 75th percentile plus 1.5 times IQR and 25th percentile minus 1.5 times IQR of all data, and any values greater than these were defined as outliers and plotted as individual points. Different letters above the boxplots indicated statistically significant differences ($p < .05$) between groups. The baseline and unhealthy Ag concentrations in the liver tissue were defined as 0.43 µg/g and 4.45 µg/g, respectively; the baseline and unhealthy Ag concentrations in the kidney tissues were defined as 0.08 µg/g and 0.33 µg/g, respectively (Chen et al., 2017).

2.7. Histopathological findings in liver and kidney tissues with different estimated silver concentrations

The FFPE samples were sectioned at 5 µm and stained with hematoxylin and eosin (H&E) for histopathological examination. The slides were comprehensively examined in a blinded fashion by a single veterinary pathologist (Wen-Ta Li), and the lesions in liver and kidney were recorded and categorized. The direct correlation between the lesions and Ag was evaluated by the intralesional aggregates of AMG positive signals. The correlation between the lesions (presented or unrepresented) and estimated Ag concentrations were analysed by Chi-square test or Fisher exact test. The liver tissues with estimated Ag concentrations ≤ 0.43 , 0.43–4.45, and ≥ 4.45 µg/g were respectively classified into baseline, intermediate, and unhealthy groups; the kidney tissues with estimated Ag concentrations ≤ 0.08 , 0.08–0.33, and ≥ 0.33 µg/g were respectively classified into baseline, intermediate, and unhealthy groups.

3. Results

3.1. Patterns of AMG positive signals in the liver and kidney tissues

Different patterns of AMG positive signals were detected in the liver and kidney tissues of cetaceans. Because the AMG positive signals may be interfered by other heavy metals, the liver and kidney tissues with Ag concentrations higher than baselines measured by ICP-MS were used as the positive group to demonstrate the Ag distribution. In the livers of positive group (5 individuals, Table 2), the AMG positive signals were diffusely/evenly distributed in hepatic parenchyma and were variably sized brown to black dots in hepatocytes and Kupffer cells (Fig. 2A and B). In the kidneys of positive group (3 individuals, Table 2), the AMG positive signals were variably-sized brown to black dots and unevenly distributed in the epithelial cells of some proximal renal tubules in the renal cortex (Fig. 2C and D). Golden-yellow to brown AMG positive signals in the basement membranes of renal tubules and glomeruli and amorphous golden-yellow to brown AMG positive signals on the surface of epithelial cells of proximal renal tubules were found in one individual (*Lagenodelphis hosei*; field code: TP20110830) (Fig. 2E). In contrast, absent to minimal AMG positive signals (the majority being brown to black dots) were noted in the livers (Fig. 2F) and kidneys (Fig. 2G) of individuals with Ag concentrations lower than baselines (Table 2).

Table 2

The results of ICP-MS and AMG positivity values from six cetaceans. Gg = *Grampus griseus*, Ko = *Kogia* spp., Lh = *Lagenodelphis hosei*, Sa = *Stenella attenuata*, M = Male, F = Female, AMG = AMG positivity values quantified by imageJ, ICP-MS = Ag concentrations measured by ICP-MS (µg/g, dry weight).

Field number	Species	Sex	Age class	Liver		Kidney	
				AMG	ICP-MS	AMG	ICP-MS
TP20111116	Gg	M	Adult	7.48	21.82	8.82	0.42
TC20110611	Ko	M	Adult	4.50	2.77	1.52	0.05
TC20110722	Ko	M	Young	1.20	3.86	0.11	0.05
TD20110608	Lh	M	Young	0.34	0.06	0.21	0.05
TP20110830	Lh	M	Adult	6.21	14.93	9.43	1.04
IL20110101	Sa	F	Young	2.67	1.73	5.26	0.14

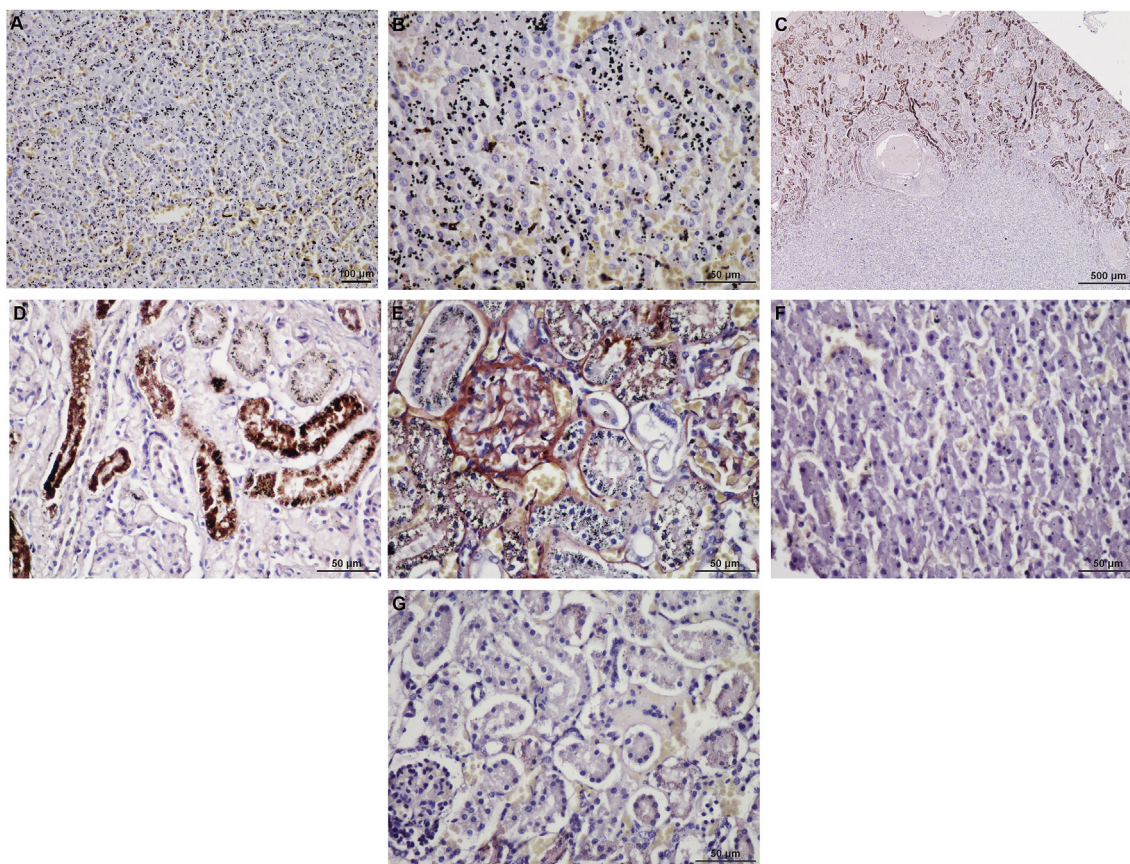


Fig. 2. Representative photographs of the Autometallography (AMG) positive signals in the liver and kidney tissues of cetacean. Silver enhancement method with hematoxylin as counterstain. (A) The AMG positive signals in the liver with a higher Ag concentration (14.93 µg/g) are diffusely and evenly distributed in the hepatic parenchyma (*Lagenodelphis hosei* (Lh); field code: TP20110830). (B) Higher magnification of Fig. 1A. The AMG positive signals are variably sized brown to black dots in hepatocytes and Kupffer cells. (C) The AMG positive signals in the kidney with a higher Ag concentration (1.04 µg/g) are unevenly distributed in the renal cortex (Lh; field code: TP20110830). (D) Higher magnification of Fig. 1C. The AMG positive signals are variably sized brown to black dots in the epithelial cells of proximal renal tubules. (E) Golden-yellow to brown AMG positive signals on the basement membranes of renal tubules and glomeruli and amorphous golden-yellow to brown AMG positive signals on the surface of epithelial cells of proximal renal tubules are occasionally found in the kidney tissue of one individual (Lh; field code: TP20110830). (F) Scattered AMG positive signals of brown to black dots are observed in the liver with a lower Ag concentration (0.06 µg/g) (Lh; field code: TD20110608) (G) Scattered AMG positive signals of brown to black dots are observed in the liver with a lower Ag concentration (0.05 µg/g) (Lh; field code: TD20110608). (For interpretation of the references to colour in this figure legend, the reader is referred to the Web version of this article.)

3.2. Establishment of the Cetacean Histological Ag Assay (CHAA)

The results of ICP-MS and AMG positivity values in the six stranded cetaceans are summarized in Table 2. Significant positive correlations between the results of ICP-MS and AMG positivity values were found in the liver (Pearson's $r = 0.88$; $p = .0204$) and kidney (Pearson's $r = 0.83$; $p = .0393$) tissues. The regression models to establish the CHAA for livers and kidneys, including linear regression, quadratic regression, cubic regression and linear regression through origin, were statistically compared, and linear regression through origin was the preferred regression model for the CHAA (Table 3). The regression equations of the CHAA for livers and kidneys were respectively $Y = 2.249 \times X$ (adjusted $R^2 = 0.74$) and $Y = 0.07288 \times X$ (adjusted $R^2 = 0.69$) (Fig. 3A and B). The mean standard deviations from six FFPE tissue sections with known Ag concentrations to evaluate the accuracy of the CHAA were 3.24 and 0.16 for livers and kidneys, respectively. In addition, the mean standard deviations of three repeated measurements of the same FFPE tissue sections with known Ag concentrations to evaluate the consistency of CHAA were 2.8 and 0.35 for livers and kidneys, respectively.

3.3. Estimation of Ag concentrations of the liver and kidney tissues by CHAA

The estimated Ag concentrations presented as mean \pm SD of each cetacean species are summarized in Table 1. The ranges of estimated Ag concentrations were 0.06–28.39 and 0–1.6 µg/g in the liver and kidney tissues, respectively. There was a significant age-dependent increase of Ag concentration in the liver (12.82 ± 5.3 and 3.0 ± 3.4 µg/g) and kidney (0.63 ± 0.43 and 0.08 ± 0.10 µg/g) tissues (Fig. 4A), and the Ag concentrations of liver tissues (10.49 ± 6.48 µg/g) were significantly higher than those of kidney tissues (0.50 ± 0.45 µg/g) (Fig. 4B). No significant difference in Ag concentrations between sexes in the liver and kidney tissues was observed (Fig. 4C), nor was a significant difference in Ag concentrations in the liver tissues found among these cetacean species. In approximately 50% of the individuals, the estimated Ag concentrations of the liver tissues were higher than the unhealthy Ag concentration (Fig. 4D). The Ag concentrations in the kidney tissues of Fa (0.93 ± 0.45 µg/g) were significant higher than those of Ko (0.38 ± 0.37 µg/g), Tt (0.32 ± 0.45 µg/g) and Sb (0.12 ± 0.13 µg/g). In approximately 30% of the individuals, the estimated Ag

Table 3

The comparisons among different regression models to establish the Cetacean Histology Ag Assay (CHAA) for liver and kidney tissues of cetaceans by the extra sum-of-squares F test and Akaike's information criterion (AIC).

	Extra sum-of-squares F test					
	CHAA for liver			CHAA for kidney		
Null hypothesis	Linear regression through origin			Linear regression through origin		
Alternative hypothesis	Linear	Quadratic	Cubic	Linear	Quadratic	Cubic
P value	0.4644	0.1065	0.2621	0.8201	0.354	0.4559
Conclusion ($\alpha = 0.05$)	Not reject	Not reject	Not reject	Not reject	Not reject	Not reject
Preferred model	Linear regression through origin			Linear regression through origin		
F (DFn, DFd)	0.6529 (1,4)	5.174 (2,3)	2.969 (3,2)	0.05895 (1,4)	1.497 (2,3)	1.332 (3,2)
	AIC					
	CHAA for liver			CHAA for kidney		
Simpler model	Linear regression through origin			Linear regression through origin		
Probability it is correct	98.95%	>99.99%	N.A.	99.30%	>99.99%	N.A.
Alternative model	Linear	Quadratic	Cubic ^a	Linear	Quadratic	Cubic ^a
Probability it is correct	1.05%	<0.01%	N.A.	0.70%	<0.01%	N.A.
Ratio of probabilities	94.29		N.A.	142.04		N.A.
Preferred model	Linear regression through origin			Linear regression through origin		
Difference in corrected AIC	-9.093	-31.04	N.A.	-9.912	-35.85	N.A.

^a Cannot be calculated due to too few points.

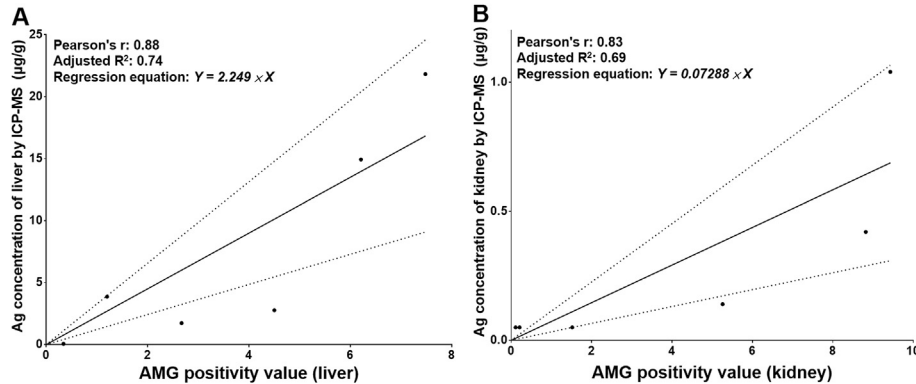


Fig. 3. Linear regression through origin for estimated Ag concentrations in the (A) liver and (B) kidney of 6 cetaceans (2 *Kogia* spp., 1 *Grampus griseus*, 2 *Lagenodelphis hosei* and 1 *Stenella attenuata*) with known Ag concentrations from autometallography positivity values. 95% confidence bands of the best-fit line of the regression line are shown as a dotted line.

concentrations of the kidney tissues were higher than the un-healthy Ag concentration (Fig. 4E).

3.4. Histopathological findings in liver and kidney tissues with different estimated silver concentrations

A variety of lesions were observed in the liver and kidney tissues of stranded cetaceans. The lesions found in liver tissues included hyaline inclusion (n = 58), non-specific reactive hepatitis (n = 51), severe congestion (n = 38), vacuolar degeneration (n = 37), multifocal necrosis (n = 2), extramedullary hematopoiesis (n = 2), periportal fibrosis (n = 2), and fibrotic nodule (n = 1). On the other hand, vacuolar degeneration of the proximal renal tubular epithelium (n = 10), hyaline droplets in the proximal renal tubular epithelium (n = 9), interstitial nephritis (n = 3), glomerulonephropathy (n = 2), interstitial fibrosis (n = 2), pyelonephritis (n = 2), suppurative nephritis (n = 1) were found in the kidney tissues. However, no lesions with marked intralésional aggregates of AMG positive signals were observed. The lesions with >3 frequencies (n > 3) were used in the correlation analysis, but there was no statistically significant correlation between these lesions and Ag concentrations. The frequencies and percentages of lesions presented in the liver and kidney tissues with baseline, intermediate

and high Ag concentrations were summarized in Table 5.

4. Discussion

After intravenous injection of dextrin-silver colloid in laboratory rats, Ag was largely distributed in the spleen, liver and bone marrow, but the exact location of Ag deposition on the suborgan and cell levels was still undetermined (Gammill et al., 1950). Afterward, the technique of AMG for visualizing the metal elements with light and electron microscopy was described in 1981, and that technique has been improved with specific procedures over the years to detect different trace metals in various tissues of humans and animals (Dimitriadis et al., 2003; Loumbourdis and Danscher, 2004; Miller et al., 2016; Stoltenberg et al., 2003; Zarnescu et al., 2017; Zhu et al., 2012). The use of AMG to detect Ag in Wistar rats with intraperitoneal injection of silver lactate demonstrated the suborgan and cell level distributions of Ag, including 1) lysosomes of proximal renal tubular epithelium, mesangial cells, hepatocytes, macrophages (such as Kupffer cells and glial cells) and motor neurons; 2) basal lamina (a portion of basement membrane) of glomeruli, renal tubules, epidermis, and mucosal epithelium of tongue; 3) interstitium of renal papilla; 4) pheochromocytes of adrenal glands (Danscher, 1981). The AMG positive signals in F334

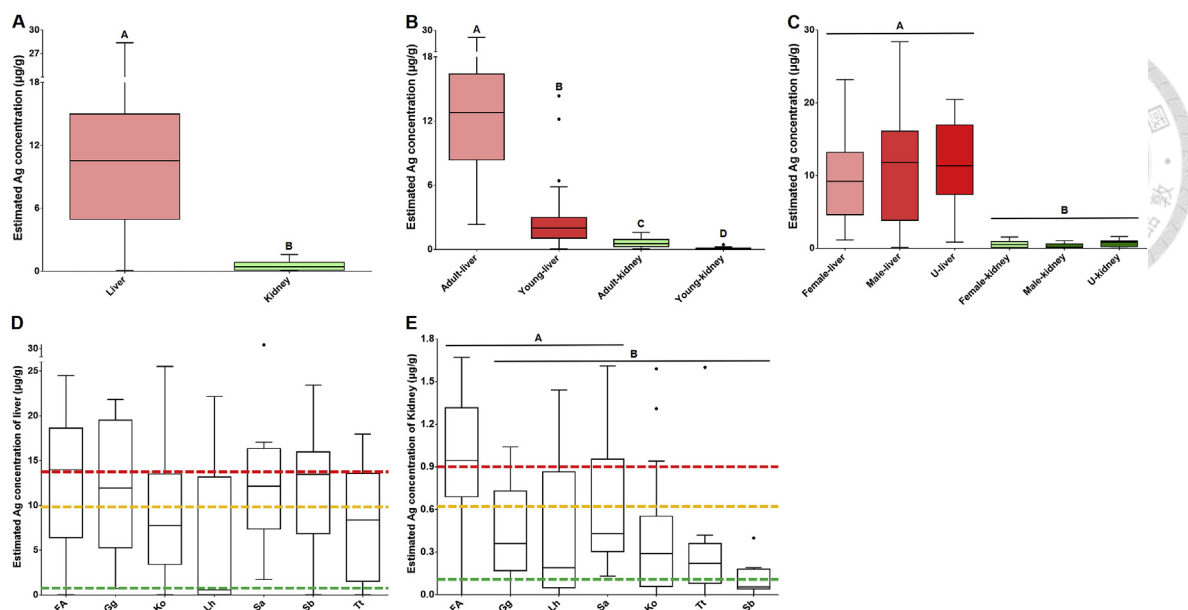


Fig. 4. Ag concentrations of cetacean tissues divided by different parameters, including (A) sample type (livers and kidneys), (B) age classes and sample type, (C) sex and sample type, (D) and (E) species and sample types. Fa = *Feresa attenuata*, Gg = *Grampus griseus*, Ko = *Kogia* spp., Lh = *Lagenodelphis hosei*, Sa = *Stenella attenuata*, Sb = *Steno bredanensis*, Tt = *Tursiops truncatus*. The bar in the middle of the box represents the median, and the bottom and top of the box describe the first and third quartiles. The whiskers show the 75th percentile plus 1.5 times IQR and 25th percentile minus 1.5 times IQR of all data, and any values greater than these are defined as outliers and plotted as individual points. Significant differences between groups at $p < .05$, Mann-Whitney *U* test (Fig. 3A) or Kruskal-Wallis Test (Fig. 3B–E) are indicated by different letters. The green, yellow, and red dashed lines indicate the upper limits of the baseline, and unhealthy and critically dangerous concentrations of Ag in the liver and kidney tissues of cetaceans. (For interpretation of the references to colour in this figure legend, the reader is referred to the Web version of this article.)

rats with oral administration of AgNPs (60 nm in diameter) were golden-yellow to brown positive signals and mainly located in the basement membranes of renal tubules, glomeruli, and transitional epithelium of the urinary bladder (Kim et al., 2009). A previous study also demonstrated that AMG positive signals (black dots) were observed in alveolar macrophages, ependymal cells, the choroid plexus, and the perivascular regions of the lung and renal cortex in laboratory rats after intranasal exposure of AgNPs (18–19 nm in diameter) (Miller et al., 2016).

It is evident that Ag can bind to metallothionein (MT), selenium (Se) and high-molecular-weight substances (HMWS) in the livers of cetaceans and mainly accumulates in nuclear, lysosomal, and mitochondrial fractions, as shown by cell fractionation analysis (Ikemoto et al., 2004a, b; Kunito et al., 2004). In the present study, the AMG positive signals in the liver tissues of cetaceans were brown to black dots in hepatocytes and Kupffer cells, similar to the results of a previous study conducted in 1981 (Danscher, 1981). Therefore, it is presumed that Ag is conjugated with MT, Se and HMWS, and then mainly accumulates in lysosomes of hepatocytes of cetaceans. The AMG positivity signals in the kidney tissues of cetaceans were mainly located in the proximal renal tubules of the renal cortex. A previous study applied autofluorescent signals and immunohistochemistry to localize Ag-MT complexes in the kidneys of laboratory rats with intraperitoneal injection of silver lactate, and it was found that they were exclusively located in the proximal renal tubules of the renal cortex (Kurasaki et al., 2000). Previous studies have indicated that the proximal renal tubular epithelium of S1 and S2 segments have active endocytosis with abundant intracytoplasmic lysosomes, and heavy metals can be uptaken by tubular epithelium via endocytosis (Barbier et al., 2005; Cristofori et al., 2007). Therefore, our findings may suggest that Ag/Ag compounds in cetacean kidneys are reabsorbed by the proximal renal tubular epithelium.

Our study also found differences in the AMG positive signals as

compared to previous studies (Danscher, 1981; Kim et al., 2009). Since the basement membrane was considered the major location of Ag deposition after oral administration of AgNO₃ in laboratory rats (Boudreau et al., 2016; McGiven et al., 1977; Walker, 1972), it was surprising that the AMG positivity signals in the basement membrane of renal tubules and glomeruli were rarely found in kidney tissues of cetaceans. Although the mechanism of Ag deposition in the basement membrane is still largely unknown, it can be associated with the high affinity of Ag to the abundant negatively-charged sulfhydryl and/or disulfide groups in the basement membrane (Boudreau et al., 2016; Walker, 1971, 1972). Furthermore, in previous studies, AMG positivity signals were observed in the nucleus of the interstitial cells of the inner renal medulla (Kim et al., 2009), but not in our study. The above differences indicate that the metabolic profile of Ag in cetaceans is different from that in laboratory rats.

The underlying mechanisms that cause the different metabolic profile of Ag in cetaceans are still undetermined, but several possibilities should be considered. First, cetaceans may have different physiological characteristics, and the composition of the basement membrane in cetaceans could be different from those of laboratory rats or other animals. Second, cetaceans may be exposed to different types of Ag/Ag compounds, which could be quite different from the Ag/Ag compounds used in previous studies on laboratory animals. Third, cetaceans are exposed to varieties of contaminants; thus, the interactions between Ag/Ag compounds and other contaminants in cetaceans may also affect the process of Ag deposition. In addition, cetaceans may expose to Ag/Ag compounds at extremely low concentration and for relatively long period of time, which are different from laboratory animals and may affect the process of Ag deposition.

Based on the significantly higher concentrations and diffuse distribution patterns of Ag in the livers of these seven cetacean species, it is most likely that the liver is the main storage organ for

Table 4Silver (Ag) concentrations (mean \pm stand deviation, $\mu\text{g/g}$ dry wt.) of the liver and kidney tissues of cetaceans in various studies worldwide.

Location	Oceans	Time period	Species	Liver		Kidney		References
				N	Mean \pm SD	N	Mean \pm SD	
Alaska, US	Arctic	1989–1990	<i>Delphinapterus leucas</i>	14	86.44 \pm 83.63 ^a	–	–	(Becker et al., 1995)
Alaska, US	Arctic	1989–1990	<i>Globicephala melas</i>	8	0.53 \pm 0.36 ^a	–	–	(Becker et al., 2000)
Alaska, US	Arctic	1992–1999	<i>Delphinapterus leucas</i>	48	42.37 \pm 29.3 ^a	–	–	(Dehn et al., 2006; Woshner et al., 2001)
Alaska, US	Arctic	1983–2001	<i>Balaena mysticetus</i>	127	0.43 \pm 0.93 ^a	–	–	(Dehn et al., 2006; RJ et al., 1995; Woshner et al., 2001)
Alaska, US	Arctic	1983–2001	<i>Balaena mysticetus</i>	82	0.46 \pm 1.09 ^a	86	0.04 \pm 0.04 ^a	(Rosa et al., 2008)
Spain	North Atlantic	2004–2008	<i>Delphinus delphis</i>	100	0.69 \pm 0.69 ^a	98	<0.31 ^a	(Mendez-Fernandez et al., 2014)
Spain	North Atlantic	2004–2009	<i>Globicephala melas</i>	8	0.43 \pm 0.69 ^a	6	<0.31 ^a	(Mendez-Fernandez et al., 2014)
Spain	North Atlantic	2004–2010	<i>Phocoena phocoena</i>	14	3.44 \pm 3.5 ^a	12	<0.31 ^a	(Mendez-Fernandez et al., 2014)
Spain	North Atlantic	2004–2011	<i>Stenella coeruleoalba</i>	18	0.99 \pm 0.99 ^a	16	<0.31 ^a	(Mendez-Fernandez et al., 2014)
Spain	North Atlantic	2004–2012	<i>Tursiops truncatus</i>	8	0.66 \pm 0.63 ^a	6	<0.31 ^a	(Mendez-Fernandez et al., 2014)
Carolina, US	North Atlantic	1990–2011	<i>Kogia sima</i>	12	3.12 \pm 1.06 ^a	9	N.D.	(Reed et al., 2015)
Argentina	South Atlantic	2010–2011	<i>Cephalorhynchus commersonii</i>	7	5.4 \pm 5	6	1.2 \pm 2.7	(Caceres-Saez et al., 2013)
Brazil	South Atlantic	1997–2002	<i>Delphinus capensis</i>	1	2.71 ^a	–	–	(Kunito et al., 2004)
Brazil	South Atlantic	1997–2000	<i>Pontoporia blainvillei</i>	23	7.93 \pm 13.54 ^a	–	–	(Kunito et al., 2004)
Brazil	South Atlantic	1997–1999	<i>Sotalia guianensis</i>	20	6.28 \pm 4.29 ^a	–	–	(Kunito et al., 2004)
Brazil	South Atlantic	1997–2003	<i>Stenella coeruleoalba</i>	1	10.57 ^a	–	–	(Kunito et al., 2004)
Brazil	South Atlantic	1997–2001	<i>Stenella frontalis</i>	2	4.96 ^a	–	–	(Kunito et al., 2004)
Brazil	South Atlantic	N.A.	<i>Sotalia guianensis</i>	19	0.79 \pm 0.89	–	–	(Seixas et al., 2009)
Alaska, US	North Pacific	1992–1996	<i>Delphinapterus leucas</i>	6	22.4 \pm 13.78 ^a	–	–	(Becker et al., 2000)
Taiwan	North Pacific	1994–1995	<i>Grampus griseus</i>	2	0.46 \pm 0.12	–	–	(Chen et al., 2017)
Taiwan	North Pacific	2001–2012	<i>Grampus griseus</i>	12	5.87 \pm 10.80	12	0.19 \pm 0.22	(Chen et al., 2017)
Taiwan	North Pacific	2001–2012	<i>Kogia simus</i>	–	–	6	0.28 \pm 0.36	(Chen et al., 2017)
Taiwan	North Pacific	1994–1995	<i>Stenella attenuata</i>	4	0.42 \pm 0.16	–	–	(Chen et al., 2017)
Taiwan	North Pacific	2001–2012	<i>Stenella attenuata</i>	9	1.45 \pm 1.99	10	0.24 \pm 0.20	(Chen et al., 2017)
Russia	North Pacific	2001	<i>Eschrichtius robustus</i>	29	0.33 \pm 0.46 ^a	–	–	(Dehn et al., 2006)
Japan	North Pacific	1997–1998	<i>Phocoenoides dalli</i>	6	4.29 \pm 3.63	6	–	(Ikemoto et al., 2004a)
Russia	North Pacific	1994	<i>Eschrichtius robustus</i>	5	1.02 \pm 0.2 ^a	–	–	(Tilbury et al., 2002)
Taiwan	North Pacific	1999–2016	<i>Feresa attenuata</i>	22	12.95 \pm 6.64	22	0.91 \pm 0.43	This study
Taiwan	North Pacific	1999–2016	<i>Grampus griseus</i>	5	12.67 \pm 7.09	5	0.43 \pm 0.36	This study
Taiwan	North Pacific	1999–2016	<i>Kogia spp.</i>	38	9.32 \pm 6.08	38	0.38 \pm 0.36	This study
Taiwan	North Pacific	1999–2016	<i>Lagenodelphis hosei</i>	13	6.96 \pm 6.87	13	0.44 \pm 0.46	This study
Taiwan	North Pacific	1999–2016	<i>Stenella attenuata</i>	13	12.65 \pm 6.28	13	0.63 \pm 0.44	This study
Taiwan	North Pacific	1999–2016	<i>Steno bredanensis</i>	8	11.89 \pm 6.13	8	0.14 \pm 0.13	This study
Taiwan	North Pacific	1999–2016	<i>Tursiops truncatus</i>	11	9.27 \pm 5.6	11	0.33 \pm 0.42	This study
New Zealand	South Pacific	1999–2005	<i>Delphinus capensis</i>	3	2.65 \pm 0.99 ^a	3	0.15 \pm 0 ^a	(Stockin et al., 2007)

^a Wet weight basis concentration has been converted to dry weight basis concentration by assuming that moisture content was 69.73% for liver and 77.32 for kidney (Yang and Miyazaki, 2003).

Table 5

The lesions presented in the liver and kidney tissues of stranded cetaceans with high, intermediate and baseline Ag concentrations.

Lesions ^a	Ag concentration ^b	High N = 83	Intermediate N = 24	Baseline N = 3	Significance ^d
Liver ^e	Severe congestion	31 (42.5%)	7 (29.2%)	0 (0.0%)	NS
	Vacuolar degeneration of hepatocytes	29 (33.3%)	7 (29.2%)	1 (33.3%)	NS
	Non-specific reactive hepatitis	41 (47.1%)	10 (41.7%)	0 (0.0%)	NS
	Hyaline inclusions in hepatocytes	47 (54.0%)	9 (37.5%)	2 (66.7%)	NS
Lesions ^a	Ag concentration ^c	High N = 60	Intermediate N = 27	Baseline N = 23	Significance ^d
Kidney	Vacuolar degeneration of proximal renal tubular epithelium	5 (8.3%)	3 (11.1%)	2 (8.7%)	NS
	Hyaline droplets in the proximal renal tubular epithelium	11 (19.3%)	4 (14.8%)	4 (17.4%)	NS

^a The lesions with >3 frequencies ($n > 3$) were used in the correlation analysis.

^b The liver tissues with estimated Ag concentrations ≤ 0.43 , 0.43 – 4.45 , and ≥ 4.45 $\mu\text{g/g}$ were respectively classified into baseline, intermediate, and high group (Chen et al., 2017).

^c The kidney tissues with estimated Ag concentrations ≤ 0.08 , 0.08 – 0.33 , and ≥ 0.33 $\mu\text{g/g}$ were respectively classified into baseline, intermediate, and high groups (Chen et al., 2017).

^d p -value $< .05$ was considered statistically significant. NS = No significance.

^e Because the observed values were less than 5 in some cells of the contingency table, Fisher's exact test was used.

Ag/Ag compounds, but the kidneys may be a transit station for the metabolism of Ag/Ag compounds in cetaceans. Although the metabolism of Ag is still largely unknown in animals, a presumptive metabolic pathway of Ag in cetaceans is advanced based on our results and previous studies focused on heavy metals metabolism

(Fig. 5). It is presumed that Ag/Ag compounds can enter the cetacean body through food intake and then be delivered to the liver through the gastrointestinal tract and portal circulation (Loeschner et al., 2011; van der Zande et al., 2012). Previous studies found that Ag can bind to the Se and HMWS, and Se is a component of the

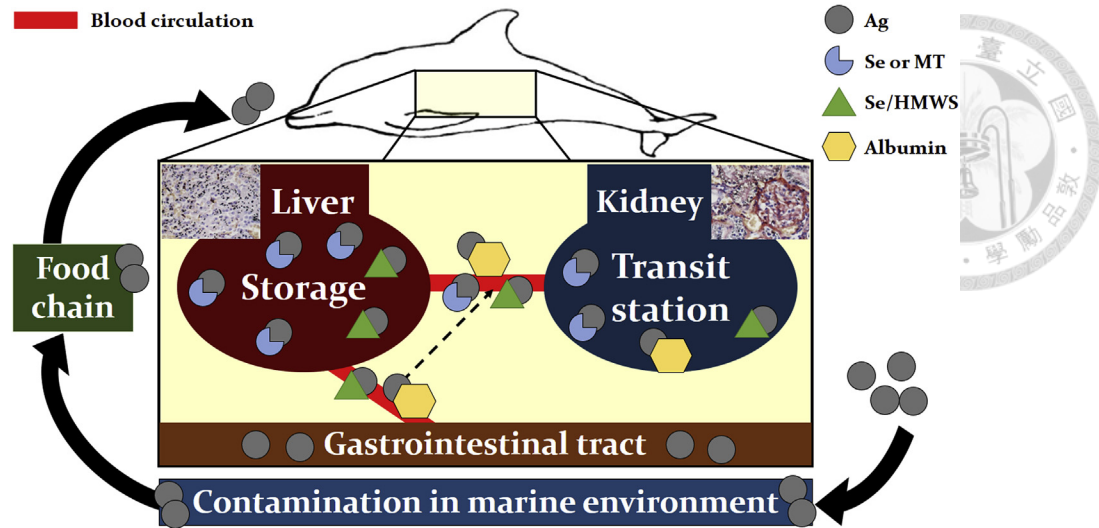


Fig. 5. Presumptive metabolic pathway of Ag in cetaceans. Se = selenium; MT = metallothionein; HMWS = high-molecular-weight substances.

HMWS in plasma protein (Ikemoto et al., 2004a; Naganuma and Imura, 1983; Yoneda and Suzuki, 1997a, b). Besides, previous studies also suggested that the heavy metals can bind rapidly to albumin in plasma (Barbier et al., 2005). Therefore, the Ag/Ag compounds during the portal circulation is considered to be conjugated with proteins, including Se, HMWS or albumin. Most of the Ag/Ag compounds with proteins (Se, HMWS or albumin) conjugation are uptaken by hepatocytes, degraded in lysosomes, released into the cytoplasm of hepatocytes, conjugated with MT, Se or HMWS, and stored in the lysosomes of hepatocytes (Ikemoto et al., 2004a, b; Kunito et al., 2004). Some of the Ag/Ag compounds with protein (Se, HMWS or albumin) conjugation may still remain in blood circulation, or those with MT, Se or HMWS conjugation in hepatocytes may be released into blood circulation during renewal of hepatocytes (Barbier et al., 2005; Loeschner et al., 2011; van der Zande et al., 2012). The Ag/Ag compounds in blood circulation can be subsequently delivered to multiple organs, such as the kidneys (Loeschner et al., 2011; van der Zande et al., 2012). In the kidneys, Ag/Ag compounds with MT, Se, HMWS or albumin conjugation can penetrate through the glomeruli and then be reabsorbed by proximal renal tubular epithelium (Barbier et al., 2005; Cristofori et al., 2007; Kurasaki et al., 2000).

The significant positive correlation between the results of ICP-MS and AMG positivity values suggests that the areas of AMG positivity signals can be a parameter for estimating the Ag concentration. Therefore, the CHAA was developed based on the AMG positivity values and regression model. Generally, a more complicated model with more parameters fits the data better than the simpler one (in other words, it has a relatively high adjusted R^2), but it is necessary to statistically evaluate whether the differences among these regression models are sufficient to justify a preference for the more complicated model. Hence, these regression models were compared statistically (Liang et al., 2017; Spiess and Neumeyer, 2010), and the results showed that linear regression through origin was preferred for the CHAA in both the livers and kidneys of cetaceans. The adjusted R^2 of the CHAA for livers (0.74) and kidneys (0.69) indicates that most of the response is attributed to Ag concentration, but some undetermined factors still influence the CHAA for the liver and kidney tissues of cetaceans. One of the possible factors influencing the CHAA for the liver and kidney tissues of cetaceans is the differences among cetacean species. The samples with known Ag concentrations in the current study were

collected from cetaceans of four different species, which have different habitats, prey, and physiological characteristics (Baird, 2009; Louella and Dolar, 2009; McAlpine, 2009; Perrin, 2009). Therefore, it is rational to consider that the models for estimating the Ag concentration by AMG positivity values may be different for different cetacean species. The best way to improve the effect size (adjusted R^2) of our models is to increase the sample sizes of each cetacean species with known Ag concentrations determined by ICP-MS. Furthermore, if the sample sizes are large enough, more accurate models for estimating the Ag concentration can be developed for each cetacean species.

Considering the mean SDs of the accuracy tests of the CHAA (liver: 3.24; kidney: 0.16) and the precision tests of the semi-quantitative analysis for AMG positivity (liver: 2.8; kidney: 0.35), the accuracy errors of the CHAA may be largely attributable to the errors in the semi-quantitative analysis for AMG positivity. In particular, the mean SD in the precision test of the semi-quantitative analysis in the kidney tissues of cetaceans is larger than that of the accuracy test in the CHAA for kidneys ($0.35 > 0.16$). Therefore, the accuracy of the CHAA for kidneys may be lower than that for livers, and it might be associated with the uneven distribution of the AMG positivity signals and the relatively low Ag concentrations in the kidney tissues of cetaceans. In contrast, the accuracy of the CHAA for livers is not affected by the above factors because of the even distribution of AMG positive signals and the relatively high Ag concentrations in the liver tissues of cetaceans. This phenomenon also explains the relatively lower adjusted R^2 in the CHAA for kidneys, and the reliability of the CHAA for kidneys is low.

Intracytoplasmic hyaline inclusions of hepatocytes were commonly found in the stranded cetaceans of each species in this study. The hyaline inclusions are most likely associated with hepatocellular hypoxia due to impaired blood circulation during stranding, but other possibilities such as morbillivirus infection and toxic effect of contaminants have been postulated (Jaber et al., 2004). Non-specific reactive hepatitis, characterized by inflammatory cells infiltrations in portal areas and/or in the parenchyma without the presence of hepatocellular necrosis, represents a non-specific response to the extrahepatic diseases and/or previous intrahepatic inflammatory diseases (Jaber et al., 2004; van den Ingh et al., 2006). Severe congestion of liver is most frequently observed in the *Kogia* spp. (34/38), and this lesion has been associated with

dilated cardiomyopathy in this species (Bossart et al., 1985, 2007). Vacuolar degeneration of hepatocytes is not uncommon in stranded cetaceans with metabolic disorders due to toxic injuries and/or nutritional deficiencies (Jaber et al., 2004). The meanings of hyaline droplets and vacuolar degeneration of renal tubular epithelium in cetaceans are still undetermined. In laboratory rats and mice, the presence of hyaline droplets indicated that the low molecular weight protein is accumulated within lysosomes due to impairment of tubular reabsorption/hydrolysis, which is associated with increased filtered protein loads or decreased catabolism (Frazier et al., 2012). The vacuolar degeneration of proximal renal tubular epithelium may be a preceding and reversible change of tubular degeneration/necrosis, but may be a post-mortem change and can be observed in healthy animals (Frazier et al., 2012). As above, the lesions found in liver and kidney tissues are non-specific, and no marked intralosomal aggregates of AMG positive signals are noted. Besides, there was no statistically significant correlation between these lesions and Ag concentrations of liver and kidney tissues of cetaceans, and thus there is no direct evidence of Ag deposition induced lesions in the liver and kidney tissues of cetaceans. However, stranded cetaceans are not laboratory animals and not well controlled to expose to a single contaminant. Therefore, further investigations are warranted to study the systemic Ag distribution, the cause of death/stranding, and the infectious diseases in stranded cetaceans with different Ag concentrations for comprehensively evaluating the negative health effects caused by Ag in cetaceans.

Although there is no statistically significant correlation between the observed lesions and Ag concentrations in the liver and kidney tissues, the Ag concentrations of cetaceans in the present study are relatively higher than those reported in previous studies conducted in other marine regions, with the exceptions of *Delphinapterus leucas* in the Arctic Ocean and *Sotalia guianensis* and *Pontoporia blainvillei* in the South Atlantic Ocean (Table 4). The Ag concentrations found in the present study also indicate that Ag contamination is relatively more severe in the North-western Pacific Ocean than in other marine regions of the world. In addition, most of the estimated Ag concentrations in the liver and kidney tissues of stranded cetaceans in Taiwan are markedly higher than the baseline concentrations (Chen et al., 2017), and this finding further suggests that the Ag contamination in the North-western Pacific Ocean may have caused detrimental effects on the health of cetaceans.

In addition, a significant age-dependent increase in the Ag concentration estimated by the CHAA was found in the present study, and similar phenomena have been reported in a variety of cetacean species (Becker et al., 1995; Reed et al., 2015; Romero et al., 2017; Seixas et al., 2009). This data indicates that the Ag deposition in cetaceans aggravate with time, and thus the source of Ag deposition is most likely from their prey. The tissues of cetaceans in this study were from 7 different species and have different habitats and prey, but there are no significant difference in Ag concentrations between different cetacean species. This finding also suggests that the Ag contamination may exist in all aspects of the marine ecosystem. Therefore, it is necessary to raise the public awareness and encourage more studies about Ag contamination.

5. Conclusions

In summary, the present study localized Ag by AMG and developed a model called the CHAA to estimate the Ag concentrations in liver and kidney tissues from 7 cetacean species. The Ag distribution pattern in cetaceans was different from those in previous studies conducted in laboratory rats, and this difference may suggest that cetaceans have a different metabolic profile of Ag.

Therefore, a presumptive metabolic pathway of Ag in cetaceans is advanced. Furthermore, our results suggest that Ag contamination is more severe in cetaceans living in the North-western Pacific Ocean than in cetaceans living in other marine regions of the world and may have detrimental effects on their health condition.

Declaration of interest statement

The authors report no conflicts of interest.

Acknowledgments

We thank the Taiwan Cetacean Stranding Network for sample collection and storage, including the Taiwan Cetacean Society, Taipei; the Cetacean Research Laboratory (Prof. Lien-Siang Chou), the Institute of Ecology and Evolutionary Biology, National Taiwan University, Taipei; the National Museum of Marine Biology and Aquarium (Dr. Chiou-Ju Yao), Taichung; and the Marine Biology & Cetacean Research Center, National Cheng-Kung University. This study is partially supported by the Ministry of Science & Technology, Taiwan under Grant MOST 106-2313-B-002-054-.

Appendix A. Supplementary data

Supplementary data related to this article can be found at <https://doi.org/10.1016/j.envpol.2018.01.010>.

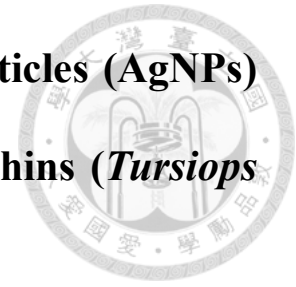
References

- Ajmal, C.M., Menamparambath, M.M., Choi, H.R., Baik, S., 2016. Extraordinarily high conductivity of flexible adhesive films by hybrids of silver nanoparticle-nanowires. *Nanotechnology* 27, 225603. <https://doi.org/10.1088/0957-4484/27/22/225603>.
- Anderson, D.S., Patchin, E.S., Silva, R.M., Uyeminami, D.L., Sharmah, A., Guo, T., Das, G.K., Brown, J.M., Shannahan, J., Gordon, T., Chen, L.C., Pinkerton, K.E., Van Winkle, L.S., 2015. Influence of particle size on persistence and clearance of aerosolized silver nanoparticles in the rat lung. *Toxicol. Sci.* 144, 366–381. <https://doi.org/10.1093/toxsci/kfv005>.
- Baird, R.W., 2009. Risso's dolphin: *Grampus griseus*. In: Perrin, William F., Würsig, B., Thewissen, J.G.M. (Eds.), *Encyclopedia of Marine Mammals*, second ed. Academic Press, London, pp. 975–976.
- Barbier, O., Jacquillet, G., Tauc, M., Cugnion, M., Poujeol, P., 2005. Effect of heavy metals on, and handling by, the kidney. *Nephron. Physiol.* 99, p105–110. <https://doi.org/10.1159/000083981>.
- Becker, P., Krahn, M., Mackey, E., Demiralp, R., Schantz, M., Epstein, M., Donais, M., Porter, B., Muir, D., Wise, S., 2000. Concentrations of Polychlorinated Biphenyls (PCB's) Chlorinated Pesticides and Heavy Metals and Other Elements in Tissues of Belugas *Delphinapterus leucas* from Cook Inlet Alaska.
- Becker, P.R., Mackey, E.A., Demiralp, R., Suydam, R., Early, G., Koster, B.J., Wise, S.A., 1995. Relationship of silver with selenium and mercury in the liver of two species of toothed whales (odontocetes). *Mar. Pollut. Bull.* 30, 262–271. [https://doi.org/10.1016/0025-326X\(94\)00176-A](https://doi.org/10.1016/0025-326X(94)00176-A).
- Bischoff, K., Lamm, C., Erb, H.N., Hillebrandt, J.R., 2008. The effects of formalin fixation and tissue embedding of bovine liver on copper, iron, and zinc analysis. *J. Vet. Diagn. Invest.* 20, 220–224. <https://doi.org/10.1177/104063870802000213>.
- Bonta, M., Torok, S., Hegedus, B., Dome, B., Limbeck, A., 2017. A comparison of sample preparation strategies for biological tissues and subsequent trace element analysis using LA-ICP-MS. *Anal. Bioanal. Chem.* 409, 1805–1814. <https://doi.org/10.1007/s00216-016-0124-6>.
- Bornhorst, J.A., Hunt, J.W., Urry, F.M., McMillin, G.A., 2005. Comparison of sample preservation methods for clinical trace element analysis by inductively coupled plasma mass spectrometry. *Am. J. Clin. Pathol.* 123, 578–583. <https://doi.org/10.1309/L241-WUER-8831-GLWB>.
- Bossart, G.D., 2011. Marine mammals as sentinel species for oceans and human health. *Vet. Pathol.* 48, 676–690. <https://doi.org/10.1177/0300985810388525>.
- Bossart, G.D., Hensley, G., Goldstein, J.D., Kroell, K., Manire, C.A., Defran, R.H., Reif, J.S., 2007. Cardiomyopathy and myocardial degeneration in stranded pygmy (*Kogia breviceps*) and dwarf (*Kogia sima*) sperm whales. *Aquat. Mamm.* 33, 214–222. <https://doi.org/10.1578/AM.33.2.2007.214>.
- Bossart, G.D., Odell, D.K., Altman, N.H., 1985. Cardiomyopathy in stranded pygmy and dwarf sperm whales. *J. Am. Vet. Med. Assoc.* 187, 1137–1140.
- Boudreau, M.D., Imam, M.S., Paredes, A.M., Bryant, M.S., Cunningham, C.K., Felton, R.P., Jones, M.Y., Davis, K.J., Olson, G.R., 2016. Differential effects of silver nanoparticles and silver ions on tissue accumulation, distribution, and toxicity in the Sprague Dawley rat following daily oral gavage administration for 13

- weeks. *Toxicol. Sci.* 150, 131–160. <https://doi.org/10.1093/toxsci/kfv318>.
- Buffet, P.E., Zalouk-Vergnoux, A., Chatel, A., Berthet, B., Metais, I., Perrein-Ettajani, H., Poirier, L., Luna-Acosta, A., Thomas-Guyon, H., Risso-de Faverney, C., Guibolini, M., Gilliland, D., Valsami-Jones, E., Mouneyrac, C., 2014. A marine mesocosm study on the environmental fate of silver nanoparticles and toxicity effects on two endobenthic species: the ragworm *Hediste diversicolor* and the bivalve mollusc *Scrobicularia plana*. *Sci. Total Environ.* 470–471, 1151–1159. <https://doi.org/10.1016/j.scitotenv.2013.10.114>.
- Caceres-Saez, I., Ribeiro Guevara, S., Dellabianca, N.A., Goodall, R.N., Cappozzo, H.L., 2013. Heavy metals and essential elements in Commerson's dolphins (*Cephalorhynchus c. commersonii*) from the southwestern South Atlantic Ocean. *Environ. Monit. Assess.* 185, 5375–5386. <https://doi.org/10.1007/s10661-012-2952-y>.
- Chen, M.H., Shih, C.C., Chou, C.L., Chou, L.S., 2002. Mercury, organic-mercury and selenium in small cetaceans in Taiwanese waters. *Mar. Pollut. Bull.* 45, 237–245. [https://doi.org/10.1016/S0025-326X\(02\)00095-4](https://doi.org/10.1016/S0025-326X(02)00095-4).
- Chen, M.H., Zhuang, M.F., Chou, L.S., Liu, J.Y., Shih, C.C., Chen, C.Y., 2017. Tissue concentrations of four Taiwanese toothed cetaceans indicating the silver and cadmium pollution in the western Pacific Ocean. *Mar. Pollut. Bull.* <https://doi.org/10.1016/j.marpolbul.2017.03.028>.
- Cristofori, P., Zanetti, E., Fregona, D., Piaia, A., Trevisan, A., 2007. Renal proximal tubule segment-specific nephrotoxicity: an overview on biomarkers and histopathology. *Toxicol. Pathol.* 35, 270–275. <https://doi.org/10.1080/01926230601187430>.
- Dansch, G., 1981. Light and electron microscopic localization of silver in biological tissue. *Histochemistry* 71, 177–186.
- Dansch, G., 1991. Applications of autometallography to heavy metal toxicology. *Pharmacol. Toxicol.* 68, 414–423.
- Dehn, L.A., Follmann, E.H., Thomas, D.L., Sheffield, G.G., Rosa, C., Duffy, L.K., O'Hara, T.M., 2006. Trophic relationships in an Arctic food web and implications for trace metal transfer. *Sci. Total Environ.* 362, 103–123. <https://doi.org/10.1016/j.scitotenv.2005.11.012>.
- Deroulers, C., Ameisen, D., Badoual, M., Gerin, C., Granier, A., Lartaud, M., 2013. Analyzing huge pathology images with open source software. *Diagn. Pathol.* 8 <https://doi.org/10.1186/1746-1596-8-92>.
- Dimitriadis, V.K., Domouhtsidou, G.P., Raftopoulou, E., 2003. Localization of Hg and Pb in the palps, the digestive gland and the gills in *Mytilus galloprovincialis* (L.) using autometallography and X-ray microanalysis. *Environ. Pollut.* 125, 345–353. [https://doi.org/10.1016/S0269-7491\(03\)00122-2](https://doi.org/10.1016/S0269-7491(03)00122-2).
- Farre, M., Gajda-Schrantz, K., Kantiani, L., Barcelo, D., 2009. Ecotoxicity and analysis of nanomaterials in the aquatic environment. *Anal. Bioanal. Chem.* 393, 81–95. <https://doi.org/10.1007/s00216-008-2458-1>.
- Frazier, K.S., Seely, J.C., Hard, G.C., Betton, G., Burnett, R., Nakatsuji, S., Nishikawa, A., Durchfeld-Meyer, B., Bube, A., 2012. Proliferative and nonproliferative lesions of the rat and mouse urinary system. *Toxicol. Pathol.* 40, 145–86S. <https://doi.org/10.1177/0192623312438736>.
- Gammill, J.C., Wheeler, B., Carothers, E.L., Hahn, P.F., 1950. Distribution of radioactive silver colloids in tissues of rodents following injection by various routes. *Proc Soc Exp Biol Med* 74, 691–695.
- Ge, L., Li, Q., Wang, M., Ouyang, J., Li, X., Xing, M.M., 2014. Nanosilver particles in medical applications: synthesis, performance, and toxicity. *Int. J. Nanomed.* 9, 2399–2407. <https://doi.org/10.2147/IJN.S55015>.
- Geraci, J.R., Lounsbury, V.J., 2005. Specimen and data collection, marine mammals ashore: a field guide for strandings. *Natl. Aquarium Baltimore* 167–230.
- Hansen, S.F., Heggelund, L.R., Besora, P.R., Mackevica, A., Boldrin, A., Baun, A., 2016. Nanoproducts – what is actually available to European consumers? *Environ. Sci. -Nano* 3, 169–180. <https://doi.org/10.1039/c5en00182j>.
- Hohn, A.A., 2009. Age estimation. In: Würsig, B., Thewissen, J.G.M. (Eds.), *Encyclopedia of Marine Mammals*, second ed. Academic Press, London, pp. 11–17.
- Ikemoto, T., Kunito, T., Anan, Y., Tanaka, H., Baba, N., Miyazaki, N., Tanabe, S., 2004a. Association of heavy metals with metallothionein and other proteins in hepatic cytosol of marine mammals and seabirds. *Environ. Toxicol. Chem.* 23, 2008–2016. <https://doi.org/10.1897/03-456>.
- Ikemoto, T., Kunito, T., Tanaka, H., Baba, N., Miyazaki, N., Tanabe, S., 2004b. Detoxification mechanism of heavy metals in marine mammals and seabirds: interaction of selenium with mercury, silver, copper, zinc, and cadmium in liver. *Arch. Environ. Contam. Toxicol.* 47, 402–413. <https://doi.org/10.1007/s00244-004-3188-9>.
- Jaber, J.R., Perez, J., Arbelo, M., Andrada, M., Hidalgo, M., Gomez-Villamandos, J.C., Van Den Ingh, T., Fernandez, A., 2004. Hepatic lesions in cetaceans stranded in the Canary Islands. *Vet. Pathol.* 41, 147–153. <https://doi.org/10.1354/vp.41-2-147>.
- Jensen, E.C., 2013. Quantitative analysis of histological staining and fluorescence using ImageJ. *Anat. Rec. -Adv. Integrat. Anat. Evol. Biol.* 296, 378–381. <https://doi.org/10.1002/ar.22641>.
- Kim, W.Y., Kim, J., Park, J.D., Ryu, H.Y., Yu, I.J., 2009. Histological study of gender differences in accumulation of silver nanoparticles in kidneys of Fischer 344 rats. *J. Toxicol. Environ. Health A* 72, 1279–1284. <https://doi.org/10.1080/15287390903212287>.
- Kokkat, T.J., Patel, M.S., McGarvey, D., LiVolsi, V.A., Baloch, Z.W., 2013. Archived formalin-fixed paraffin-embedded (FFPE) blocks: a valuable underexploited resource for extraction of DNA, RNA, and protein. *Biopreserv. Biobanking* 11, 101–106. <https://doi.org/10.1089/bio.2012.0052>.
- Kunito, T., Nakamura, S., Ikemoto, T., Anan, Y., Kubota, R., Tanabe, S., Rosas, F.C., Fillmann, G., Readman, J.W., 2004. Concentration and subcellular distribution of trace elements in liver of small cetaceans incidentally caught along the Brazilian coast. *Mar. Pollut. Bull.* 49, 574–587. <https://doi.org/10.1016/j.marpolbul.2004.03.009>.
- Kurasaki, M., Okabe, M., Saito, S., Yamanoshita, O., Hosokawa, T., Saito, T., 2000. Histochemical characterization of silver-induced metallothionein in rat kidney. *J. Inorg. Biochem.* 78, 275–281.
- Levard, C., Hotze, E.M., Lowry, G.V., Brown Jr., G.E., 2012. Environmental transformations of silver nanoparticles: impact on stability and toxicity. *Environ. Sci. Technol.* 46, 6900–6914. <https://doi.org/10.1021/es2037405>.
- Liang, C.S., Ho, P.S., Yen, C.H., Chen, C.Y., Kuo, S.C., Huang, C.C., Yeh, Y.W., Ma, K.H., Huang, S.Y., 2017. The relationship between the striatal dopamine transporter and novelty seeking and cognitive flexibility in opioid dependence. *Prog Neuro-psychopharmacol Biol Psychiatry* 74, 36–42. <https://doi.org/10.1016/j.pnpbp.2016.12.001>.
- Louella, M., Dolar, L., 2009. Fraser's dolphin: *Lagenodelphis hosei*. In: Würsig, B., Thewissen, J.G.M. (Eds.), *Encyclopedia of Marine Mammals*, second ed. Academic Press, London, pp. 469–471.
- Loeschner, K., Hadrup, N., Qvortrup, K., Larsen, A., Gao, X., Vogel, U., Mortensen, A., Lam, H.R., Larsen, E.H., 2011. Distribution of silver in rats following 28 days of repeated oral exposure to silver nanoparticles or silver acetate. *Part. Fibre Toxicol.* 8, 18.
- Loumbourdis, N.S., Danscher, G., 2004. Autometallographic tracing of mercury in frog liver. *Environ. Pollut.* 129, 299–304. <https://doi.org/10.1016/j.envpol.2003.10.010>.
- Massarsky, A., Trudeau, V.L., Moon, T.W., 2014. Predicting the environmental impact of nanosilver. *Environ. Toxicol. Pharmacol.* 38, 861–873. <https://doi.org/10.1016/j.etap.2014.10.006>.
- McAlpine, D.F., 2009. Pygmy and dwarf sperm whales: *Kogia breviceps* and *K. sima*. In: Würsig, B., Thewissen, J.G.M. (Eds.), *Encyclopedia of Marine Mammals*, second ed. Academic Press, London, pp. 936–938.
- McGIVEN, A.R., DAY, W.A., HUNT, J.S., 1977. Glomerular lesions in argyric NZB/NZW mice. *Br. J. Exp. Pathol.* 58, 57–62.
- Mendez-Fernandez, P., Webster, L., Chouvelon, T., Bustamante, P., Ferreira, M., Gonzalez, A.F., Lopez, A., Moffat, C.F., Pierce, G.J., Read, F.L., Russell, M., Santos, M.B., Spitz, J., Vingada, J.V., Caurant, F., 2014. An assessment of contaminant concentrations in toothed whale species of the NW Iberian Peninsula: part II. Trace element concentrations. *Sci. Total Environ.* 484, 206–217. <https://doi.org/10.1016/j.scitotenv.2014.03.001>.
- Miller, D.L., Yu, I.J., Genter, M.B., 2016. Use of autometallography in studies of nanosilver distribution and toxicity. *Int. J. Toxicol.* 35, 47–51. <https://doi.org/10.1177/10915818156166602>.
- Naganuma, A., Imura, N., 1983. Mode of in vitro interaction of mercuric mercury with selenite to form high-molecular weight substance in rabbit blood. *Chem. Biol. Interact.* 43, 271–282.
- Nowack, B., Krug, H.F., Height, M., 2011. 120 years of nanosilver history: implications for policy makers. *Environ. Sci. Technol.* 45, 1177–1183. <https://doi.org/10.1021/es103316q>.
- Nuttall, K.L., Gordon, W.H., Ash, K.O., 1995. Inductively coupled plasma mass spectrometry for trace element analysis in the clinical laboratory. *Ann. Clin. Lab. Sci.* 25, 264–271.
- Parlee, S.D., Lentz, S.I., Mori, H., MacDougald, O.A., 2014. Quantifying size and number of adipocytes in adipose tissue. *Meth. Enzymol.* 537, 93–122. <https://doi.org/10.1016/B978-0-12-411619-1.00006-9>.
- Perrin, W.F., 2009. Pantropical spotted dolphin: *Stenella attenuata*. In: Würsig, B., Thewissen, J.G.M. (Eds.), *Encyclopedia of Marine Mammals*, second ed. Academic Press, London, pp. 819–821.
- Polanowski, A.M., Robbins, J., Chandler, D., Jarman, S.N., 2014. Epigenetic estimation of age in humpback whales. *Mol Ecol Resour* 14, 976–987. <https://doi.org/10.1111/1755-0998.12247>.
- Reed, L.A., McFee, W.E., Pennington, P.L., Wirth, E.F., Fulton, M.H., 2015. A survey of trace element distribution in tissues of the dwarf sperm whale (*Kogia sima*) stranded along the South Carolina coast from 1990–2011. *Mar. Pollut. Bull.* 100, 501–506. <https://doi.org/10.1016/j.marpolbul.2015.09.005>.
- RJ, T., TL, W., EM, H., 1995. *Toxicological Studies in Tissues of the Beluga Whale Delphinapterus leucas along Northern Alaska with an Emphasis on Public Health Implications of Subsistence Utilization*. Final report to the Alaska Beluga Whale Committee. Department of Wildlife Management, North Slope Borough, Barrow, Alaska.
- Romero, M.B., Polizzi, P., Chiodi, L., Robles, A., Das, K., Gerpe, M., 2017. Metals as chemical tracers to discriminate ecological populations of threatened Franciscana dolphins (*Pontoporia blainvillei*) from Argentina. *Environ Sci Pollut Res Int* 24, 3940–3950. <https://doi.org/10.1007/s11356-016-7970-9>.
- Rosa, C., Blake, J.E., Bratton, G.R., Dehn, L.A., Gray, M.J., O'Hara, T.M., 2008. Heavy metal and mineral concentrations and their relationship to histopathological findings in the bowhead whale (*Balaena mysticetus*). *Sci. Total Environ.* 399, 165–178. <https://doi.org/10.1016/j.scitotenv.2008.01.062>.
- Seixas, T.G., Kehrig, H.A., Di Benedetto, A.P., Souza, C.M., Malm, O., Moreira, I., 2009. Essential (Se, Cu) and non-essential (Ag, Hg, Cd) elements: what are their relationships in liver of *Sotalia guianensis* (Cetacea, Delphinidae)? *Mar. Pollut. Bull.* 58, 629–634. <https://doi.org/10.1016/j.marpolbul.2008.12.005>.
- Shu, J., Dolman, G.E., Duan, J., Qiu, G., Ilyas, M., 2016. Statistical colour models: an automated digital image analysis method for quantification of histological biomarkers. *Biomed. Eng. Online* 15, 46. <https://doi.org/10.1186/s12938-016-0161-6>.
- Spieß, A.N., Neumeier, N., 2010. An evaluation of R2 as an inadequate measure for

- nonlinear models in pharmacological and biochemical research: a Monte Carlo approach. *BMC Pharmacol.* 10, 6. <https://doi.org/10.1186/1471-2210-10-6>.
- Stockin, K.A., Law, R.J., Duignan, P.J., Jones, G.W., Porter, L., Mirimin, L., Meynier, L., Orams, M.B., 2007. Trace elements, PCBs and organochlorine pesticides in New Zealand common dolphins (*Delphinus* sp.). *Sci. Total Environ.* 387, 333–345. <https://doi.org/10.1016/j.scitotenv.2007.05.016>.
- Stoltenberg, M., Danscher, G., 2000. Histochemical differentiation of autometallographically traceable metals (Au, Ag, Hg, Bi, Zn): protocols for chemical removal of separate autometallographic metal clusters in Epon sections. *Histochem. J.* 32, 645–652.
- Stoltenberg, M., Larsen, A., Kemp, K., Bloch, D., Weihe, P., 2003. Autometallographic tracing of mercury in pilot whale tissues in the Faroe Islands. *Int. J. Circumpolar Health* 62, 182–189. <https://doi.org/10.3402/ijch.v62i2.17552>.
- Tilbury, K.L., Stein, J.E., Krone, C.A., Brownell Jr., R.L., Blokhin, S.A., Bolton, J.L., Ernest, D.W., 2002. Chemical contaminants in juvenile gray whales (*Eschrichtius robustus*) from a subsistence harvest in Arctic feeding grounds. *Chemosphere* 47, 555–564. [https://doi.org/10.1016/S0045-6535\(02\)00061-9](https://doi.org/10.1016/S0045-6535(02)00061-9).
- Tran, J.Q., Dranikov, A., Iannucci, A., Wagner, W.P., LoBello, J., Allen, J., Weiss, G.J., 2014. Heavy metal content in thoracic tissue samples from patients with and without NSCLC. *Lung Canc. Int* 2014, 853158. <https://doi.org/10.1155/2014/853158>.
- Vance, M.E., Kuiken, T., Vejerano, E.P., McGinnis, S.P., Hochella Jr., M.F., Rejeski, D., Hull, M.S., 2015. Nanotechnology in the real world: redeveloping the nanomaterial consumer products inventory. *Beilstein J. Nanotechnol.* 6, 1769–1780. <https://doi.org/10.3762/bjnano.6.181>.
- van den Ingh, T.S.G.A.M., Van Winkle, T., Cullen, J.M., Charles, J.A., Desmet, V.J., 2006. Morphological Classification of Parenchymal Disorders of the Canine and Feline Liver: 2. Hepatocellular Death, Hepatitis and Cirrhosis. In: *WSAVA Liver Standardization*, Rothuizen, J., Bunch, S.E., Charles, J.A., Cullen, J.M., Desmet, V.J., Szatmári, V., Twedt, D.C., van den Ingh, T.S.G.A.M., Van Winkle, T., Washabau, R.J. (Eds.), *WSAVA Standards for Clinical and Histological Diagnosis of Canine and Feline Liver Diseases*. W.B. Saunders, Edinburgh, pp. 85–101.
- van der Zande, M., Vandebriel, R.J., Van Doren, E., Kramer, E., Herrera Rivera, Z., Serrano-Rojero, C.S., Gremmer, E.R., Mast, J., Peters, R.J., Hollman, P.C., Hendriksen, P.J., Marvin, H.J., Peijnenburg, A.A., Bouwmeester, H., 2012. Distribution, elimination, and toxicity of silver nanoparticles and silver ions in rats after 28-day oral exposure. *ACS Nano* 6, 7427–7442. <https://doi.org/10.1021/nn302649p>.
- Walker, F., 1971. Experimental argyria: a model for basement membrane studies. *Br. J. Exp. Pathol.* 52, 589–593.
- Walker, F., 1972. The deposition of silver in glomerular basement membrane. *Virchows Arch. B Cell Pathol.* 11, 90–96.
- Walters, C.R., Pool, E.J., Somerset, V.S., 2014. Ecotoxicity of silver nanomaterials in the aquatic environment: a review of literature and gaps in nano-toxicological research. *J Environ Sci Health A Tox Hazard Subst Environ Eng* 49, 1588–1601. <https://doi.org/10.1080/10934529.2014.938536>.
- Wang, H., Ho, K.T., Scheckel, K.G., Wu, F., Cantwell, M.G., Katz, D.R., Horowitz, D.B., Boothman, W.S., Burgess, R.M., 2014. Toxicity, bioaccumulation, and biotransformation of silver nanoparticles in marine organisms. *Environ. Sci. Technol.* 48, 13711–13717. <https://doi.org/10.1021/es502976y>.
- Woshner, V.M., O'Hara, T.M., Bratton, G.R., Suydam, R.S., Beasley, V.R., 2001. Concentrations and interactions of selected essential and non-essential elements in bowhead and beluga whales of arctic Alaska. *J. Wildl. Dis.* 37, 693–710. <https://doi.org/10.7589/0090-3558-37.4.693>.
- Yang, J., Miyazaki, N., 2003. Moisture content in Dall's porpoise (*Phocoenoides dalli*) tissues: a reference base for conversion factors between dry and wet weight trace element concentrations in cetaceans. *Environ. Pollut.* 121, 345–347. [https://doi.org/10.1016/S0269-7491\(02\)00239-7](https://doi.org/10.1016/S0269-7491(02)00239-7).
- Yoneda, S., Suzuki, K.T., 1997a. Detoxification of mercury by selenium by binding of equimolar Hg-Se complex to a specific plasma protein. *Toxicol. Appl. Pharmacol.* 143, 274–280. <https://doi.org/10.1006/taap.1996.8095>.
- Yoneda, S., Suzuki, K.T., 1997b. Equimolar Hg-Se complex binds to selenoprotein P. *Biochem. Biophys. Res. Commun.* 231, 7–11. <https://doi.org/10.1006/bbrc.1996.6036>.
- Yu, S.J., Yin, Y.G., Liu, J.F., 2013. Silver nanoparticles in the environment. *Environ Sci Process Impacts* 15, 78–92. <https://doi.org/10.1039/C2EM30595J>.
- Zarnescu, O., Petrescu, A.M., Gaspar, A., Craciunescu, O., 2017. Effect of sublethal nickel chloride exposure on crayfish, *Astacus leptodactylus* ovary: an ultrastructural, autometallographic, and electrophoretic analyses. *Microsc. Microanal.* 23, 668–678. <https://doi.org/10.1017/S1431927617000496>.
- Zhu, L., Tang, Y., Wang, H.D., Zhang, Z.Y., Pan, H., 2012. Immersion autometallographic demonstration of pathological zinc accumulation in human acute neural diseases. *Neurol. Sci.* 33, 855–861. <https://doi.org/10.1007/s10072-011-0847-2>.

**Chapter IV: Immunotoxicity of Silver Nanoparticles (AgNPs)
on the Leukocytes of Common Bottlenose Dolphins (*Tursiops
truncatus*) Scientific Reports, 2018, 8:5593**



**Wen-Ta Li¹, Hui-Wen Chang¹, Wei-Cheng Yang², Chieh Lo³, Lei-Ya Wang¹, Victor
Fei Pang¹, Meng-Hsien Chen⁴, Chian-Ren Jeng¹**

¹ Graduate Institute of Molecular and Comparative Pathobiology, National Taiwan
University, Taipei 10617, Taiwan

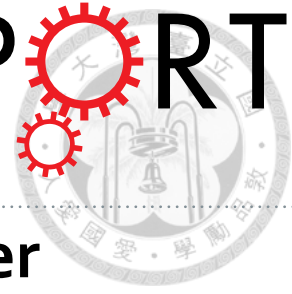
² College of Veterinary Medicine, National Chiayi University, Chiayi 60004, Taiwan

³ Farglory Ocean Park, Hualien 97449, Taiwan

⁴ Department of Oceanography and Asia-Pacific Ocean Research Center, National Sun
Yat-sen University, Kaohsiung 80424, Taiwan

*Corresponding author: crjeng@ntu.edu.tw

SCIENTIFIC REPORTS



OPEN

Immunotoxicity of Silver Nanoparticles (AgNPs) on the Leukocytes of Common Bottlenose Dolphins (*Tursiops truncatus*)

Wen-Ta Li¹, Hui-Wen Chang¹, Wei-Cheng Yang², Chieh Lo³, Lei-Ya Wang¹, Victor Fei Pang¹, Meng-Hsien Chen⁴ & Chian-Ren Jeng¹

Silver nanoparticles (AgNPs) have been extensively used and are considered as an emerging contaminant in the ocean. The environmental contamination of AgNPs is expected to increase greatly over time, and cetaceans, as the top ocean predators, will suffer the negative impacts of AgNPs. In the present study, we investigate the immunotoxicity of AgNPs on the leukocytes of cetaceans using several methods, including cytomorphology, cytotoxicity, and functional activity assays. The results reveal that 20 nm Citrate-AgNPs (C-AgNP₂₀) induce different cytomorphological alterations and intracellular distributions in cetacean polymorphonuclear cells (cPMNs) and peripheral blood mononuclear cells (cPBMCs). At high concentrations of C-AgNP₂₀ (10 and 50 µg/ml), the time- and dose-dependent cytotoxicity in cPMNs and cPBMCs involving apoptosis is demonstrated. C-AgNP₂₀ at sub-lethal doses (0.1 and 1 µg/ml) negatively affect the functional activities of cPMNs (phagocytosis and respiratory burst) and cPBMCs (proliferative activity). The current study presents the first evidence of the cytotoxicity and immunotoxicity of AgNPs on the leukocytes of cetaceans and improves our understanding of environmental safety concerning AgNPs. The dose-response data of AgNPs on the leukocytes of cetaceans are invaluable for evaluating the adverse health effects in cetaceans and for proposing a conservation plan for marine mammals.

Silver nanoparticles (AgNPs) have been extensively used in numerous commercial products including textiles, cosmetics, and health care items mainly due to their strong antimicrobial properties^{1,2}. Previous studies estimated that the production of AgNPs and the number of AgNP-containing products would increase over time^{3,4}. Furthermore, AgNPs can be released during the production, transport, use, and/or disposal of AgNP-containing products, subsequently draining into the aquatic environment and ultimately accumulating in the ocean^{5,6}. Although the fate of AgNPs in the aquatic environment is complicated and changeable, previous studies have indicated that AgNPs in the aquatic environment can remain as individual particles in suspension, aggregate, dissolve, react with different species in the environment, or be regenerated from Ag⁺ ions^{2,3}. Therefore, the extensive use and growing production of AgNP-containing products may aggravate the environmental contamination level of AgNPs, leading to concerns about the safety and environmental toxicity of AgNPs and related ecotoxicological investigations of AgNPs in the marine environment.

AgNPs may precipitate in marine sediments, be ingested by benthic organisms, and thereby enter the food chain in the marine environment⁷. The current knowledge on ecotoxicological data regarding AgNPs in the marine ecosystem is still scarce, and only limited data on the potential toxicity of Ag-NPs to marine organisms at different trophic levels has been reported^{7–12}. Their results have demonstrated that AgNPs are toxic to all tested marine organisms in a dose-dependent manner, suggesting that AgNPs may have negative effects on marine organisms at different trophic levels within the marine ecosystem. In addition, AgNPs can be transferred from one trophic level to the next via the food chain and may have negative effects on the animals at higher trophic

¹Graduate Institute of Molecular and Comparative Pathobiology, National Taiwan University, Taipei, 10617, Taiwan.

²College of Veterinary Medicine, National Chiayi University, Chiayi, 60004, Taiwan. ³Farglory Ocean Park, Hualien, 97449, Taiwan. ⁴Department of Oceanography and Asia-Pacific Ocean Research Center, National Sun Yat-sen University, Kaohsiung, 80424, Taiwan. Correspondence and requests for materials should be addressed to C.-R.J. (email: crjeng@ntu.edu.tw)

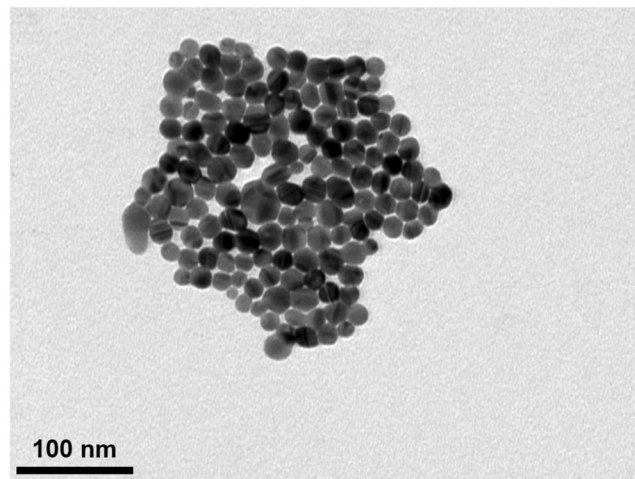


Figure 1. Characterization of C-AgNP₂₀. The representative TEM image of C-AgNP₂₀ in complete RPMI-1640.

levels, such as marine mammals^{5,7,8}. The environmental contamination level of AgNPs is expected to increase greatly in the near future^{3,4}, and marine mammals, as the top predators in the ocean, will suffer the potentially negative impacts caused by AgNPs.

Although no studies on the toxicity of AgNPs in marine mammals have been reported, AgNPs evidently induce several negative effects, such as hepatitis, bile duct hyperplasia, nephritis, neuron cell apoptosis, and alteration of gene expression of the brain, in laboratory mammals^{13–18}. Previous *in vitro* studies using different cell lines have demonstrated that AgNPs can damage DNA, cell membranes, and mitochondria through reactive oxygen species (ROS) dependent/independent pathways and thereby induce cell apoptosis and necrosis^{19,20}. Previous studies conducted in laboratory mammals including mice and rats have also demonstrated that AgNPs can enter the blood circulation through oral and inhalation exposure, and then accumulate in multiple organs^{13,16,18,21–23}. Several studies on the effects of AgNPs in human leukocytes have been recently reported^{24–32}. These studies demonstrated that AgNPs could cause several effects in human neutrophils, including morphological alterations, cytotoxicity, atypical cell death, inhibition of de novo protein synthesis, increased production of the CXCL8 chemokine (IL-8), and impaired lysosomal activity^{28–31}. Cytotoxicity and inhibition of lymphocyte proliferation in lymphocytes and macrophages were also revealed^{24–26,32}. However, the effects of AgNPs on the functional activities of human neutrophils and lymphocytes are still poorly understood. Therefore, the negative effects of AgNPs on the white blood cells of marine mammals such as cetaceans are of concern.

Despite such concern, no studies on the toxicity of AgNPs in cetaceans have been reported. Generally, *in vivo* studies are usually not feasible, and ethical issues concerning the study of immunotoxic effects caused by environmental contaminants in cetaceans are difficult to overcome, so *in vitro* study using blood samples from captive cetaceans would be a logical and crucial approach³³. Therefore, we evaluate the effects of AgNPs on the leukocytes of cetaceans by several methods, including cytomorphological examination (microscopic examination under Liu's stain/autometallographic [AMG] Ag visualization and transmission electron microscope [TEM]), cytotoxicity assays (flow cytometric analysis using Annexin V/Propidium iodide staining), and functional activity assays (ROS production, phagocytosis, and respiratory burst of polymorphonuclear cells [PMNs] and proliferative activity of peripheral blood mononuclear cells [PBMCs] by flow cytometry). Furthermore, previous studies have demonstrated that the toxicity and physicochemical characteristics of AgNPs are associated with their surface coating and size^{19,20}. The state of AgNPs and Ag in the marine environment and in the bodies of cetaceans is complicated and various, and it is not realistic to investigate all possible types of AgNPs and Ag compounds in the leukocytes of cetaceans *in vitro*. Considering the wide usage of 20 nm citrate-AgNPs (C-AgNP₂₀) in recently reported studies of human leukocytes^{26,29,30}, commercial C-AgNP₂₀ is used in the present study.

Results

Characterization of C-AgNP₂₀. The C-AgNP₂₀ suspended in complete RPMI-1640 medium (RPMI-1640 [Gibco, NY, USA] with 10% fetal bovine serum, 2mM L-glutamine, 50 IU penicillin, and 50 µg streptomycin) were spherically shaped and close to 20 nm in diameter (Fig. 1). The size distributions were 30 ± 0 (100%) and 30 ± 0 (100%) for C-AgNP₂₀ at 100 and 500 µg/ml, respectively. The values of the zeta potentials were -38.97 ± 1.33 and -44.2 ± 1.35 mV for C-AgNP₂₀ at 100 and 500 µg/ml. The Poly-dispersity Indexes (PDIs) were 0.12 ± 0.00 and 0.11 ± 0.01 , indicating that the distribution consisted of a single size mode without aggregates (The detailed information is presented in Supplementary Files).

C-AgNP₂₀ induced different cytomorphological alterations and intracellular distributions in cetacean PMNs/PBMCs. The cell size of cetacean PMNs (cPMNs) with 50 µg/ml C-AgNP₂₀ treatment was increased by the presence of variably sized intracytoplasmic vacuoles and enlarged multi-lobed nuclei (Fig. 2A), which were not observed in the control (Fig. 2B). The numbers of cetacean PBMCs (cPBMCs) with blurred cell morphology increased after exposure to 50 µg/ml C-AgNP₂₀. Although the presences of intracytoplasmic

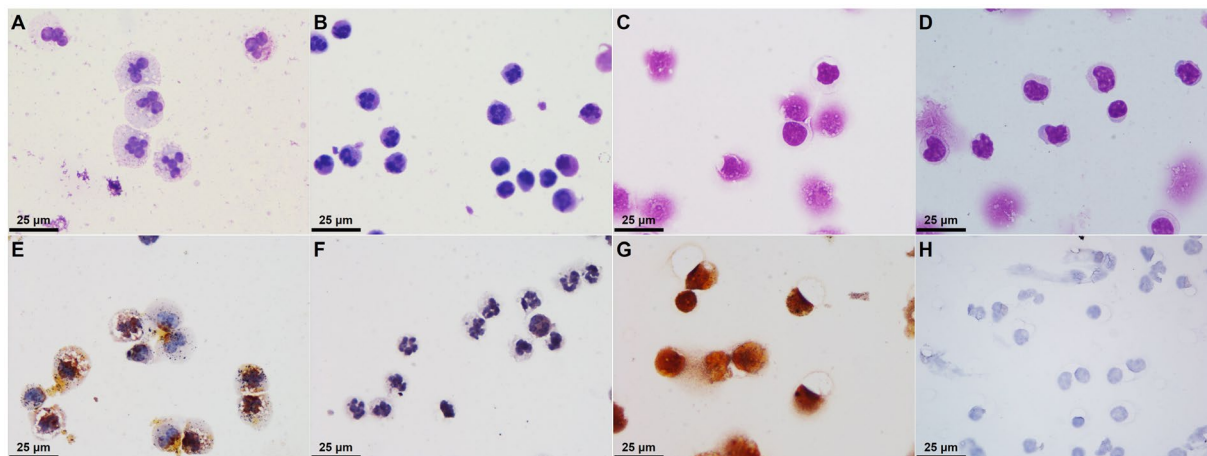


Figure 2. C-AgNP₂₀ induced different cytomorphological alterations and intracellular distributions in cPMNs and cPBMCs. Representative cytological slides stained with Liu's stain of cPMNs after 4 h of culture (A) with 50 µg/ml C-AgNP₂₀ and (B) without C-AgNP₂₀ (control), cPBMCs after 4 h of culture (C) with 50 µg/ml C-AgNP₂₀ and (D) without C-AgNP₂₀ (control); representative cytological slides stained with silver enhancement method of cPMNs after 4 h of culture (E) with 50 µg/ml C-AgNP₂₀ and (F) without C-AgNP₂₀ (control); cPBMCs after 4 h of culture (G) with 50 µg/ml C-AgNP₂₀ and (H) without C-AgNP₂₀ (control).

vacuoles were found in the cPBMCs with 50 µg/ml C-AgNP₂₀ treatment, the increased cell size of cPBMCs was unremarkable (Fig. 2C) as compared to the control (Fig. 2D). The AMG positive signals in the cPMNs were mainly intracytoplasmic black dots with the multifocal presence of an amorphous golden yellow to brown substance in the cytoplasm and nucleus (Fig. 2E). The AMG positive signals in the cPBMCs were an intracellularly diffuse, golden yellow to brown substance (Fig. 2G). No AMG positive signals were found in the controls (Fig. 2F and H). Under TEM, intracellular electron-dense structures with clear spaces were found in the intracytoplasmic vacuoles of some but not all cPMNs with 50 µg/ml C-AgNP₂₀ treatment for 4 h, but no particles of compatible size and shape with C-AgNP₂₀ were noted (Fig. 3A). No intracellular electron-dense structures were found in the control group (Fig. 3B). Nuclear membrane rupture and swollen mitochondria with cristae disruption were frequently found in the cPBMCs with 50 µg/ml C-AgNP₂₀ treatment for 4 h (Fig. 3C) but were not found in the control group (Fig. 3D).

In the flow-cytometric analysis, the inner complexity of cPMNs with 10 and 50 µg/ml C-AgNP₂₀ increased after 1 and 4 h of culture. The cell size of cPMNs with 10 and 50 µg/ml C-AgNP₂₀ increased after 1 h of culture but decreased after 4 h of culture. Decreased cell size with mildly increased inner complexity was found in cPBMCs after 1 and 4 h of culture with 10 and 50 µg/ml C-AgNP₂₀. After 16 h of culture with 10 and 50 µg/ml C-AgNP₂₀, both cPMNs and cPBMCs revealed decreased cell size and inner complexity. No marked differences were noted between the cPMN and cPBMC exposures to 0, 0.1 and 1.0 µg/ml C-AgNP₂₀ after 1 and 4 h of culture (Fig. 4A and B).

C-AgNP₂₀ induced cytotoxicity in cPMNs and cPBMCs with involvement of apoptotic pathway.

C-AgNP₂₀ (10 and 50 µg/ml) treatment significantly increased the number of apoptotic cells and late apoptotic/necrotic cells in a time- and dose-dependent manner in cPMNs and cPBMCs. Percentages of apoptotic and late apoptotic/necrotic cells of cPMNs and cPBMCs after exposure to different concentrations of C-AgNP₂₀ and incubation time are shown in Fig. 5A to D. A significant increase in the apoptotic rate was observed in the cPMNs (median ± interquartile range (IQR): 8.04 ± 5.27%; $p = 0.0003$) and cPBMCs (9.32 ± 4.36%; $p < 0.0001$) after 1 h of 50 µg/ml C-AgNP₂₀ treatment. Late apoptotic/necrotic cells in cPMNs (13.08 ± 5.92%; $p < 0.0001$) and cPBMCs (51.19 ± 28.52%; $p < 0.0001$) after 4 h and 1 h of 50 µg/ml C-AgNP₂₀ treatments, respectively, were significantly increased. The rates of late apoptotic/necrotic cells in cPBMCs with 10 and 50 µg/ml C-AgNP₂₀ after 1 and 4 h of culture were significantly higher than those of cPMNs with the same treatments ($p < 0.0001$; except the group with 10 µg/ml C-AgNP₂₀ after 1 h of culture [$p = 0.0232$]) (Fig. 5E). A marked increase in the number of apoptotic cells was noted in cPMNs without C-AgNP₂₀ after 16 h incubation, which might be similar to the spontaneous apoptosis found in human neutrophils^{29,35}.

There were no statistically significant differences in the percentages of apoptotic and late apoptotic/necrotic cells in cPMNs and cPBMCs with 0, 0.1, and 1.0 µg/ml C-AgNP₂₀ after 1 and 4 h of culture. Based on the results of morphological alterations and cytotoxicity assays, 0.1 and 1.0 µg/ml C-AgNP₂₀ were defined as the sub-lethal dose for cPMNs and cPBMCs. Representative dot plots by flow-cytometric analyses of cPMNs and cPBMCs exposed to 0, 10 and 50 µg/ml C-AgNP₂₀ for different incubation times are shown in Fig. 6. The results illustrated that cPMNs and cPBMCs exposed to C-AgNP₂₀ were apoptotic and subsequently shifted to late apoptotic/necrotic, suggesting the apoptotic pathway is involved in the cytotoxicity induced by C-AgNP₂₀.

C-AgNP₂₀ at sub-lethal dose significantly decreased the phagocytosis but increased the respiratory burst in cPMNs. The percentage of phagocytizing cPMNs was significantly decreased after 1 and 3 h of C-AgNP₂₀ (1.0 µg/ml) treatment (Fig. 7A). The number of ingested bacteria per cPMN significantly increased

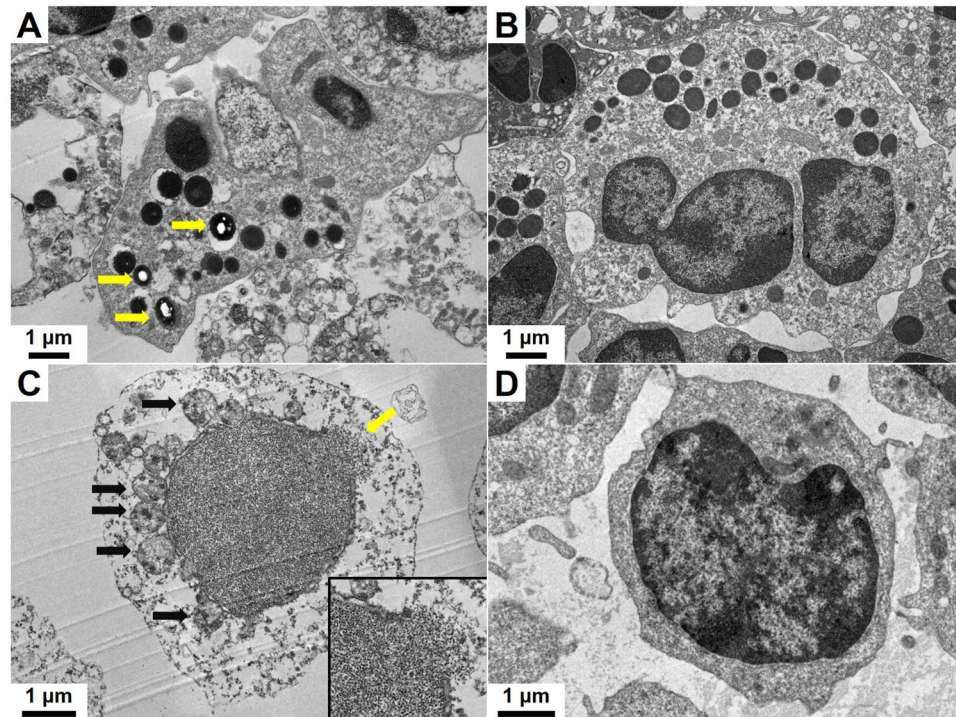


Figure 3. C-AgNP₂₀ induced different cytomorphological alterations and intracellular distributions in cPMNs and cPBMCs. Representative TEM images of ultrathin sections of cPMNs after 4 h of culture (A) with 50 µg/ml C-AgNP₂₀ and (B) without C-AgNP₂₀ (control). Intracellular electron-dense structures with clear spaces are indicated by yellow arrows. Representative TEM images of ultrathin sections of cPBMCs after 4 h of culture (C) with 50 µg/ml C-AgNP₂₀ and (D) without C-AgNP₂₀ (control). Ruptured nuclear membrane is indicated by yellow arrow, and black arrows indicate the swollen mitochondria with cristae disruption. Inset: higher power field of the ruptured nuclear membrane.

after 1 h of C-AgNP₂₀ (0.1 µg/ml) treatment, but significantly decreased after exposure to C-AgNP₂₀ (0.1 µg/ml) for 3 h and C-AgNP₂₀ (1.0 µg/ml) for 1 and 3 h (Fig. 7B). No significant difference in the percentages of oxidizing cPMNs was found after 1 and 3 h of exposure to C-AgNP₂₀ (Fig. 7C), but C-AgNP₂₀ (1.0 µg/ml) induced a significant increase in the oxidative activity per cPMN after 1 and 3 h of exposure (Fig. 7D). In order to determine whether the increased respiratory burst of cPMNs exposed to C-AgNP₂₀ was associated with oxidative killing or spontaneous ROS production, the ROS production of cPMNs induced by C-AgNP₂₀ without bacterial stimulation was performed. Our results indicated that the ROS production of cPMNs was significantly increased after exposure to 10 and 50 µg/ml C-AgNP₂₀ for 1 and 4 h exposure, but no significant differences in ROS production were noted in the cPMNs exposed to 0, 0.1 and 1.0 µg/ml C-AgNP₂₀ (Fig. 8).

C-AgNP₂₀ at sub-lethal dose significantly decreased proliferative activity of cPBMCs. C-AgNP₂₀ (10 µg/ml) caused a significant decrease in cell viability of cPBMCs after 60 h of culture (with Concanavalin A [Con A]: Me: 42.45%, $p = 0.0047$; without Con A: Me: 33.15%, $p = 0.005$) (Fig. 9A). Therefore, 0.1 and 1.0 µg/ml C-AgNP₂₀ were considered sub-lethal doses for the proliferative activity assay of cPBMCs. Con A significantly induced cell proliferative activity in cPBMCs in contrast to the cPBMCs without Con A (Fig. 9B). The Con A-induced cell proliferative activity of cPBMCs was significantly inhibited by 0.1 and 1.0 µg/ml C-AgNP₂₀ treatment (Fig. 9C).

Discussion

The present study has demonstrated the first evidence of the cytotoxicity and immunotoxicity caused by AgNPs on the leukocytes of cetaceans. Our data demonstrated that C-AgNP₂₀ at high concentrations (10 and 50 µg/ml) induced a time- and dose-dependent cytotoxicity in cPMNs and cPBMCs, and an apoptotic pathway was involved in the C-AgNP₂₀-induced cytotoxicity. The cPBMCs were more vulnerable than cPMNs to the C-AgNP₂₀-induced cytotoxic effects, suggestive of a cell-type-specific response to AgNPs. Furthermore, the functional activities of cPMNs and cPBMCs were significantly compromised by C-AgNP₂₀ at sub-lethal doses (0.1 and 1.0 µg/ml). The biodistribution of AgNPs or Ag in cetaceans is still largely unknown, but previous *in vivo* studies of AgNPs and Ag by oral exposure in laboratory rats demonstrated that the silver concentration is approximately 10 times higher in the liver than in blood or plasma^{16,21,23}. Based on the concept of these laboratory animal models, it is presumed that the Ag concentration in the blood of stranded cetaceans may range from 0.01 to 72.6 µg/ml^{34,35}. Although the state of Ag and AgNPs in the body of cetaceans is undetermined, complicated, and various, the

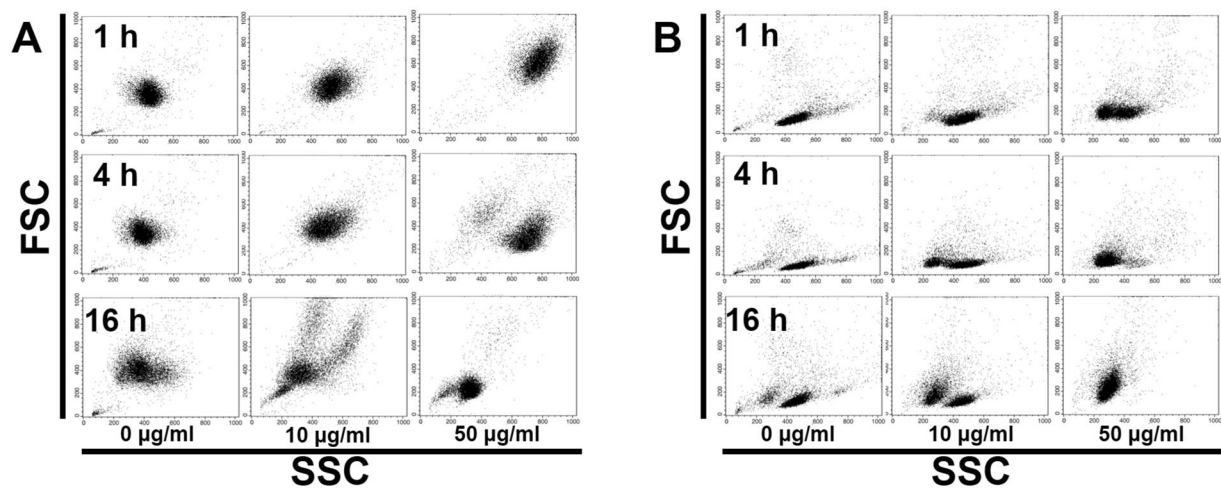


Figure 4. Representative dot plots by flow-cytometric analyses for evaluation of the cell size and inner complexity of (A) cPMNs and (B) cPBMCs.

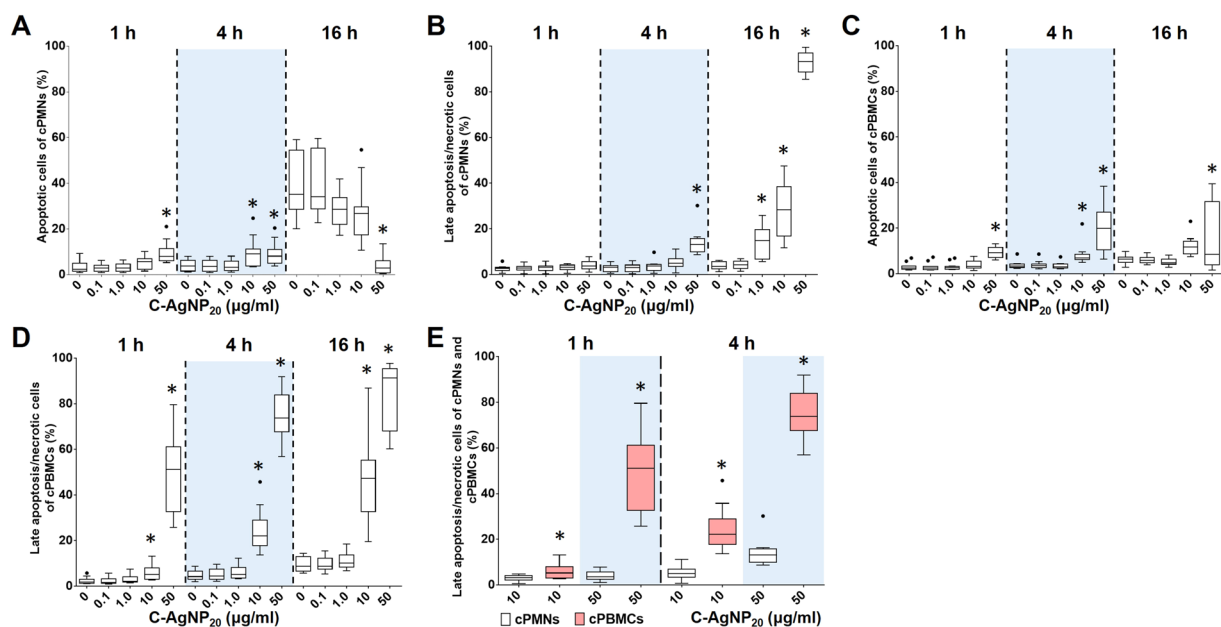


Figure 5. Cytotoxicity of C-AgNP₂₀ in cPMNs and cPBMCs. Percentages of apoptotic and late apoptotic/necrotic cells of (A and B) cPMNs and (B and C) cPBMCs after exposure to different concentrations of C-AgNP₂₀ and different incubation times. Comparison of the cytotoxicity caused by C-AgNP₂₀ in cPMNs and cPBMCs (E). The bar in the middle of the box represents the median, and the bottom and top of the box describe the first and third quartiles. The whiskers show the 75th percentile plus 1.5 times IQR and 25th percentile minus 1.5 times IQR of all data, and any values greater than these are defined as outliers and plotted as individual points. Asterisks indicate statistically significant differences from the control ($p < 0.05$, Kruskal-Wallis Test for [A to D] and Mann-Whitney U-test for [E]).

current results still suggest that the immune function of cetaceans may have been compromised by AgNPs and/or Ag, and the immunotoxic effects of AgNPs in marine mammals should not be overlooked.

Two studies have used the same C-AgNP₂₀ (Pelco[®] citrate Biopure[™] silver, Ted Pella, CA, USA) to investigate the effects of AgNPs on human PMNs^{29,30}. The characterization of the C-AgNP₂₀ has been studied, but the endotoxin level of C-AgNP₂₀ has not been investigated^{29,30}. Endotoxins are common contaminants in engineered nanomaterials and can influence the results of immunological and toxicological studies due to their marked immunostimulatory effects³⁶. Therefore, the endotoxin levels of the C-AgNP₂₀ used in the present study were investigated. These studies have demonstrated that human PMNs are well tolerant to C-AgNP₂₀, and only an increased apoptotic rate is observed after 24 h of culture with 100 µg/ml C-AgNP₂₀ treatment^{29,30}. Therefore, the lethal dose of C-AgNP₂₀ in human PMNs is considered to be 100 µg/ml. In contrast, our data indicated that the

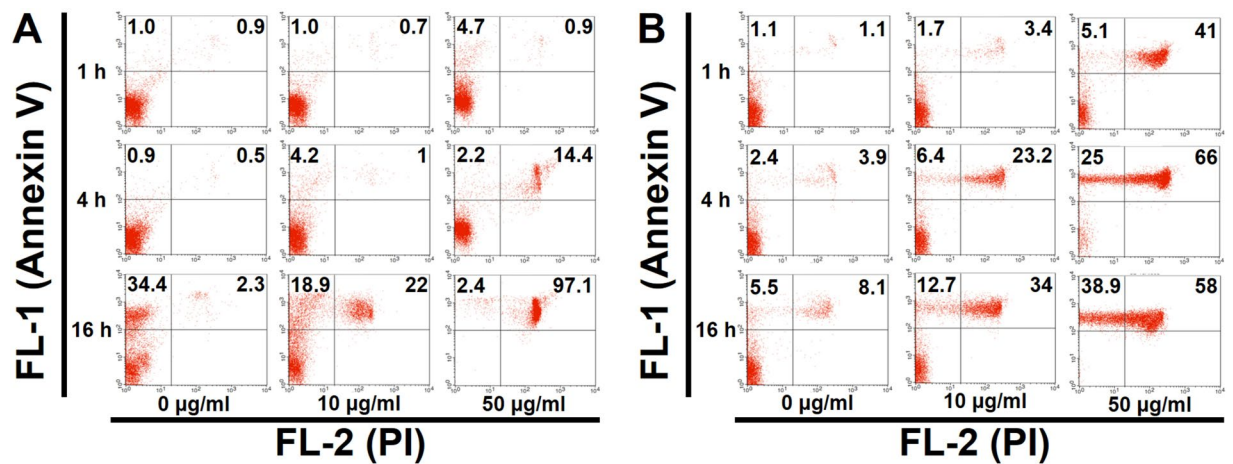


Figure 6. Representative dot plots by flow-cytometric analyses using Annexin V-FITC/PI double staining in (A) cPMNs and (B) cPBMCs exposed to different concentrations of C-AgNP₂₀ and different incubation times.

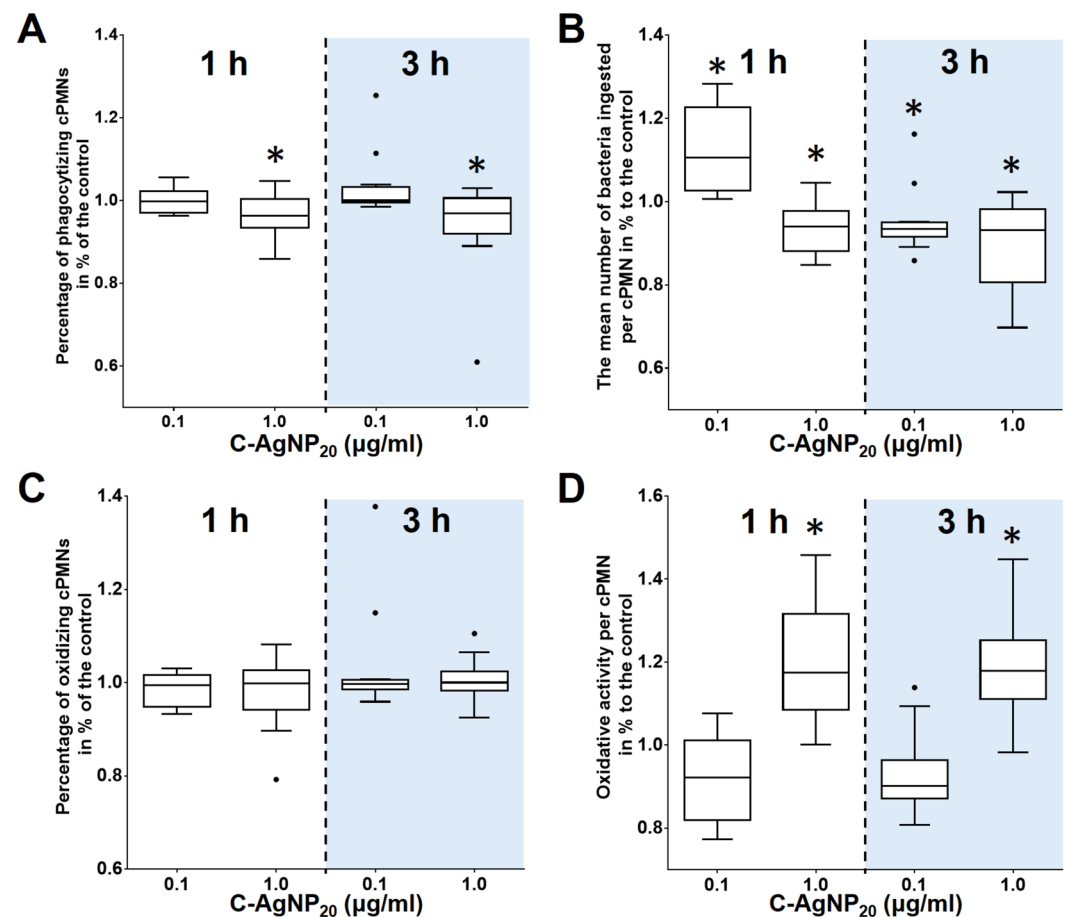


Figure 7. The negative effects of C-AgNP₂₀ on the functional activity of cPMNs. (A) percentage of phagocytizing cPMNs, (B) number of ingested bacteria per cPMN, (C) percentage of oxidizing cPMNs, and (D) oxidative activity per cPMN. The bar in the middle of the box represents the median, and the bottom and top of the box describe the first and third quartiles. The whiskers showed the 75th percentile plus 1.5 times IQR and 25th percentile minus 1.5 times IQR of all data, and any values greater than these are defined as outliers and plotted as individual points. Asterisks indicate statistically significant differences from the control ($p < 0.05$, Kruskal-Wallis Test).

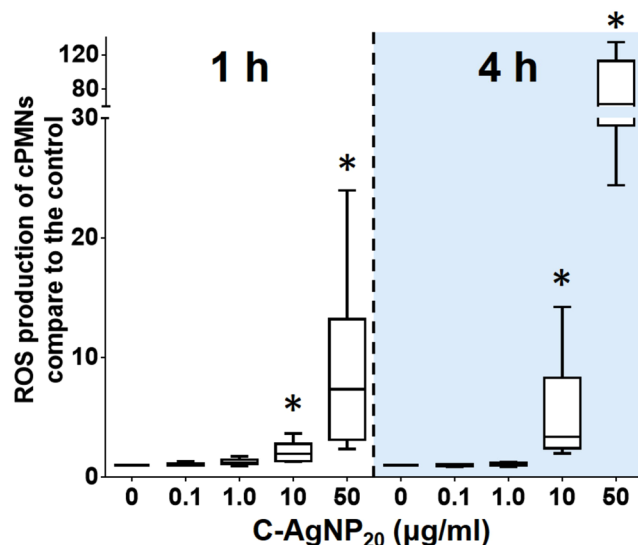


Figure 8. The ROS production of cPMNs induced by C-AgNP₂₀. The bar in the middle of the box represents the median, and the bottom and top of the box describe the first and third quartiles. The whiskers show the 75th percentile plus 1.5 times IQR and 25th percentile minus 1.5 times IQR of all data, and any values greater than these are defined as outliers and plotted as individual points. Asterisks indicate statistically significant differences from the control ($p < 0.05$, Kruskal-Wallis Test).

lethal dose of C-AgNP₂₀ in cPMNs is ≥ 10 µg/ml; hence, it might suggest that C-AgNP₂₀ cause different cytotoxic effects on cPMNs and human PMNs.

In the current study, C-AgNP₂₀ (10 and 50 µg/ml) significantly induced cytotoxicity in cPBMCs. This finding is similar to those of studies conducted in human lymphocytes with C-AgNP₂₀ treatment^{26,27}. In addition, a cell-type-specific response of human PBMCs exposed to polyvinylpyrrolidone (PVP)-coated AgNPs (55 to 90 nm) has been demonstrated and may be associated with differences in cell-type-specific uptake and intracellular distribution of AgNPs between monocytes and lymphocytes²⁵. Our data on cytotoxicity assays found that the cytotoxicity induced by C-AgNP₂₀ was significantly higher in cPBMCs than in cPMNs, which might be associated with differences in cell-type-specific uptake and intracellular distribution. The intracellular distribution of AgNPs in human neutrophils in a previous study indicated that C-AgNP₂₀ could penetrate into neutrophils and localize in intracytoplasmic vacuoles within 1 min²⁹. In contrast, the intracellular distribution of AgNPs in lymphocytes is still undetermined. A previous study found that uncoated AgNPs treatment (75 to 130 nm) could induce varying degrees of cell deformity, cell membrane damage, and vacuolization in human lymphocytes, but no AgNPs or agglomerated AgNPs were identified in lymphocytes under TEM²⁴. It is speculated that larger-sized AgNPs (75 to 130 nm) might not be able to penetrate the cell membrane and may only be uptaken by phagocytosis or endocytosis. In contrast, smaller-sized AgNPs might directly penetrate the cell membrane, and thus the interaction between smaller-sized AgNPs and cPBMCs might be different from that in the previous study using larger-sized AgNPs.

The results of TEM in our study demonstrated that C-AgNP₂₀ agglomerated in the intracytoplasmic vacuoles of cPMNs, compatible with the results of AMG visualization and a previous study conducted in human neutrophils²⁹. In addition, the presence of amorphous AMG positive signals in the cytoplasm and nucleus of cPMNs suggested that the C-AgNP₂₀ were partially dissolved, released Ag⁺ ions, and caused cytotoxicity^{37,38}. Therefore, although C-AgNP₂₀ were sequestered in the intracytoplasmic vacuoles of cPMNs, they could still induce certain negative effects due to the intracellular dissolution. Conversely, diffuse AMG positive signals found in cPBMCs suggested that the C-AgNP₂₀ might be diffusely dispersed in the cytoplasm and nuclei of cPBMCs. However, no particles of C-AgNP₂₀ were found under TEM. As above, our results suggest that the C-AgNP₂₀ directly penetrated into the cytoplasm and nuclei of cPBMCs, intracellularly dissolved (Trojan-horse type mechanism), and thereby induced a stronger cytotoxicity in cPBMCs than in cPMNs. Furthermore, it is also suggested that the cytotoxicity of C-AgNP₂₀ on cPMNs and cPBMCs may be associated with the particles themselves and the released Ag⁺ ions.

ROS are strongly bactericidal but may also cause damage to the cell itself, driving the cell into apoptosis³⁹. A previous study using citrate-coated AgNPs (20 and 70 nm) found that AgNPs did not significantly increase ROS production in human PMNs³⁰. Nevertheless, other studies using PVP-coated AgNPs (10 nm and 50 nm) and uncoated AgNPs (15 nm) demonstrated that AgNPs could increase the level of ROS production and thereby induce ROS-dependent cytotoxicity in human PMNs^{28,31}. In the current study, the increased ROS production was observed only in the cPMNs with 10 and 50 µg/ml C-AgNP₂₀ treatment, and significant cytotoxicity was observed in the cPMNs with the same treatments. Therefore, our data suggested that C-AgNP₂₀ may cause cytotoxicity in cPMNs by a ROS-dependent pathway.



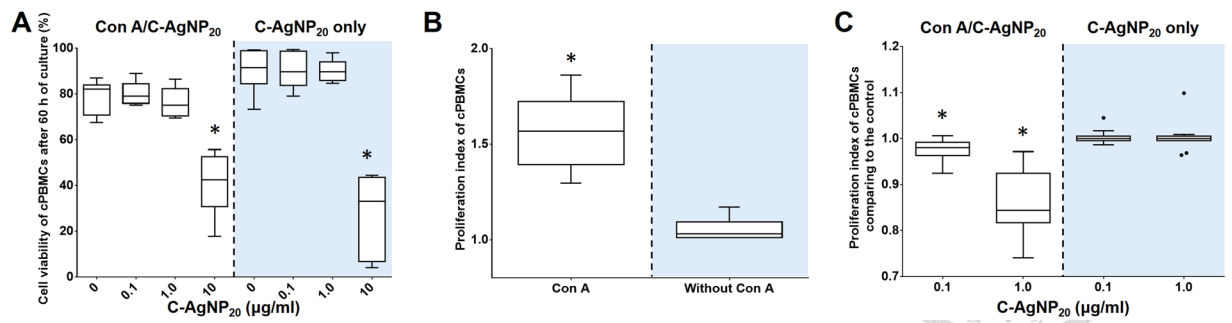


Figure 9. The negative effects of C-AgNP₂₀ on the functional activity of cPBMCs. **(A)** The cell viability of cPBMCs exposed to C-AgNP₂₀ with or without Con A stimulation after 60 h of culture. **(B)** Con A-induced proliferative activity in cPBMCs. **(C)** The effects of C-AgNP₂₀ on the proliferative activity of cPBMCs. The bar in the middle of the box represents the median, and the bottom and top of the box describe the first and third quartiles. The whiskers show the 75th percentile plus 1.5 times IQR and 25th percentile minus 1.5 times IQR of all data, and any values greater than these are defined as outliers and plotted as individual points. Asterisks indicate statistically significant differences from the control ($p < 0.05$, Kruskal-Wallis Test for [A and C]; Mann-Whitney U-test for [B]).

To determine the effects of C-AgNP₂₀ on the functional activity in cPMNs and cPBMCs, sub-lethal doses (0.1 and 1.0 µg/ml) of C-AgNP₂₀ were used in functional activity assays for both cPMNs and cPBMCs. Our data demonstrated that C-AgNP₂₀ at sub-lethal doses could suppress the phagocytosis but stimulate the respiratory burst of cPMNs. A previous study using human PMNs found that the phagocytosis and the respiratory burst were not affected by 10 µM (approximately 1 µg/mL AgNPs [2.0 nm to 34.7 nm in diameter]) after 15 min of incubation⁴⁰. Although the type and size of AgNPs and the protocol in the previous study are different from those in our study, it is still suggested that AgNPs can differently affect the functional activities of PMNs in different animal species. To our knowledge, this is the first study demonstrating that AgNPs can cause suppressive effects on the phagocytosis of PMNs, so the underlying mechanism is still poorly studied. It is speculated that the suppressive phagocytosis may be associated with the restricted expansion capability and/or the impaired phagocytosis of PMNs^{41–43}. In our study, C-AgNP₂₀ were ingested by cPMNs and agglomerated in the intracytoplasmic vacuoles, and it is possible that the expansion capability of cPMNs may be restricted by the presence of intracytoplasmic vacuoles. However, no marked morphocytological alterations were noted on the cPMNs with sub-lethal doses of C-AgNP₂₀, and thus the mechanism of suppressive phagocytosis cannot be solely explained by the restricted expansion capability. On the other hand, the process of phagocytosis in humans can be generally classified into 3 stages, (1) attachment of target particles, (2) pseudopod extensions around attached particles, and (3) engulfment of attached particles in a phagosome⁴³, and defeat in any stage can result in impaired phagocytosis. Previous studies have indicated that contaminants such as heavy metals (mercury, aluminium, and cadmium), polychlorinated biphenyls, and perfluorinated compounds mostly cause a suppressive effect on phagocytosis of cPMNs^{33,44–46}. However, the molecular mechanism of phagocytosis of PMNs in humans and animals is complicated and has not been well-studied, and the molecular mechanism and process of phagocytosis in cetaceans might be different from that in humans. Therefore, further experiments for expanding the knowledge on the molecular mechanism of phagocytosis of cPMNs are required to determine the interactions between AgNPs and phagocytosis of cPMNs.

Our data demonstrated that the respiratory burst of cPMNs was stimulated by C-AgNP₂₀. Several possible mechanisms should be considered to explain the stimulated respiratory burst of cPMNs exposed to C-AgNP₂₀. First, the increased respiratory burst of cPMNs might be associated with the spontaneous ROS production induced by C-AgNP₂₀. However, the increased respiratory burst of cPMNs in the present study cannot be solely explained by the ROS production induced by C-AgNP₂₀ because no significantly increased ROS production was observed in cPMNs exposed to 0.1 and 1.0 µg/ml C-AgNP₂₀. Hence, it is speculated that the number of C-AgNP₂₀ ingested by cPMNs increased during active phagocytosis. Bacteria with appropriate opsonisation are recognized by PMNs via specific surface receptors, and the phagocytosis of PMNs will be activated^{42,43}. In addition, a previous study of interactions between AgNPs and bacteria demonstrated that AgNPs could accumulate in the membrane of bacteria, while some of them might penetrate into the bacteria⁴⁷. Therefore, the bacteria might have been a vector for the C-AgNP₂₀ in our study. Both phenomena could increase the number of C-AgNP₂₀ ingested by cPMNs and thereby increase the ROS production of cPMNs. As above, our data suggest that the increased respiratory burst of cPMNs is associated with spontaneous ROS production induced by C-AgNP₂₀ rather than the oxidative killing of cPMNs against bacteria.

The inhibitory effect caused by C-AgNP₂₀ (0.1 and 1.0 µg/ml) on Con A-induced proliferative activity in cPBMCs was evident in our study. Previous studies have demonstrated that no inhibitory effects on the proliferative activity are noted in human PBMCs treated with <10 µg/ml uncoated AgNPs (1 to 2.5 nm and 75 to 130 nm in diameter), citrate-coated AgNPs (24.3 ± 4.5 nm), and PVP-coated AgNPs (75 ± 20 nm and 21.6 ± 4.8 nm in diameter)^{24–26,32}. This difference suggests that C-AgNP₂₀ can cause proliferative arrest of cPBMCs at relatively lower concentration (≤1 µg/ml), and further implies that cPBMCs are more vulnerable than are human PBMCs. The possible mechanisms on the proliferative arrest induced by C-AgNP₂₀ in cPBMCs include cell cycle arrest,

intracellular calcium transients, chromosomal aberrations, and cytoskeleton deformations^{48–51}. The mechanism of AgNPs on the proliferative arrest in cPBMCs needs further investigation.

The current study presents the first evidence of the cytotoxicity and immunotoxicity of AgNPs on the leukocytes of cetaceans and improves our understanding of environmental safety concerning AgNPs. The dose-response data of AgNPs on the leukocytes of cetaceans are invaluable for evaluating the adverse health effects in cetaceans and for proposing a conservation plan for marine mammals. Furthermore, the suppressive effects on the phagocytosis of cPMNs caused by AgNPs, which were not found in previous human studies, indicate that the underlying immunotoxic mechanisms of AgNPs on the leukocytes of cetaceans may be different from those of humans. Considering the differences of cytotoxicity and immunotoxicity caused by AgNPs between the leukocytes of humans and cetaceans, it is suggested that AgNPs can cause different effects in different animal species in the ecosystem. To comprehensively evaluate the negative impacts of AgNPs on the biosphere, it is crucial to conduct more research to accumulate data on the biological effects of AgNPs in different animal species. However, the differences of AgNP-induced toxicity in different cells/animals may be also associated with the different state (such as coating, sizes, and the intracellular Ag⁺ ions release) of the AgNPs used in the *in vitro/in vivo* models. In addition, a recent study found that AgNPs could be generated from AgNO₃ in culture medium, and the toxic effects induced by Ag⁺ ions and/or AgNPs may not be completely separated by using AgNO₃ as a reference for *in vitro* models with AgNPs⁵². Therefore, further investigations to determine the underlying cytotoxic and immunotoxic mechanisms of AgNPs on the leukocytes of cetaceans with comprehensive AgNPs characterization and a suitable reference of Ag⁺ ions are warranted.

Methods

All the experiments were performed in accordance with international guidelines^{53,54} and the manual for exposure control of nanoparticles in nanotechnology laboratories, which is published by the Institute of Labor, Occupational Safety and Health, Ministry of Labor, Executive Yuan, Taiwan. All reagents were purchased from Sigma-Aldrich (MO, USA) unless otherwise indicated.

AgNPs characterization. C-AgNP₂₀ (Pelco[®] citrate Biopure[™] silver) was purchased from Ted Pella (CA, USA). The AgNPs had been extensively washed without centrifugation to remove trace elements of the supernatant (<0.00001% of trace elements). TEM for determining surface area and size/shape distributions, UV-visible spectroscopy for measuring the optical properties, DLS for determining the particle hydrodynamic diameter and zeta potential were performed by the manufacturer and previous studies^{29,30}. The endotoxin level of C-AgNP₂₀ suspension was examined by ToxinSensor[™] Single Test Kit (GenScript, NJ, USA) and was lower than or equal to 0.015 EU/ml. For characterization, the C-AgNP₂₀ obtained from the manufacturer were suspended in complete RPMI-1640 medium at a concentration of 50 µg/ml, and then examined using a JEM-1400 TEM (JEOL, Japan). Briefly, the C-AgNP₂₀ with complete RPMI-1640 was dropped on the TEM grids, stood for 30 min, and then dried with tissue paper (placed on the border of the grid to absorb the liquid). The size distribution and zeta potential were determined by dynamic light scattering (DLS) through Zetasizer Nano-ZS (Malvern Instruments Inc., MA, USA). Because 1) the relatively high recommended concentration (>100 µg/ml for) of nanoparticles for DLS, and 2) the difficulty on performing DLS in cell culture medium, only 100 and 500 µg/ml C-AgNP₂₀ in 2 mM citrate buffer (pH 7.4) were measured through Zetasizer Nano-ZS in the present study⁵⁵. Measurements were performed in triplicate and shown as means ± SD. The C-AgNP₂₀ were diluted to 1, 10, 100, and 500 µg/ml with 2 mM citrate buffer and instantly used for subsequent experiments. Two mM citrate buffer was used as a vehicle control (0 µg/ml C-AgNP₂₀).

Blood sample collection. Voluntary blood samples were collected from captive dolphins in accordance with international guidelines, and the protocol had been reviewed and approved by the Council of Agriculture of Taiwan (Approval number 1051700175). Samples from six bottlenose dolphins (*Tursiops truncatus*) in Farglory Ocean Park were obtained on a monthly basis from 2015 to 2017. Blood samples were obtained from clinically healthy dolphins with confirmation by history, physical examination, complete blood count, and biochemistry. Forty millilitres of heparin-anticoagulated whole blood were collected, stored, and shipped at 4 °C within 8 hours for subsequent experiments.

Blood sample preparation for subsequent experiments. For cytomorphological examinations, cytotoxicity assays, the detection of ROS production of cPMNs, and functional activity assays of cPBMCs, cetacean peripheral blood leukocytes (cPBLs) were isolated by a slow spin method and a density gradient centrifugation method with minor modifications⁵⁶. The isolated cPBLs were resuspended in RPMI-1640 (Gibco) with 10% ethylenediaminetetraacetic acid (EDTA) and subsequently used in the isolation of cPBMCs by density gradient centrifugation method. After centrifugation at 1200 × g for 30 min at 20 °C, the cPBMCs were collected from the cell layer between the RPMI-1640 (Gibco) and Ficoll-Paque PLUS (GE Healthcare, Uppsala, Sweden), washed with RPMI-1640 twice (if the cells were utilized in proliferative activity assay, the cells were washed with PBS once, and the procedures in the section of “functional activity assay of PBMCs” were followed), and resuspended to a final concentration of 1 × 10⁷ cells/ml in complete RPMI-1640 medium. The bottom sediment was collected and erythrocytes were lysed (Keogh *et al.* 2011). The cPMNs were washed and resuspended to a final concentration of 1 × 10⁷ cells/ml in complete RPMI-1640 medium. The cell viability of cPMNs and cPBMCs was determined by the trypan blue exclusion method using a hemacytometer, and the cell purity based on the cell size (forward-scattered light; FSC) and inner complexity (side-scattered light; SSC) of cPMNs and cPBMCs were determined by FACScalibur flow cytometry (BD, CA, USA). The cPMNs with higher than 90% viability and 90% purity and the cPBMCs with higher than 90% viability and 80% purity were used in this study. The isolated

cPMNs and cPBMCs were kept on ice until utilized in subsequent experiments. For evaluating the effects of C-AgNP₂₀ on the functional activity of cPMNs, the white blood cell (WBC) count of the whole blood sample was determined by VetAutoread Hematology Analyzer (IDEXX Laboratories, ME, USA), and the concentration of WBC of the whole blood sample was adjusted to a final concentration of 5.56×10^6 cells/ml.

Cytomorphological examinations and AMG silver visualization. Freshly isolated cPMNs and cPBMCs (1×10^6 cells/ml in complete RPMI-1640 medium) were exposed to C-AgNP₂₀ at concentrations of 0 and 50 $\mu\text{g/ml}$ in duplicate. After 4 h of culture in an atmosphere of 5% CO₂ at 37 °C, cells were cytocentrifuged (28 \times g; 10 min). One of the cytology slides was stained with Liu's stain (Tonyar Biotech, Taipei, Taiwan) according to the manufacturer's instructions. Another cytology slide was fixed with 100% methanol for 10 min at -20 °C, stained by silver enhancement method^{15,57,58}, and counterstained with hematoxylin for 30 sec. AMG positive signals included golden yellow to black dots to an amorphous golden yellow substance. Freshly isolated cPMNs and cPBMCs (1×10^7 cells/ml in complete RPMI-1640 medium) were exposed to C-AgNP₂₀ at concentrations of 0 and 50 $\mu\text{g/ml}$ for 4 h, fixed with glutaraldehyde (2.5%), and examined using a JEM-1400 TEM (JEOL).

Cytotoxicity assays of cPMNs and cPBMCs. The cytotoxicity of C-AgNP₂₀ in cPMNs and cPBMCs was evaluated by the Annexin V-FITC/PI Apoptosis Detection Kit (Strong Biotech, Taipei, Taiwan) according to the manufacturer's instructions. Briefly, freshly isolated cPMNs and cPBMCs were seeded in 96-well plates at a density of 5×10^5 cells/well and exposed to C-AgNP₂₀ at concentrations of 0, 0.1, 1.0, 10, and 50 $\mu\text{g/ml}$. After 1, 4, and 16 h of culture, cells were collected and resuspended in binding buffer for further analysis by FACScalibur flow cytometry (BD). A total of 8,000 events/sample were acquired. The sub-lethal doses of C-AgNP₂₀ for cPMNs and cPBMCs were determined and further used in the functional activity assays.

Functional activity assays of cPMNs. The effects of C-AgNP₂₀ on the phagocytosis and respiratory burst of cPMNs were separately evaluated by the previously established protocol with minor modifications⁵⁹. Briefly, 200 μl of heparinized whole blood samples was seeded in 48-well plates at a density of 1×10^6 cells/well with or without sub-lethal doses of C-AgNP₂₀ in duplicate. After 1 and 3 h of culture, 40 μl PI labelled *Staphylococcus aureus* (PI-staph) and unlabeled *S. aureus* (U-staph) were added for evaluating phagocytosis and respiratory burst, respectively. The whole blood samples with PI-staph or U-staph were incubated for 30 min in a shaking incubator (200 rpm) at 37 °C. PI-staph and U-staph were added for the final ratio of 30:1 (bacteria to leukocyte) to all relevant tubes. Subsequently, 10 μl DPBS and 10 μl DCFH-DA were added to the whole blood samples with PI-staph and U-staph, respectively. Further incubation for 20 min in a shaking incubator (200 rpm) at 37 °C was performed. Subsequently, the erythrocytes were lysed, washed, and resuspended in 350 μl cold DPBS with 1% paraformaldehyde⁵⁹. The ROS production of cPMNs induced by C-AgNP₂₀ without bacterial stimulation was determined according to previous studies^{30,31}. Briefly, freshly-isolated cPMNs were seeded in 96-well plates at a density of 5×10^5 cells/well with different concentrations of C-AgNP₂₀ (0, 0.1, 1.0, 10, and 50 $\mu\text{g/ml}$) in duplicate. After 1 and 4 h of culture, cPMNs were collected, washed and resuspended in DPBS for flow-cytometric analysis.

Functional activity assay of cPBMCs. To evaluate the effect of C-AgNP₂₀ on the functional activity of cPBMCs, the cell viability of cPBMCs exposed to C-AgNP₂₀ at concentrations of 0, 0.1, 1.0 and 10 $\mu\text{g/ml}$ with or without 2 $\mu\text{g/ml}$ Concanavalin A (Con A; from *Canavalia exsiformis*, Sigma-Aldrich, MO, USA) after 60 h of culture was determined by PI staining method with flow-cytometric analysis³¹. The sub-lethal dose of C-AgNP₂₀ for cPBMCs was used in the functional activity assay of cPBMCs. The effects of C-AgNP₂₀ on the proliferative activity of cPBMCs with or without Con A (Sigma-Aldrich) were evaluated by flow cytometry using the Vybrant CFDA SE cell Tracer Kit (Molecular Probes, Oregon, USA) according to the manufacturer's instructions with minor modifications. Briefly, cPBMCs were isolated, washed, and then resuspended in 5 ml DPBS with 10 mM Carboxyfluorescein succinimidyl ester (CFDA-SE). The cPBMCs were seeded in 96-well plates at a density of 3×10^5 cells/well, and exposed to sub-lethal doses of C-AgNP₂₀ with or without 2 $\mu\text{g/ml}$ Con A. After 60 h of culture, cells were collected, resuspended in 200 μl of Accutase (StemPro® Accutase®, Thermo Fisher Scientific, MA, USA), and incubated for 20 min. The cells were gently resuspended and transferred into 5 ml centrifuge tubes with cold 150 μl DPBS for flow-cytometric analysis using Modfit LT 3.0 software (Verity Software House, ME, USA).

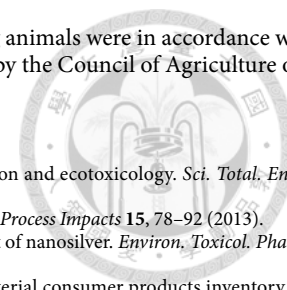
Statistical analysis. All experiments were independently repeated twice in duplicate (N = 12), except the experiments of (1) cell viability of cPBMCs after 60 h of culture and (2) detection of ROS production of cPMNs (N = 6). In all experiments, the results from duplicates were averaged. Individual differences in the ROS production of cPMNs and the functional activity assays of cPMNs and cPBMCs were observed in our study. To compensate for the individual differences, the results at different concentrations of C-AgNP₂₀ for each individual were calculated as percentages of the results of the control⁶⁰. Our data were first checked by Shapiro-Wilk normality test and Brown-Forsythe test, and results indicated that the assumptions of normality and/or equal variance were violated. Therefore, Kruskal-Wallis Test (post hoc test: Dunn's multiple comparison test) was subsequently performed on the data, and the results in each experiment were compared to the control. Exceptionally, the Mann-Whitney U-test was used to compare (1) the cytotoxicity caused by C-AgNP₂₀ between cPMNs and cPBMCs, and (2) the proliferation index between cPBMCs with or without Con A. A p value <0.05 was considered statistically significant, and the analysis was performed in Prism (GraphPad Software, CA, USA). All data were plotted on box-plot graphics. The bar in the middle of the box represented the second quartile (median), and the bottom and top of the box described the first and third quartiles. The whiskers showed the 75th percentile plus 1.5 times IQR and 25th percentile minus 1.5 times IQR of all data, and any values that are greater than these are

defined as outliers and plotted as individual points. Asterisks above the boxplots indicated statistically significant differences compared to the control of each experiment.

Ethical approval. All procedures performed in this study involving animals were in accordance with international guidelines, and the protocol had been reviewed and approved by the Council of Agriculture of Taiwan (Approval number 1051700175).

References

- McGillicuddy, E. *et al.* Silver nanoparticles in the environment: Sources, detection and ecotoxicology. *Sci. Total. Environ.* **575**, 231–246 (2017).
- Yu, S. J., Yin, Y. G. & Liu, J. F. Silver nanoparticles in the environment. *Environ. Sci. Process Impacts* **15**, 78–92 (2013).
- Massarsky, A., Trudeau, V. L. & Moon, T. W. Predicting the environmental impact of nanosilver. *Environ. Toxicol. Pharmacol.* **38**, 861–873 (2014).
- Vance, M. E. *et al.* Nanotechnology in the real world: Redeveloping the nanomaterial consumer products inventory. *Beilstein J. Nanotechnol.* **6**, 1769–1780 (2015).
- Farre, M., Gajda-Schranz, K., Kantiani, L. & Barcelo, D. Ecotoxicity and analysis of nanomaterials in the aquatic environment. *Anal. Bioanal. Chem.* **393**, 81–95 (2009).
- Walters, C. R., Pool, E. J. & Somerset, V. S. Ecotoxicity of silver nanomaterials in the aquatic environment: a review of literature and gaps in nano-toxicological research. *J. Environ. Sci. Health A Tox. Hazard Subst. Environ. Eng.* **49**, 1588–1601 (2014).
- Wang, H. *et al.* Toxicity, bioaccumulation, and biotransformation of silver nanoparticles in marine organisms. *Environ. Sci. Technol.* **48**, 13711–13717 (2014).
- Buffet, P. E. *et al.* A marine mesocosm study on the environmental fate of silver nanoparticles and toxicity effects on two endobenthic species: the ragworm *Hediste diversicolor* and the bivalve mollusc *Scrobicularia plana*. *Sci. Total. Environ.* **470–471**, 1151–1159 (2014).
- Gambardella, C. *et al.* Effect of silver nanoparticles on marine organisms belonging to different trophic levels. *Mar. Environ. Res.* **111**, 41–49 (2015).
- Garcia-Alonso, J. *et al.* Toxicity and accumulation of silver nanoparticles during development of the marine polychaete *Platynereis dumerilii*. *Sci. Total. Environ.* **476–477** (2014).
- Huang, J., Cheng, J. & Yi, J. Impact of silver nanoparticles on marine diatom *Skeletonema costatum*. *J. Appl. Toxicol.* **36**, 1343–1354 (2016).
- Ringwood, A. H., McCarthy, M., Bates, T. C. & Carroll, D. L. The effects of silver nanoparticles on oyster embryos. *Mar. Environ. Res.* **69**(Suppl), S49–51 (2010).
- Espinosa-Cristobal, L. F. *et al.* Toxicity, distribution, and accumulation of silver nanoparticles in Wistar rats. *J. Nanopart. Res.* **15**, <https://doi.org/10.1007/s11051-013-1702-6> (2013).
- Hadrup, N. *et al.* Subacute oral toxicity investigation of nanoparticulate and ionic silver in rats. *Arch. Toxicol.* **86**, 543–551 (2012).
- Kim, Y. S. *et al.* Twenty-eight-day oral toxicity, genotoxicity, and gender-related tissue distribution of silver nanoparticles in Sprague-Dawley rats. *Inhal. Toxicol.* **20**, 575–583 (2008).
- Loeschner, K. *et al.* Distribution of silver in rats following 28 days of repeated oral exposure to silver nanoparticles or silver acetate. *Part. Fibre Toxicol.* **8**, 18, <https://doi.org/10.1186/1743-8977-8-18> (2011).
- Sardari, R. R. R. *et al.* Toxicological effects of silver nanoparticles in rats. *Afr. J. Microbiol. Res.* **6**, 5587–5593 (2012).
- Shahare, B. & Yashpal, M. Toxic effects of repeated oral exposure of silver nanoparticles on small intestine mucosa of mice. *Toxicol. Mech. Methods* **23**, 161–167 (2013).
- Kim, S. & Ryu, D. Y. Silver nanoparticle-induced oxidative stress, genotoxicity and apoptosis in cultured cells and animal tissues. *J. Appl. Toxicol.* **33**, 78–89 (2013).
- Zhang, T., Wang, L., Chen, Q. & Chen, C. Cytotoxic potential of silver nanoparticles. *Yonsei Med. J.* **55**, 283–291 (2014).
- Lee, J. H. *et al.* Biopersistence of silver nanoparticles in tissues from Sprague-Dawley rats. *Part. Fibre Toxicol.* **10**, 36, <https://doi.org/10.1186/1743-8977-10-36> (2013).
- Sung, J. H. *et al.* Subchronic inhalation toxicity of silver nanoparticles. *Toxicol. Sci.* **108**, 452–461 (2009).
- van der Zande, M. *et al.* Distribution, elimination, and toxicity of silver nanoparticles and silver ions in rats after 28-day oral exposure. *ACS Nano* **6**, 7427–7442 (2012).
- Ghosh, M. *et al.* *In vitro* and *in vivo* genotoxicity of silver nanoparticles. *Mutat. Res.* **749**, 60–69 (2012).
- Greulich, C. *et al.* Uptake and intracellular distribution of silver nanoparticles in human mesenchymal stem cells. *Acta. Biomater.* **7**, 347–354 (2011).
- Huang, H. *et al.* An evaluation of blood compatibility of silver nanoparticles. *Sci. Rep.* **6**, 25518, <https://doi.org/10.1038/srep25518> (2016).
- Ivask, A. *et al.* DNA melting and genotoxicity induced by silver nanoparticles and graphene. *Chem. Res. Toxicol.* **28**, 1023–1035 (2015).
- Liz, R., Simard, J. C., Leonardi, L. B. & Girard, D. Silver nanoparticles rapidly induce atypical human neutrophil cell death by a process involving inflammatory caspases and reactive oxygen species and induce neutrophil extracellular traps release upon cell adhesion. *Int. Immunopharmacol.* **28**, 616–625 (2015).
- Poirier, M., Simard, J. C., Antoine, F. & Girard, D. Interaction between silver nanoparticles of 20 nm (AgNP₂₀) and human neutrophils: induction of apoptosis and inhibition of de novo protein synthesis by AgNP₂₀ aggregates. *J. Appl. Toxicol.* **34**, 404–412 (2014).
- Poirier, M., Simard, J. C. & Girard, D. Silver nanoparticles of 70 nm and 20 nm affect differently the biology of human neutrophils. *J. Immunotoxicol.* **13**, 375–385 (2016).
- Soares, T. *et al.* Size-dependent cytotoxicity of silver nanoparticles in human neutrophils assessed by multiple analytical approaches. *Life Sci.* **145**, 247–254 (2016).
- Shin, S. H., Ye, M. K., Kim, H. S. & Kang, H. S. The effects of nano-silver on the proliferation and cytokine expression by peripheral blood mononuclear cells. *Int. Immunopharmacol.* **7**, 1813–1818 (2007).
- Desforges, J. P. *et al.* Immunotoxic effects of environmental pollutants in marine mammals. *Environ. Int.* **86**, 126–139 (2016).
- Chen, M. H. *et al.* Tissue concentrations of four Taiwanese toothed cetaceans indicating the silver and cadmium pollution in the western Pacific Ocean. *Mar. Pollut. Bull.* **124**, 993–1000 (2017).
- Li, W. T. *et al.* Investigation of silver (Ag) deposition in tissues from stranded cetaceans by autometallography (AMG). *Environ. Pollut.* **235**, 534–545 (2018).
- Dobrovolskaia, M. A. & McNeil, S. E. Endotoxin and engineered nanomaterials in *Handbook of immunological properties of engineered nanomaterials* (eds Dobrovolskaia, M. A. & McNeil, S. E.) 77–115 (World Scientific, 2013).
- Park, E. J., Yi, J., Kim, Y., Choi, K. & Park, K. Silver nanoparticles induce cytotoxicity by a Trojan-horse type mechanism. *Toxicol. In Vitro* **24**, 872–878 (2010).



38. Singh, R. P. & Ramarao, P. Cellular uptake, intracellular trafficking and cytotoxicity of silver nanoparticles. *Toxicol. Lett.* **213**, 249–259 (2012).
39. Bylund, J., Björnsdóttir, H., Sundqvist, M., Karlsson, A. & Dahlgren, C. Measurement of respiratory burst products, released or retained, during activation of professional phagocytes in *Neutrophil methods and protocols* (eds Quinn, M. T. & DeLeo, F. R.) 321–338 (Humana Press, 2014).
40. Haase, H., Fahmi, A. & Mahltig, B. Impact of silver nanoparticles and silver ions on innate immune cells. *J Biomed. Nanotechnol.* **10**, 1146–1156 (2014).
41. Evans, E. Kinetics of granulocyte phagocytosis: rate limited by cytoplasmic viscosity and constrained by cell size. *Cell Motil. Cytoskeleton* **14**, 544–551 (1989).
42. Lee, W. L., Harrison, R. E. & Grinstein, S. Phagocytosis by neutrophils. *Microbes Infect.* **5**, 1299–1306 (2003).
43. van Kessel, K. P., Bestebroer, J. & van Strijp, J. A. Neutrophil-Mediated Phagocytosis of *Staphylococcus aureus*. *Front. Immunol.* **5**, 467, <https://doi.org/10.3389/fimmu.2014.00467> (2014).
44. Camara Pellisso, S., Munoz, M. J., Carballo, M. & Sanchez-Vizcaino, J. M. Determination of the immunotoxic potential of heavy metals on the functional activity of bottlenose dolphin leukocytes *in vitro*. *Vet Immunol. Immunopathol.* **121**, 189–198 (2008).
45. Fair, P. A. *et al.* Associations between perfluoroalkyl compounds and immune and clinical chemistry parameters in highly exposed bottlenose dolphins (*Tursiops truncatus*). *Environ. Toxicol. Chem.* **32**, 736–746 (2013).
46. Schwacke, L. H. *et al.* Anaemia, hypothyroidism and immune suppression associated with polychlorinated biphenyl exposure in bottlenose dolphins (*Tursiops truncatus*). *Proc. Biol. Sci.* **279**, 48–57 (2012).
47. Sondi, I. & Salopek-Sondi, B. Silver nanoparticles as antimicrobial agent: a case study on *E. coli* as a model for Gram-negative bacteria. *J. Colloid Interface Sci.* **275**, 177–182 (2004).
48. Asharani, P. V., Hande, M. P. & Valiyaveetil, S. Anti-proliferative activity of silver nanoparticles. *BMC Cell Biol.* **10**, 65, <https://doi.org/10.1186/1471-2121-10-65> (2009).
49. Eom, H. J. & Choi, J. p38 MAPK activation, DNA damage, cell cycle arrest and apoptosis as mechanisms of toxicity of silver nanoparticles in Jurkat T cells. *Environ. Sci. Technol.* **44**, 8337–8342 (2010).
50. Kim, J. A., Aberg, C., Salvati, A. & Dawson, K. A. Role of cell cycle on the cellular uptake and dilution of nanoparticles in a cell population. *Nat. Nanotechnol.* **7**, 62–68 (2011).
51. Panzarini, E. *et al.* Glucose capped silver nanoparticles induce cell cycle arrest in *HeLa* cells. *Toxicol. In Vitro* **41**, 64–74 (2017).
52. Hansen, U. & Thunemann, A. F. Considerations using silver nitrate as a reference for *in vitro* tests with silver nanoparticles. *Toxicol. In Vitro* **34**, 120–122 (2016).
53. American Society for Testing and Materials. Standard guide for handling unbound engineered nanoscale particles in occupational settings. <https://compass.astm.org/download/E2535.19973.pdf> (2013).
54. British Standard Institute. Nanotechnologies – Part 2: Guide to safe handling and disposal of manufactured nanomaterials. <https://shop.bsigroup.com/upload/Shop/Download/Nano/PD6699-2.pdf> (2007).
55. Bhattacharjee, S. DLS and zeta potential - What they are and what they are not? *J. Control Release* **235**, 337–351 (2016).
56. Bossart, G. D. *et al.* Hematological, Biochemical, and Immunological Findings in Atlantic Bottlenose Dolphins (*Tursiops truncatus*) with Orogenital Papillomas. *Aquat. Mamm.* **34**, 166–177 (2008).
57. Loch, L. J., Smidt, K., Rungby, J., Stoltenberg, M. & Larsen, A. Uptake of silver from metallic silver surfaces induces cell death and a pro-inflammatory response in cultured J774 macrophages. *Histol. Histopathol.* **26**, 689–697 (2011).
58. Miller, D. L., Yu, I. J. & Genter, M. B. Use of Autometallography in Studies of Nanosilver Distribution and Toxicity. *Int. J. Toxicol.* **35**, 47–51 (2016).
59. Keogh, M. J. *et al.* Simultaneous measurement of phagocytosis and respiratory burst of leukocytes in whole blood from bottlenose dolphins (*Tursiops truncatus*) utilizing flow cytometry. *Vet. Immunol. Immunopathol.* **144**, 468–475 (2011).
60. Levin, M. *et al.* Immunomodulatory effects upon *in vitro* exposure of California sea lion and southern sea otter peripheral blood leukocytes to domoic acid. *J. Wildl. Dis.* **46**, 541–550 (2010).

Acknowledgements

We thank all the personnel at Farglory Ocean Park (FOP) for assisting in sample collection, the dolphins at FOP for blood donation, and Dr. Bang-Yeh Liou for sample transportation. The authors also acknowledge the support of the Ministry of Science & Technology, Taiwan under Grant MOST 106-2313-B-002-054.

Author Contributions

W.-T.L., conception and design, experiment performance, analysis/interpretation of data, manuscript writing; L.-Y.W., experiment performance, and analysis/interpretation of data; H.-W.C., W.-C.Y., V.F.P. and M.-H.C., conception and design and analysis/interpretation of data; C.L., conception/design and sample collection; C.-R.J., analysis/interpretation of data, critical revision and final approval of the manuscript.

Additional Information

Supplementary information accompanies this paper at <https://doi.org/10.1038/s41598-018-23737-0>.

Competing Interests: The authors declare no competing interests.

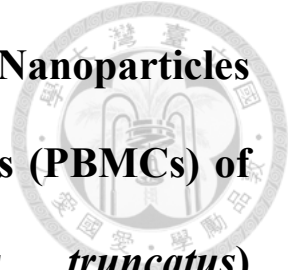
Publisher's note: Springer Nature remains neutral with regard to jurisdictional claims in published maps and institutional affiliations.



Open Access This article is licensed under a Creative Commons Attribution 4.0 International License, which permits use, sharing, adaptation, distribution and reproduction in any medium or format, as long as you give appropriate credit to the original author(s) and the source, provide a link to the Creative Commons license, and indicate if changes were made. The images or other third party material in this article are included in the article's Creative Commons license, unless indicated otherwise in a credit line to the material. If material is not included in the article's Creative Commons license and your intended use is not permitted by statutory regulation or exceeds the permitted use, you will need to obtain permission directly from the copyright holder. To view a copy of this license, visit <http://creativecommons.org/licenses/by/4.0/>.

© The Author(s) 2018

**Chapter V: Th2 Cytokine Bias Induced by Silver Nanoparticles
(AgNPs) in Peripheral Blood Mononuclear Cells (PBMCs) of
Common Bottlenose Dolphins (*Tursiops truncatus*)
(Manuscript in Submission)**



Wen-Ta Li¹, Lei-Ya Wang¹, Hui-Wen Chang¹, Wei-Cheng Yang², Chieh Lo³, Victor Fei Pang¹, Meng-Hsien Chen⁴, Chian-Ren Jeng¹

¹ Graduate Institute of Molecular and Comparative Pathobiology, National Taiwan University, Taipei 10617, Taiwan

² College of Veterinary Medicine, National Chiayi University, Chiayi 60004, Taiwan

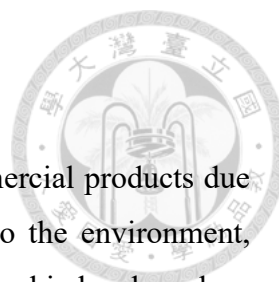
³ Farglory Ocean Park, Hualien 97449, Taiwan

⁴ Department of Oceanography and Asia-Pacific Ocean Research Center, National Sun Yat-sen University, Kaohsiung 80424, Taiwan

Corresponding author: Chian-Ren Jeng¹

No. 1, Sec. 4, Roosevelt Rd., Taipei 10617, Taiwan

Email address: crjeng@ntu.edu.tw



Abstract

Background

Silver nanoparticles (AgNPs) have been widely used in many commercial products due to their excellent antibacterial ability. The AgNPs are released into the environment, gradually accumulate in the ocean, and may affect animals at high trophic level, such as cetaceans and humans, via the food chain. Hence, the negative health impacts caused by AgNPs in cetaceans are of concern. Cytokines play a major role in the modulation of immune system and can be classified into two types, Th1 and Th2. Th1/Th2 balance can be evaluated by the ratios of their polarizing cytokines (i.e., interferon [IFN]- γ /Interleukin [IL]-4), and animals with imbalanced Th1/Th2 response may become more susceptible to certain kinds of infection. Therefore, the present study evaluated the *in vitro* cytokine responses of cetacean peripheral blood mononuclear cells (cPBMCs) to 20 nm citrate-AgNPs (C-AgNP₂₀) by quantitative reverse transcriptase polymerase chain reaction (qRT-PCR).

Methods

Blood samples were collected from six common bottlenose dolphins (*Tursiops truncatus*) in Farglory Ocean Park. The cPBMCs were isolated and utilized for evaluating the *in vitro* cytokine responses of cPBMCs to C-AgNP₂₀ by qRT-PCR. The cytokines evaluated included IL-2, IL-4, IL-10, IL-12, interferon (IFN)- γ , and tumor necrosis factor (TNF)- α . The geometric means of two housekeeping genes (HKGs), glyceraldehyde 3-phosphate dehydrogenase (GAPDH) and β 2-microglobulin (B2M), of each sample were determined and used to normalize the mRNA expression levels of target genes.

Results

The ratio of late apoptotic/necrotic cells of cPBMCs significantly increased with or without concanavalin A (ConA) stimulation after 24 h of 10 μ g/ml C-AgNP₂₀ treatment. At 4 h of culture, the mRNA expression level of IL-10 was significantly decreased with 1 μ g/ml C-AgNP₂₀ treatment. At 24 h of culture with 1 μ g/ml C-AgNP₂₀, the mRNA expression levels of all cytokines were significantly decreased, with the exceptions of IL-4 and IL-10. The IFN- γ /IL-4 ratio was significantly decreased at 24 h of culture with 1 μ g/ml C-AgNP₂₀ treatment, and the IL-12/IL-4 ratio was significantly decreased at 4 or 24 h of culture with 0.1 or 1 μ g/ml C-AgNP₂₀ treatment, respectively. Furthermore, the mRNA expression level of TNF- α was significantly decreased by 1 μ g/ml C-AgNP₂₀ after 24 h of culture.

Discussion

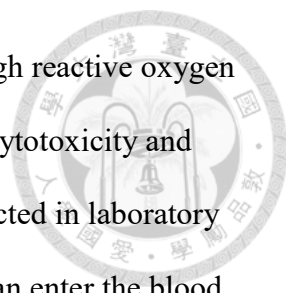
The present study demonstrated that the sublethal dose of C-AgNP₂₀ ($\leq 1 \mu\text{g/ml}$) has an inhibitory effect on the cytokine mRNA expression levels of cPBMCs with the evidence of Th2 cytokine bias and significantly decreased the mRNA expression level of TNF- α . Th2 cytokine bias is associated with enhanced immunity against parasites but decreased immunity to intracellular microorganisms. TNF- α is a contributing factor for the inflammatory response against the infection of intracellular pathogens. In summary, our data indicate that C-AgNP₂₀ suppresses the cellular immune response and thereby increases the susceptibility of cetaceans to infection by intracellular microorganisms.



Introduction

The application of silver nanoparticles (AgNPs) in industry and in consumer products has increased, and the production of AgNPs and the number of AgNP-containing products will increase over time (Massarsky et al. 2014). AgNPs can be released during the production, transport, decay, use, and/or disposal of AgNP-containing products, subsequently draining into the surface water and then accumulating in the marine environment (Farre et al. 2009; Walters et al. 2014). Therefore, the increasing use and growing production of AgNPs, as potential sources of Ag contamination, raise public concerns about the environmental toxicity of Ag (Li et al. 2018a). Previous research has demonstrated that AgNPs can precipitate in marine sediments, be ingested by benthic organisms (such as benthic invertebrate species), enter and be transferred from one trophic level to the next via the food chain, and thereby cause negative effects on the animals at different trophic levels, such as algae, invertebrates and fishes (Buffet et al. 2014; Farre et al. 2009; Gambardella et al. 2015; Huang et al. 2016b; Wang et al. 2014). Previous studies have demonstrated that AgNPs are toxic to all tested marine organisms in a dose-dependent manner, indicating that AgNPs may have negative effects on marine organisms at different trophic levels of the marine environment. Immunotoxic effects of AgNPs have been demonstrated in some aquatic animals such as Nile tilapia and mussel (Gagne et al. 2013; Thummabancha et al. 2016). Nevertheless, to date the potential toxicity of AgNPs on marine mammals such as cetaceans has not been sufficiently studied.

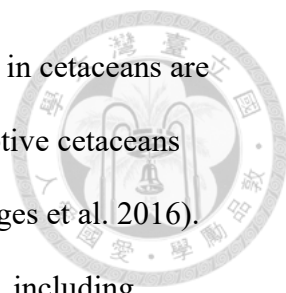
AgNPs have been demonstrated to cause several negative effects, such as hepatitis, nephritis, neuron cell apoptosis, and alteration of gene expression of the brain, on laboratory mammals (Espinosa-Cristobal et al. 2013; Sardari et al. 2012; Shahare & Yashpal 2013). *In vitro* studies using different cell lines have also indicated that AgNPs



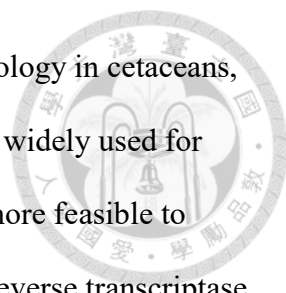
can cause damage to DNA, cell membranes, and mitochondria through reactive oxygen species (ROS) dependent/independent pathways and further induce cytotoxicity and genotoxicity (Kim & Ryu 2013). In addition, previous studies conducted in laboratory mammals, including mice and rats, have demonstrated that AgNPs can enter the blood circulation through alimentary tracts and then deposit in multiple organs (Espinosa-Cristobal et al. 2013; Lee et al. 2013; Shahare & Yashpal 2013; van der Zande et al. 2012). Considering the negative effects of AgNPs and the presence of AgNPs in blood circulation, the negative effects of AgNPs on leukocytes should be of concern. Previous studies have demonstrated that AgNPs can cause several negative effects on human polymorphonuclear leukocytes (PMNs) and peripheral blood mononuclear cells (PBMCs). These studies demonstrated that AgNPs could cause morphological alterations, cytotoxicity, atypical cell death, inhibition of de novo protein synthesis, increased production of the CXCL8 chemokine (IL-8), and impaired lysosomal activity in human neutrophils (Poirier et al. 2014; Poirier et al. 2016; Soares et al. 2016). Only a few studies have investigated the toxicity of AgNPs on human PBMCs, which have shown that AgNPs can cause cytotoxicity and functional perturbations, including inhibition of proliferative activity and cytokine production (Franco-Molina et al. 2016; Ghosh et al. 2012; Huang et al. 2016a; Orta-Garcia et al. 2015; Paino & Zucolotto 2015; Shin et al. 2007).

The environmental contamination level of AgNPs is expected to increase greatly in the near future, and cetaceans, as the top predators in the ocean, will suffer the potentially negative impacts caused by AgNPs. Besides, immunotoxic effects of AgNPs have been demonstrated previously in humans and aquatic animals. Therefore, it is crucial to investigate the immunotoxic effects caused by AgNPs in cetaceans.

Generally, *in vivo* experiments are rarely feasible, and the ethical issues concerning the



study of immunotoxic effects caused by environmental contaminants in cetaceans are difficult to overcome, so *in vitro* study using blood samples from captive cetaceans would be a logical and crucial approach (Beineke et al. 2010; Desforges et al. 2016). Cytokines play a major role in the modulation of the immune system, including lymphocyte proliferation/differentiation, lymphoid development, cell trafficking, and inflammatory response through the interactions between the cytokines themselves and the surface receptors of many different cells (Owen et al. 2013; Tizard 2013a). Previous studies have found that the sequence homology of cytokines among terrestrial and aquatic mammals is low, but conserved molecule regions can still be found on biologically active areas in marine mammals, such as the receptor binding sites of cytokines, suggesting a conserved biological activity of cytokines in both terrestrial and aquatic mammal species (Beineke et al. 2004; Beineke et al. 2010). Therefore, the functions of cytokines on the immune system in cetaceans may be similar to those in mice and humans. Cytokines can be classified into two groups, Th1 and Th2, and their secretion pattern is associated with the balance of Th1 and Th2 responses (Kidd 2003; Owen et al. 2013; Tizard 2013b). Th1 response promotes cell-mediated immune response and thus enhances the immunity against intracellular microorganisms, such as *Toxoplasma gondii* and *Brucella* spp., and a variety of viruses. In contrast, Th2 response is associated with enhanced immunity against parasites but decreased immunity to intracellular microorganisms (Owen et al. 2013; Tizard 2013b). The Th1/Th2 balance can be evaluated by the ratios of their polarizing cytokines (i.e., interferon [IFN]- γ /interleukin [IL]-4), and animals with imbalanced Th1/Th2 response (Th1/Th2 polarization) may become more susceptible to certain kinds of infection (Owen et al. 2013; Raphael et al. 2015; Tizard 2013b).



Cytokine profiling is still a relatively new field of immunotoxicology in cetaceans, and thus the enzyme-linked immunosorbent assay (ELISA) kit is not widely used for cytokine profiling in cetaceans (Desforges et al. 2016). Hence, it is more feasible to study the cytokine profiling by molecular biology (i.e., quantitative reverse transcriptase polymerase chain reaction; qRT-PCR). Therefore, the present study evaluates the *in vitro* cytokine responses of cPBMCs to C-AgNP₂₀ by qRT-PCR. The cytokines measured were as follows: polarizing cytokines of Th1 (IL-12 and IFN- γ) and Th2 (IL-4), and some pro- and anti-inflammatory cytokines (IL-2, IL-10, and tumor necrosis factor [TNF]- α).

Materials and methods

AgNPs characterization

Considering the extensive use of 20 nm citrate-AgNPs (C-AgNP₂₀) in recently reported studies of cetacean and human blood cells (Huang et al. 2016a; Li et al. 2018b; Poirier et al. 2014; Poirier et al. 2016), commercial C-AgNP₂₀ (Pelco[®] citrate Biopure[™] silver; Ted Pella, CA, USA) was chosen. The C-AgNP₂₀ had been extensively washed (without centrifugation) so that the level of trace elements becomes less than 0.000001%. Transmission electron microscopy (TEM) for determining surface area and size/shape distributions, UV-visible spectroscopy for measuring the optical properties, particle hydrodynamic diameter and zeta potential, and dynamic light scattering (DLS) for determining the size distribution were performed according to the manufacturer's instructions and previous studies (Poirier et al. 2014; Poirier et al. 2016). The endotoxin level of C-AgNP₂₀ suspension was examined by ToxinSensor[™] Single Test Kit (GenScript, NJ, USA), and it was lower than or equal to 0.015 EU/ml. For characterization, the C-AgNP₂₀ obtained from the manufacturer were suspended in complete RPMI-1640 medium (RPMI-1640 [Gibco, NY, USA] with 10% fetal bovine serum, 2mM L-glutamine, 50 IU penicillin, and 50 μ g streptomycin) at a concentration of 50 μ g/ml, and then examined using a JEM-1400 (JEOL, Japan) TEM. The size distribution and zeta potential of the C-AgNP₂₀ were determined through Zetasizer Nano-ZS (Malvern Instruments Inc., MA, USA) (Table 1). Measurements were performed by using 100 and 500 μ g/ml C-AgNP₂₀ in 2 mM citrate buffer (pH 7.4). The C-AgNP₂₀ were

diluted to 1, 10, and 100 $\mu\text{g/ml}$ with 2 mM citrate buffer and instantly used for subsequent experiments. Two mM citrate buffer was used as a vehicle control (0 $\mu\text{g/ml}$ C-AgNP₂₀).

Animals and blood sample collection

All procedures involving animals were conducted in accordance with international guidelines, and the protocol had been reviewed and approved by the Council of Agriculture of Taiwan (Approval number 1051700175). Voluntary blood samples were obtained from six clinically healthy bottlenose dolphins (*Tursiops truncatus*) with confirmation by physical examination, complete blood count, and biochemistry on a monthly basis from 2015 to 2017 at Farglory Ocean Park. Forty millilitres of heparin-anticoagulated whole blood were collected, stored, and shipped at 4 °C within 8 hours for subsequent experiments.

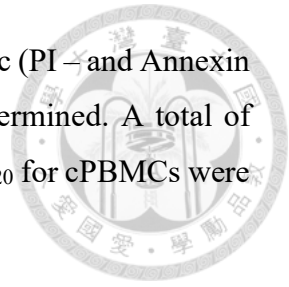
Isolation of cPBMCs

Cetacean peripheral blood leukocytes (cPBLs) were collected by slow spin method with minor modifications (Bossart et al. 2008). The isolated cPBLs were resuspended in RPMI-1640 (Gibco, NY, USA) with 10% ethylenediaminetetraacetic acid (EDTA) and subsequently used in the isolation of cPBMCs by density gradient centrifugation method. After centrifugation at 1200 $\times g$ for 30 min at 20 °C, the cPBMCs were collected from the cell layer between the RPMI-1640 (Gibco) and Ficoll-Paque PLUS (GE Healthcare, Uppsala, Sweden), washed with RPMI-1640 twice, resuspended to a final concentration of 1×10^7 cells/ml in complete RPMI-1640 media, and kept on ice until they were utilized in subsequent experiments. The cell viability of cPBMCs was determined by the trypan blue exclusion method using a hemacytometer, and the cell purity based on the cell size (forward-scattered light; FSC) and inner complexity (side-scattered light; SSC) of cPBMCs were determined by FACScalibur flow cytometry (BD, CA, USA). The cPBMCs with higher than 90% viability and 80% purity were used in this study.

Determination of the sub-lethal dose of C-AgNP₂₀ on cPBMCs with/without concanavalin A (ConA)

The cytotoxicity of C-AgNP₂₀ on cPBMCs was evaluated by the Annexin V-FITC/PI Apoptosis Detection Kit (Strong Biotech, Taipei, Taiwan) according to the manufacturer's instructions. Freshly-isolated cPBMCs were seeded in 96-well plates at a density of 5×10^5 cells/well and exposed to C-AgNP₂₀ at concentrations of 0, 0.1, 1.0 and 10 $\mu\text{g/ml}$ with or without 2 $\mu\text{g/ml}$ ConA (Sigma-Aldrich, MO, USA). After 24 h of culture, cells were collected and resuspended in binding buffer for further analysis by

FACScalibur flow cytometry (BD). The percentages of early apoptotic (PI – and Annexin +) and late apoptotic/necrotic cells (PI + and Annexin +) were determined. A total of 8,000 events/sample were acquired. The sub-lethal doses of C-AgNP₂₀ for cPBMCs were determined and subsequently used in the cytokine expression assay.



qRT-PCR efficiency of each primer sets

The primer sets used in cytokine expression assay are summarized in Table 2. The amplification efficiency (E) of qRT-PCR with each primer set was evaluated by the slope and R² of standard curves using the equation: $E = 10^{-(1/\text{slope})} - 1$ (Svec et al. 2015). The standard templates for qRT-PCR with target primer sets were prepared by serial dilution of PCR products, which were amplified from cDNA samples of isolated cPBMCs with target primer sets. The PCR product was 500-fold diluted with subsequent six steps of serial 10-fold dilutions, and subsequently used for qRT-PCR. The Cycle threshold (Ct) values of each dilution were evaluated by qRT-PCR with each primer set to generate the standard curves.

Extraction of RNA, synthesis of cDNA and qRT-PCR

Total RNA was extracted from blood samples by RNeasy[®] Mini Kit (Qiagen, Valencia, CA, USA) according to the manufacturer's instructions. The RNA samples were treated with genomic DNA (gDNA) wipeout solution (Qiagen). Treated samples were then tested by qRT-PCR to confirm the absence of residue gDNA prior to cDNA synthesis. The QuantiTect[®] Reverse Transcription kit (Qiagen) was used for cDNA synthesis. The reverse transcription was conducted within 4 hours after RNA extraction. The cDNA from each sample was stored at -20 °C for qRT-PCR. The qRT-PCR was performed on Mastercycler[®] ep realplex (Eppendorf, Hamburg, Germany). Each reaction contained 10 µl of SYBR[®] Advantage[®] qPCR Premix (Clontech, California, USA), 7.2 µl of RNase/DNase-free sterile water, 0.4 µl of each 10 mM forward/reverse primers, and 2 µl of DNA template, and the final volume of each reaction was 20 µl. Two microliters of RNase/DNase-free sterile water was used as the non-template negative control. The thermocycle conditions were set as follows: initial denaturation at 95 °C for 30 s and 40 cycles of denaturation at 95 °C for 10 s, annealing at 60 °C for 20 s, and extension at 72 °C for 30 s with fluorescence detection. Furthermore, the melting curve analysis was performed at the end to identify non-specific amplification. All PCR protocols were performed in accordance with the Minimum Information for Publication of Quantitative

Real-Time PCR Experiments (MIQE) guidelines (Bustin et al. 2009; Taylor & Mrkusich 2014).

Time kinetics of mRNA expression levels of selected cytokines of cPBMCs

To evaluate the time kinetics of mRNA expression levels of selected cytokines in cPBMCs with ConA, the cytokine gene expression levels of cPBMCs with ConA (0.5 µg/ml) were determined by qRT-PCR (N=4). Freshly-isolated cPBMCs were seeded in 96-well plates at a density of 5×10^5 cells/well and incubated for 0, 4, 8, 12, 16, 20 and 24 h of culture in a humidified atmosphere of 5 % CO₂ at 37 °C. Then the cPBMCs were collected for subsequent mRNA extraction, complementary DNA (cDNA) synthesis, and qRT-PCR. The cPBMCs with 0 h incubation were used as control for the calculation of cytokine expression level by $\Delta\Delta CT$ method. In addition, the geometric means of two housekeeping genes (HKGs), glyceraldehyde 3-phosphate dehydrogenase (GAPDH) and $\beta 2$ -microglobulin (B2M), of each sample were determined and used to normalize the expression levels of target genes (Hellemans et al. 2007; Vandesompele et al. 2002).

Effects of C-AgNP₂₀ on mRNA expression levels of selected cytokines of cPBMCs

The cPBMCs were seeded in 96-well plates at a density of 5×10^5 cells/well and exposed to sub-lethal doses of C-AgNP₂₀ with 0.5 µg/ml ConA for 4 and 24 h of culture in a humidified atmosphere of 5 % CO₂ at 37 °C. After incubation, the cPBMCs were collected for subsequent mRNA extraction, cDNA synthesis, and qRT-PCR. PBMCs with 4 and 24 h incubation without C-AgNP₂₀ treatment were used as control for the calculation of cytokine expression level by $\Delta\Delta CT$ method. In addition, the geometric means of two HKGs, GAPDH and B2M, of each sample were determined and used to normalize the expression levels of target genes (Hellemans et al. 2007; Vandesompele et al. 2002). The experiment was independently repeated twice in duplicate (N=12).

Statistical analysis

In all experiments, the results from duplicates were averaged. To compensate for individual differences, the results at different concentrations of C-AgNP₂₀ for each individual were calculated as percentages of the results of the control (exposed to 0 µg/ml C-AgNP₂₀). In addition, Th1/Th2 ratios at different concentrations of C-AgNP₂₀ were determined by the cytokine mRNA ratios of Th1 (IL-12 or INF- γ) and Th2 (IL-4) polarizing cytokines and then compared to the control. Our data were first checked by Shapiro-Wilk normality test and Brown-Forsythe test, and the results indicated that the assumptions of normality and/or equal variance were violated. Therefore, the Kruskal-

Wallis Test (post hoc test: Dunn's multiple comparison test) was subsequently performed on the data. A p value < 0.05 was considered statistically significant, and the analysis was performed in Prism (GraphPad Software, CA, USA). All data were plotted on box-plot graphics. The bar in the middle of the box represented the second quartile (median), and the bottom and top of the box described the first and third quartiles. The whiskers showed that the 75th percentile plus 1.5 times IQR and 25th percentile minus 1.5 times IQR of all data, and any values that greater than these were defined as outliers and plotted as individual points. Asterisks above the boxplots indicated statistically significant differences compared to the control of each experiment.

Results

Characterization of C-AgNP₂₀

The C-AgNP₂₀ in complete RPMI-1640 media were spherical and close to 20 nm in diameter (Fig. 1). The size distributions and zeta potentials of C-AgNP₂₀ (100 or 500 $\mu\text{g/ml}$) in 2 mM citrate buffer are illustrated in Table 1. The size distributions were 30.27 ± 0.18 (100%) and 29.64 ± 0.30 (100%) for C-AgNP₂₀ at 100 and 500 $\mu\text{g/ml}$, respectively. The values of the zeta potential were -38.97 ± 1.33 and -44.2 ± 1.35 mV for C-AgNP₂₀ at 100 and 500 $\mu\text{g/ml}$, respectively. Furthermore, the Poly-dispersity Indexes (PDIs) were 0.12 ± 0.00 and 0.11 ± 0.01 , indicating that the composition of C-AgNP₂₀ in the stock was in a single size mode without aggregates.

Sub-lethal dose of C-AgNP₂₀ in cPBMCs with or without ConA stimulation

The treatment of C-AgNP₂₀ at 10 $\mu\text{g/ml}$ significantly increased the ratios of late apoptotic/necrotic cells in cPBMCs with or without ConA stimulation. The ratios of early apoptotic and late apoptotic/necrotic cells of cPBMCs with different concentrations of C-AgNP₂₀ as compared to the control are presented in Fig. 2. After 24 h of 10 $\mu\text{g/ml}$ C-AgNP₂₀ treatment, the ratios of late apoptotic/necrotic cells of cPBMCs significantly increased with (median \pm interquartile range (IQR): 3.55 ± 3.42 ; $p=0.0073$) or without ConA stimulation (median \pm IQR: 1.78 ± 2.24 ; $p=0.0103$). In contrast, no statistically significant increases in the ratios of apoptotic and late apoptotic/necrotic cells in cPBMCs were found after 24 h culture with 0.1 and 1.0 $\mu\text{g/ml}$ C-AgNP₂₀ treatments. Therefore,

0.1 and 1.0 $\mu\text{g/ml}$ C-AgNP₂₀ were defined as the sub-lethal doses for cPBMCs and used in the subsequent mRNA expression levels of selected cytokines in cPBMCs to C-AgNP₂₀.

qRT-PCR efficiency of each primer set

Amplification efficiency (E) values for selected HKGs and cytokine genes, including GAPDH, B2M, IL-2, IL-4, IL-10, and IL-12, IFN- γ , and TNF- α , ranged from 91.08 to 101.48% with $R^2 > 0.99$. The results are summarized in Table 2.

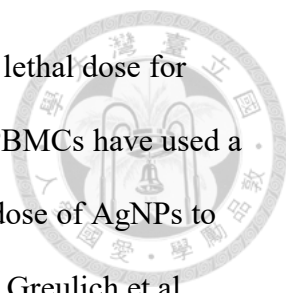
Time kinetics of mRNA expression levels of selected cytokines of cPBMCs with ConA stimulation

The mRNA expression levels of IL-2 and TNF- α were significantly increased at 4 h of culture, gradually decreased from 8 to 20 h of culture, and then mildly but not significantly increased at 24 h of culture. The mRNA expression level of IFN- γ was significantly increased at 4 h of culture, gradually decreased at 8 and 12 h of culture, and then increased from 16 to 24 h of culture. In addition, IL-4, IL-10, and IL-12 were significantly increased at 4 h of culture and gradually decreased over time. Therefore, the time points chosen for the following experiments were 4 h and 24 h. All the results are illustrated in Fig. 3.

Effects of C-AgNP₂₀ on mRNA expression levels of selected cytokines in cPBMCs

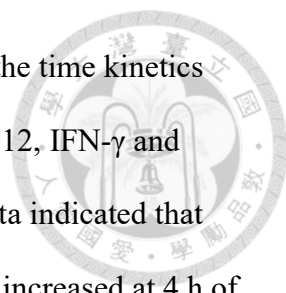
At 4 h of culture, the mRNA expression level of IL-10 was significantly decreased (median \pm IQR: 0.7864 ± 0.2355 ; $p=0.0049$) at 1 $\mu\text{g/ml}$ C-AgNP₂₀, but no significant differences were observed in the mRNA expression levels of other cytokine genes at 0.1 or 1 $\mu\text{g/ml}$ C-AgNP₂₀ (Figs. 4). Following 24 h of culture with 1 $\mu\text{g/ml}$ C-AgNP₂₀, the mRNA expression levels of IL-2, IL-12, IFN- γ , and TNF- α were significantly decreased, but no significant difference was found in those of IL-4 and IL-10. Furthermore, the mRNA expression levels of IL-12 (median \pm IQR: 0.8337 ± 0.2088 ; $p=0.0339$) and IFN- γ (median \pm IQR: 0.7894 ± 0.389 ; $p=0.0164$) were also significantly decreased at 0.1 $\mu\text{g/ml}$ C-AgNP₂₀ (Figs. 4). The Th1/Th2 bias was defined by the ratios of Th1 and Th2 polarizing cytokines. The IFN- γ /IL-4 ratio was significantly decreased following 24 h of culture with 1 $\mu\text{g/ml}$ C-AgNP₂₀, and the IL-12/IL-4 ratio was significantly decreased following 4 or 24 h of culture with 0.1 or 1 $\mu\text{g/ml}$ C-AgNP₂₀ treatments. Overall, the *in vitro* cytokine responses of cPBMCs with C-AgNP₂₀ treatments were biased toward Th2 cytokine response (Fig. 5).

Discussion



Our data indicated that the concentration of 10 $\mu\text{g/ml}$ C-AgNP₂₀ was lethal dose for cPBMCs after 24 h of culture. Although previous studies of human PBMCs have used a variety of AgNPs (including different sizes and coatings), the lethal dose of AgNPs to human PBMCs is generally higher than 10 $\mu\text{g/ml}$ (Ghosh et al. 2012; Greulich et al. 2011; Huang et al. 2016a; Orta-Garcia et al. 2015; Paino & Zucolotto 2015; Shin et al. 2007). Therefore, our data suggest that cPBMCs may be more vulnerable than human PBMCs to the cytotoxic effects of C-AgNP₂₀. However, previous studies have demonstrated that the toxicity and physicochemical characteristics of AgNPs are associated with their surface coating and size (Kim & Ryu 2013), and thus further investigation using the same AgNPs from the same manufacturer is necessary to compare the differences of susceptibility between cetaceans and humans. In addition, the negative effects of AgNPs with different sizes and coatings on the cPBMCs are also worth to be further studied.

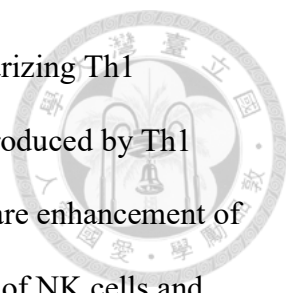
It has been demonstrated that ConA (a selective T-cell mitogen) induces proliferative activity and gene expression of cytokines in bottlenose dolphins, but no information is available regarding the time course (Hofstetter et al. 2017; Segawa et al. 2013; Sitt et al. 2008). Previous studies on ConA-induced cytokine mRNA expression levels of cPBMCs only presented one or two time points (Segawa et al. 2013; Sitt et al. 2008). Sitt et al. (2008) quantified the ConA-induced cytokine mRNA expression levels of cPBMCs after 48 h of treatment, but the reason for choosing this time point was not explained. Their results showed that the mRNA expression levels of IL-2, IL-4, IL-12, and IFN- γ in cPBMCs are induced after 48 h of ConA stimulation, but those of IL-10 and TNF- α were not increased (Sitt et al. 2008). The other study demonstrated that the mRNA expression level of IL-10 in cPBMCs increased after 6 h of ConA stimulation (Segawa et al. 2013). Therefore, to apply appropriate time points for studying the effects



of C-AgNP₂₀ on the cytokine mRNA expression levels of cPBMCs, the time kinetics (from 0 to 24 h) of mRNA expression levels of IL-2, IL-4, IL-10, IL-12, IFN- γ and TNF- α in cPBMCs with ConA stimulation were investigated. Our data indicated that the mRNA expression levels of all cytokine genes were significantly increased at 4 h of ConA stimulation and then gradually decreased with time. A longer incubation time was not possible in our study because the cell numbers of isolated cPBMCs were insufficient.

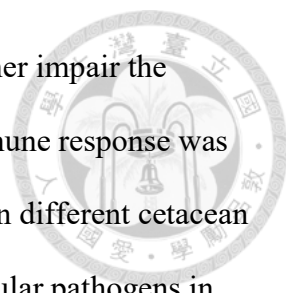
Previous studies have investigated the negative effects of AgNPs on cytokines in human PBMCs (Franco-Molina et al. 2016; Greulich et al. 2011; Shin et al. 2007). Uncoated AgNPs (1.5 nm; 1 to 2.5 nm in diameter) significantly inhibited the phytohemagglutinin (PHA)-induced IL-5, IFN- γ , and TNF- α production respectively at concentrations $\geq 10 \mu\text{g/ml}$, $\geq 3 \mu\text{g/ml}$, and $\geq 3 \mu\text{g/ml}$ in human PBMCs (Shin et al. 2007). It was reported that uncoated AgNPs (100 nm; 90 to 190 nm in diameter) at $0.0175 \mu\text{g/ml}$ can inhibit both PHA and ConA-induced IL-2 production in human PBMCs (Franco-Molina et al. 2016). Furthermore, polyvinylpyrrolidone (PVP)-coated AgNPs ($75 \pm 20 \text{ nm}$) of 5 to $20 \mu\text{g/ml}$ significantly increased the generations of IL-6 and IL-8 but significantly decreased the release of IL-1ra from human PBMCs, while PVP-coated AgNPs did not affect the productions of IL-2, IL-4 and TNF- α (Greulich et al. 2011). As mentioned above, the effects of AgNPs on cytokine production in human PBMCs remain inconclusive.

The mRNA expression levels of IL-4 and IFN- γ were mildly increased and that of IL-12 was seemingly unaffected at 4 h of C-AgNP₂₀ treatment. IL-4, as a polarizing Th2 cytokine, is mainly produced by T cells (especially the Th2 subset) and mast cells, and it promotes the differentiation of naïve T cells to Th2 cells, stimulates the growth and differentiation of B cells, and induces class switching to IgE, which may promote



allergic responses (Owen et al. 2013; Tizard 2013b). IFN- γ , as a polarizing Th1 cytokine and a key mediator of cell-mediated immune response, is produced by Th1 cells, cytotoxic T cells, and NK cells. The major functions of IFN- γ are enhancement of Th1 differentiation, inhibition of Th2 differentiation, and activations of NK cells and macrophages (Owen et al. 2013; Tizard 2013b). IL-12 is also a polarizing Th1 cytokine and is produced by dendritic cells, monocytes, macrophages and B cells. IL-12 induces differentiation of Th1 cells, increases IFN- γ production by T cells and NK cells, and enhances NK and cytotoxic T cell activity (Owen et al. 2013; Tizard 2013b). This mixed pattern of Th1 and Th2 cytokines may be indicative of a mixed Th1/Th2 cytokine response of cPBMCs at 4 h of C-AgNP₂₀ treatment. However, considering the significant decrease in the IL-12/IL-4 ratio, Th2 cytokine response is still predominant in cPBMCs following 4 h of C-AgNP₂₀ treatment. The mRNA expression levels of IL-12 and IFN- γ were significantly decreased by 0.1 or 1 $\mu\text{g/ml}$ C-AgNP₂₀, and that of IL-4 was seemingly unaffected, in cPBMCs following 24 h of culture. The significantly decreased Th1/Th2 (i.e., IFN- γ /IL-4 and IL-12/IL-4) ratios suggested that the immune response of cPBMCs following 24 h of C-AgNP₂₀ treatment is Th2 biased.

Furthermore, the mRNA expression level of TNF- α was significantly decreased by 1 $\mu\text{g/ml}$ C-AgNP₂₀ after 24 h of culture. TNF- α is a cytokine specifically useful to measure the inflammatory state of an animal and it is primarily produced by macrophages and both Th1 and Th2 cells in response to both acute and chronic conditions (Eberle et al. 2018). Previous studies have demonstrated that TNF- α is a contributing factor in the inflammatory response against infection of intracellular micropathogens such as *Plasmodium* spp., *T. gondii*, *Leishmania major*, and *Trypanosoma* spp. (Korner et al. 2010). Hence, our data indicate that C-AgNP₂₀ induced a Th2 biased immune response and suppressed the mRNA expression level of TNF- α in



cPBMCs, which may weaken the cellular immune response and further impair the immunity against intracellular organisms and virus. Similar Th2 immune response was observed in other studies that evaluated the expression of cytokines in different cetacean tissues (Jaber et al. 2010). A variety of infections caused by intracellular pathogens in cetaceans have been reported and may be associated with the mass stranding events of cetaceans (Cvetnic et al. 2016; Domingo et al. 1990; Domingo et al. 1992; Dubey et al. 2007; Dubey et al. 2008; Mazzariol et al. 2016; Mazzariol et al. 2017). In addition, previous studies suggested that Ag contamination exists in all aspects of the marine ecosystem, and cetaceans may have been negatively affected by Ag contamination (Becker et al. 1995; Caceres-Saez et al. 2013; Chen et al. 2017; Dehn et al. 2006; Kunito et al. 2004; Li et al. 2018a; Mendez-Fernandez et al. 2014; Reed et al. 2015; Rosa et al. 2008; Seixas et al. 2009; Woshner et al. 2001). The direct correlation between the infection of intracellular pathogens and the severity of Ag contamination in cetaceans is worth studying.

Following 4 h of 1 µg/ml C-AgNP₂₀ treatment, the mRNA expression level of IL-10 was significantly decreased and that of IL-2 was mildly increased. In other words, mRNA expression levels of IL-2 and IL-10 were respectively upregulated and downregulated by C-AgNP₂₀ in cPBMCs. Subsequently, the mRNA expression level of IL-2 was significantly decreased, and that of IL-10 seemingly unaffected, in cPBMCs following 24 h of treatment of 1 µg/ml C-AgNP₂₀. IL-2, which is produced by activated T cells, can stimulate proliferation and differentiation of T and B cells and activates NK cells (Owen et al. 2013; Tizard 2013b). However, a growing body of evidence has indicated that IL-2 is crucial for the development and function of regulatory T cells (Treg cells), which secrete effector cytokines, such as IL-10, to control and modulate the immunity to self, neoplasia, microorganisms, and grafts (Owen et al. 2013; Pérol &

Piaggio 2016). Considering the roles of IL-2 and IL-10 in immune tolerance, it is speculated that C-AgNP₂₀ may play a significant role in peripheral immune tolerance by regulating the balance between IL-2 and IL-10 (Pérol & Piaggio 2016; Veiopoulou et al. 2004).

The effect of C-AgNP₂₀ on the ConA-induced mRNA expression levels of the selected cytokines in cPBMCs is mainly inhibitory. A previous study found that PVP-AgNPs (10, 25, 40, 45, and 110 nm in diameter) could bind to RNA polymerase, disturb the process of RNA transcription, and thus decreased the overall RNA synthesis in mouse erythroid progenitor cells (Wang et al. 2013). Although the down-regulation of mRNA expression levels may be associated with decreased RNA synthesis due to the direct interaction between C-AgNP₂₀ and RNA polymerase, it cannot fully explain the unaffected Th2 cytokines (IL-4 and IL-10) of cPBMCs in this study. On the other hand, the ConA-induced proliferative activity of cPBMCs is inhibited by 0.1 and 1.0 µg/ml C-AgNP₂₀ (Li et al. 2018b), and this phenomenon may be associated with the decreased mRNA expression levels of IL-2, IL-12, IFN-γ, and TNF-α and/or a suppressive effect on DNA/RNA synthesis induced by ConA. Further investigation on the underlying mechanism of AgNPs in cetacean leukocytes is important to ascertain the negative health impact caused by AgNPs on cetaceans, and such investigation would improve the understanding of the potential hazards of AgNPs to environmental condition and human health.

Furthermore, although the biodistribution of AgNPs or Ag in cetaceans is still undetermined, previous *in vivo* studies of AgNPs by oral exposure in laboratory rats demonstrated that the Ag concentration in the liver is approximately 10 times higher than that in the blood or plasma (Lee et al. 2013; Loeschner et al. 2011; van der Zande et al. 2012). Based on these animal models, it is presumed that the Ag concentrations in the blood of cetaceans may range from 0.01 to 72.6 µg/ml (Chen et al. 2017; Li et al. 2018a).

Although previous studies have indicated that the status of AgNPs in the aquatic environment is complicated and variable (i.e., the concentrations of AgNPs and other Ag/Ag compounds are still undetermined in cetaceans)(Levard et al. 2012; Massarsky et al. 2014), our data suggest that cetaceans may be negatively affected by AgNPs.

Conclusions

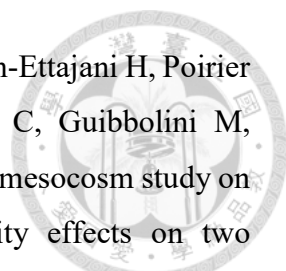
The present study has demonstrated 1) the sublethal dose of C-AgNP₂₀ to cPBMCs ($\leq 1 \mu\text{g/ml}$), 2) the time kinetics of mRNA expression levels of selected cytokines in cPBMCs, and 3) the inhibitory effect of C-AgNP₂₀ (0.1 and 1 $\mu\text{g/ml}$) on the mRNA expression levels of selected cytokines of cPBMCs with evidence of Th2 cytokine bias. Taken together, C-AgNP₂₀ may suppress the cellular immune response and thus inhibit the immunity against intracellular microorganisms in cetaceans.

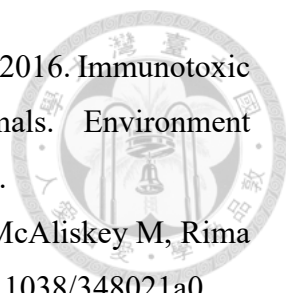
Acknowledgements


We thank all the personnel of Farglory Ocean Park for blood sample collection and storage, the dolphins in Farglory Ocean Park for donating their blood, and Dr. Bang-Yeh Liou for blood sample transportation.


References

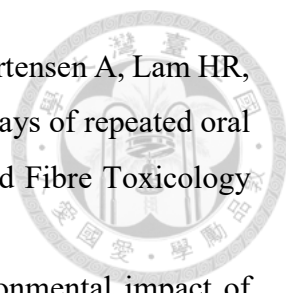
- Becker P, Mackey E, Demiralp R, Suydam R, Early G, Koster B, Wise S. 1995. Relationship of silver with selenium and mercury in the liver of two species of toothed whales (odontocetes). *Marine Pollution Bulletin* 30:262-271. DOI: 10.1016/0025-326X(94)00176-A.
- Beineke A, Siebert U, van Elk N, Baumgartner W. 2004. Development of a lymphocyte-transformation-assay for peripheral blood lymphocytes of the harbor porpoise and detection of cytokines using the reverse-transcription polymerase chain reaction. *Veterinary Immunology and Immunopathology* 98:59-68. DOI: 10.1016/j.vetimm.2003.10.002.
- Beineke A, Siebert U, Wohlsein P, Baumgartner W. 2010. Immunology of whales and dolphins. *Veterinary Immunology and Immunopathology* 133:81-94. DOI: 10.1016/j.vetimm.2009.06.019.
- Bossart GD, Romano TA, Peden-Adams MM, Rice CD, Fair PA, Goldstein JD, Kilpatrick D, Cammen K, Reif JS. 2008. Hematological, biochemical, and immunological findings in Atlantic bottlenose dolphins (*Tursiops truncatus*) with orogenital papillomas. *Aquat Mamm* 34:166-177. DOI: 10.1578/AM.34.2.2008.166.

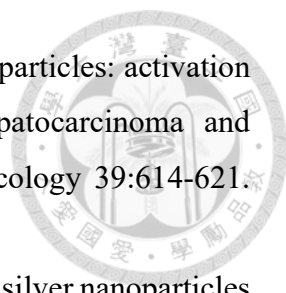
- 
- Buffet PE, Zalouk-Vergnoux A, Chatel A, Berthet B, Metais I, Perrein-Ettajani H, Poirier L, Luna-Acosta A, Thomas-Guyon H, Risso-de Faverney C, Guibbolini M, Gilliland D, Valsami-Jones E, Mouneyrac C. 2014. A marine mesocosm study on the environmental fate of silver nanoparticles and toxicity effects on two endobenthic species: the ragworm *Hediste diversicolor* and the bivalve mollusc *Scrobicularia plana*. *Science of the Total Environment* 470-471:1151-1159. DOI: 10.1016/j.scitotenv.2013.10.114.
- Bustin SA, Benes V, Garson JA, Hellemans J, Huggett J, Kubista M, Mueller R, Nolan T, Pfaffl MW, Shipley GL, Vandesompele J, Wittwer CT. 2009. The MIQE guidelines: minimum information for publication of quantitative real-time PCR experiments. *Clinical Chemistry* 55:611-622. DOI: 10.1373/clinchem.2008.112797.
- Caceres-Saez I, Ribeiro Guevara S, Dellabianca NA, Goodall RN, Cappozzo HL. 2013. Heavy metals and essential elements in Commerson's dolphins (*Cephalorhynchus c. commersonii*) from the southwestern South Atlantic Ocean. *Environmental Monitoring and Assessment* 185:5375-5386. DOI: 10.1007/s10661-012-2952-y.
- Chen IH, Chou LS, Chou SJ, Wang JH, Stott J, Blanchard M, Jen IF, Yang WC. 2015. Selection of suitable reference genes for normalization of quantitative RT-PCR in peripheral blood samples of bottlenose dolphins (*Tursiops truncatus*). *Scientific Reports* 5:15425. DOI: 10.1038/srep15425.
- Chen MH, Zhuang MF, Chou LS, Liu JY, Shih CC, Chen CY. 2017. Tissue concentrations of four Taiwanese toothed cetaceans indicating the silver and cadmium pollution in the western Pacific Ocean. *Marine Pollution Bulletin* 124:993-1000. DOI: 10.1016/j.marpolbul.2017.03.028.
- Cvetnic Z, Duvnjak S, Duras M, Gomercic T, Reil I, Zdelar-Tuk M, Spicic S. 2016. Evidence of *Brucella* strain ST27 in bottlenose dolphin (*Tursiops truncatus*) in Europe. *Veterinary Microbiology* 196:93-97. DOI: 10.1016/j.vetmic.2016.10.013.
- Dehn LA, Follmann EH, Thomas DL, Sheffield GG, Rosa C, Duffy LK, O'Hara TM. 2006. Trophic relationships in an Arctic food web and implications for trace metal transfer. *Science of the Total Environment* 362:103-123. DOI: 10.1016/j.scitotenv.2005.11.012.

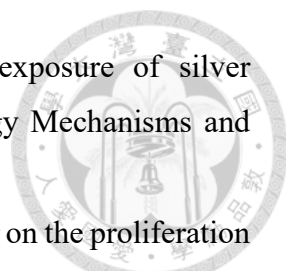
- 
- Desforges JP, Sonne C, Levin M, Siebert U, De Guise S, and Dietz R. 2016. Immunotoxic effects of environmental pollutants in marine mammals. *Environment International* 86:126-139. DOI: 10.1016/j.envint.2015.10.007.
- Domingo M, Ferrer L, Pumarola M, Marco A, Plana J, Kennedy S, McAliskey M, Rima BK. 1990. Morbillivirus in dolphins. *Nature* 348:21. DOI: 10.1038/348021a0.
- Domingo M, Visa J, Pumarola M, Marco AJ, Ferrer L, Rabanal R, Kennedy S. 1992. Pathologic and immunocytochemical studies of morbillivirus infection in striped dolphins (*Stenella coeruleoalba*). *Veterinary Pathology* 29:1-10. DOI: 10.1177/030098589202900101
- Dubey JP, Fair PA, Sundar N, Velmurugan G, Kwok OC, McFee WE, Majumdar D, Su C. 2008. Isolation of *Toxoplasma gondii* from bottlenose dolphins (*Tursiops truncatus*). *Journal of Parasitology* 94:821-823. DOI: 10.1645/GE-1444.1.
- Dubey JP, Morales JA, Sundar N, Velmurugan GV, Gonzalez-Barrientos CR, Hernandez-Mora G, Su C. 2007. Isolation and genetic characterization of *Toxoplasma gondii* from striped dolphin (*Stenella coeruleoalba*) from Costa Rica. *Journal of Parasitology* 93:710-711. DOI: 10.1645/GE-1120R.1.
- Eberle KC, Venn-Watson SK, Jensen ED, LaBresh J, Sullivan Y, Kakach L, Sacco RE. 2018. Development and testing of species-specific ELISA assays to measure IFN-gamma and TNF-alpha in bottlenose dolphins (*Tursiops truncatus*). *PLoS One* 13:e0190786. DOI: 10.1371/journal.pone.0190786
- Espinosa-Cristobal LF, Martinez-Castanon GA, Loyola-Rodriguez JP, Patino-Marin N, Reyes-Macias JF, Vargas-Morales JM, Ruiz F. 2013. Toxicity, distribution, and accumulation of silver nanoparticles in Wistar rats. *Journal of Nanoparticle Research* 15:1702. DOI: 10.1007/S11051-013-1702-6.
- Farre M, Gajda-Schranz K, Kantiani L, Barcelo D. 2009. Ecotoxicity and analysis of nanomaterials in the aquatic environment. *Analytical and Bioanalytical Chemistry* 393:81-95. DOI: 10.1007/s00216-008-2458-1.
- Franco-Molina MA, Mendoza-Gamboa E, Zarate-Triviño DG, Coronado-Cerda EE, Alcocer-González JM, Resendez-Pérez D, Rodríguez-Salazar MC, Rivera-Morales LG, Tamez-Guerra R, Rodríguez-Padilla C. 2016. In Vitro Evaluation of Colloidal Silver on Immune Function: Antilymphoproliferative Activity. *Journal of Nanomaterials* 2017:1-12. DOI: 10.1155/2016/4176212

- 
- Gambardella C, Costa E, Piazza V, Fabbrocini A, Magi E, Faimali M, Garaventa F. 2015. Effect of silver nanoparticles on marine organisms belonging to different trophic levels. *Marine Environmental Research* 111:41-49. DOI: 10.1016/j.marenvres.2015.06.001.
- Gagne F, Auclair J, Fortier M, Bruneau A, Fournier M, Turcotte P, Pilote M, Gagnon C. 2013. Bioavailability and immunotoxicity of silver nanoparticles to the freshwater mussel *Elliptio complanata*. *Journal of Toxicology and Environmental Health, Part A* 76:767-777. DOI: 10.1080/15287394.2013.818602.
- Ghosh M, J M, Sinha S, Chakraborty A, Mallick SK, Bandyopadhyay M, Mukherjee A. 2012. In vitro and in vivo genotoxicity of silver nanoparticles. *Mutation Research* 749:60-69. DOI: 10.1016/j.mrgentox.2012.08.007.
- Greulich C, Diendorf J, Gessmann J, Simon T, Habijan T, Eggeler G, Schildhauer TA, Epple M, Koller M. 2011. Cell type-specific responses of peripheral blood mononuclear cells to silver nanoparticles. *Acta Biomaterialia* 7:3505-3514. DOI: 10.1016/j.actbio.2011.05.030.
- Hellemans J, Mortier G, De Paepe A, Speleman F, Vandessompele J. 2007. qBase relative quantification framework and software for management and automated analysis of real-time quantitative PCR data. *Genome Biology* 8:R19. DOI: 10.1186/gb-2007-8-2-r19.
- Hofstetter AR, Eberle KC, Venn-Watson SK, Jensen ED, Porter TJ, Waters TE, Sacco RE. 2017. Monitoring bottlenose dolphin leukocyte cytokine mRNA responsiveness by qPCR. *PLoS One* 12:e0189437. DOI: 10.1371/journal.pone.0189437.
- Huang H, Lai W, Cui M, Liang L, Lin Y, Fang Q, Liu Y, Xie L. 2016a. An evaluation of blood compatibility of silver nanoparticles. *Scientific Reports* 6:25518. DOI: 10.1038/srep25518.
- Huang J, Cheng J, Yi J. 2016b. Impact of silver nanoparticles on marine diatom *Skeletonema costatum*. *Journal of Applied Toxicology* 36:1343-1354. DOI: 10.1002/jat.3325.
- Jaber JR, Perez J, Zafra R, Herraes P, Rodriguez F, Arbelo M, de los Monteros AE, Fernandez A. 2010. Cross-reactivity of anti-human, anti-porcine and anti-bovine cytokine antibodies with cetacean tissues. *Journal of Comparative Pathology* 143:45-51. DOI: 10.1016/j.jcpa.2010.01.001

- 
- Kidd P. 2003. Th1/Th2 balance: the hypothesis, its limitations, and implications for health and disease. *Alternative medicine review* 8:223-246.
- Kim S, Ryu DY. 2013. Silver nanoparticle-induced oxidative stress, genotoxicity and apoptosis in cultured cells and animal tissues. *Journal of Applied Toxicology* 33:78-89. DOI: 10.1002/jat.2792.
- Korner H, McMorran B, Schluter D, Fromm P. 2010. The role of TNF in parasitic diseases: still more questions than answers. *International Journal for Parasitology* 40:879-888. DOI: 10.1016/j.ijpara.2010.03.011.
- Kunito T, Nakamura S, Ikemoto T, Anan Y, Kubota R, Tanabe S, Rosas FC, Fillmann G, Readman JW. 2004. Concentration and subcellular distribution of trace elements in liver of small cetaceans incidentally caught along the Brazilian coast. *Marine Pollution Bulletin* 49:574-587. DOI: 10.1016/j.marpolbul.2004.03.009
- Lee JH, Kim YS, Song KS, Ryu HR, Sung JH, Park JD, Park HM, Song NW, Shin BS, Marshak D, Ahn K, Lee JE, Yu IJ. 2013. Biopersistence of silver nanoparticles in tissues from Sprague-Dawley rats. *Particle and Fibre Toxicology* 10:36. DOI: 0.1186/1743-8977-10-36.
- Levard C, Hotze EM, Lowry GV, Brown GE, Jr. 2012. Environmental transformations of silver nanoparticles: impact on stability and toxicity. *Environmental Science and Technology* 46:6900-6914. DOI: 10.1021/es2037405.
- Li WT, Chang HW, Chen MH, Chiou HY, Liou BY, Pang VF, Yang WC, Jeng CR. 2018a. Investigation of silver (Ag) deposition in tissues from stranded cetaceans by autometallography (AMG). *Environmental Pollution* 235:534-545. DOI: 10.1016/j.envpol.2018.01.010.
- Li WT, Chang HW, Yang WC, Lo C, Wang LY, Pang VF, Chen MH, Jeng CR. 2018b. Immunotoxicity of Silver Nanoparticles (AgNPs) on the Leukocytes of Common Bottlenose Dolphins (*Tursiops truncatus*). *Sci Rep* 8:5593. DOI: 10.1038/s41598-018-23737-0.
- Liz R, Simard JC, Leonardi LB, Girard D. 2015. Silver nanoparticles rapidly induce atypical human neutrophil cell death by a process involving inflammatory caspases and reactive oxygen species and induce neutrophil extracellular traps release upon cell adhesion. *International Immunopharmacology* 28:616-625. DOI: 10.1016/j.intimp.2015.06.030.

- 
- Loeschner K, Hadrup N, Qvortrup K, Larsen A, Gao X, Vogel U, Mortensen A, Lam HR, Larsen EH. 2011. Distribution of silver in rats following 28 days of repeated oral exposure to silver nanoparticles or silver acetate. *Particle and Fibre Toxicology* 8:18. DOI: 10.1186/1743-8977-8-18.
- Massarsky A, Trudeau VL, Moon TW. 2014. Predicting the environmental impact of nanosilver. *Environmental Toxicology and Pharmacology* 38:861-873. DOI: 10.1016/j.etap.2014.10.006.
- Mazzariol S, Centelleghé C, Beffagna G, Povinelli M, Terracciano G, Cocumelli C, Pintore A, Denurra D, Casalone C, Pautasso A, Di Francesco CE, Di Guardo G. 2016. Mediterranean fin whales (*Balaenoptera physalus*) threatened by dolphin morbillivirus. *Emerging Infectious Diseases* 22:302-305. DOI: 10.3201/eid2202.15-0882.
- Mazzariol S, Centelleghé C, Di Provvido A, Di Renzo L, Cardeti G, Cersini A, Fichi G, Petrella A, Di Francesco CE, Mignone W, Casalone C, Di Guardo G. 2017. Dolphin morbillivirus associated with a mass stranding of sperm whales, Italy. *Emerging Infectious Diseases* 23:144-146. DOI: 10.3201/eid2301.160239.
- Mendez-Fernandez P, Webster L, Chouvelon T, Bustamante P, Ferreira M, Gonzalez AF, Lopez A, Moffat CF, Pierce GJ, Read FL, Russell M, Santos MB, Spitz J, Vingada JV, Caurant F. 2014. An assessment of contaminant concentrations in toothed whale species of the NW Iberian Peninsula: part II. Trace element concentrations. *Science of the Total Environment* 484:206-217. DOI: 10.1016/j.scitotenv.2014.03.001.
- Orta-Garcia ST, Plascencia-Villa G, Ochoa-Martinez AC, Ruiz-Vera T, Perez-Vazquez FJ, Velazquez-Salazar JJ, Yacamán MJ, Navarro-Contreras HR, Perez-Maldonado IN. 2015. Analysis of cytotoxic effects of silver nanoclusters on human peripheral blood mononuclear cells 'in vitro'. *Journal of Applied Toxicology* 35:1189-1199. DOI: 10.1002/jat.3190.
- Owen JA, Punt J, Stranford SA, Jones PP, Kuby J. 2013. *Kuby immunology*. New York: W.H. Freeman.
- Pérol L, Piaggio E. 2016. New molecular and cellular mechanisms of tolerance: tolerogenic actions of IL-2. In: Cuturi MC, Anegón I, eds. *Suppression and regulation of immune responses: methods and protocols, volume II*. New York: Humana Press, 11-28.

- 
- Paino IM, Zucolotto V. 2015. Poly(vinyl alcohol)-coated silver nanoparticles: activation of neutrophils and nanotoxicology effects in human hepatocarcinoma and mononuclear cells. *Environmental Toxicology and Pharmacology* 39:614-621. DOI: 10.1016/j.etap.2014.12.012.
- Poirier M, Simard JC, Antoine F, Girard D. 2014. Interaction between silver nanoparticles of 20 nm (AgNP₂₀) and human neutrophils: induction of apoptosis and inhibition of *de novo* protein synthesis by AgNP₂₀ aggregates. *Journal of Applied Toxicology* 34:404-412. DOI: 10.1002/jat.2956.
- Poirier M, Simard JC, Girard D. 2016. Silver nanoparticles of 70 nm and 20 nm affect differently the biology of human neutrophils. *Journal of Immunotoxicology* 13:375-385. DOI: 10.3109/1547691X.2015.1106622.
- Raphael I, Nalawade S, Eagar TN, Forsthuber TG. 2015. T cell subsets and their signature cytokines in autoimmune and inflammatory diseases. *Cytokine* 74:5-17. DOI: 10.1016/j.cyto.2014.09.011.
- Reed LA, McFee WE, Pennington PL, Wirth EF, Fulton MH. 2015. A survey of trace element distribution in tissues of the dwarf sperm whale (*Kogia sima*) stranded along the South Carolina coast from 1990-2011. *Marine Pollution Bulletin* 100:501-506. DOI: 10.1016/j.marpolbul.2015.09.005.
- Rosa C, Blake JE, Bratton GR, Dehn LA, Gray MJ, and O'Hara TM. 2008. Heavy metal and mineral concentrations and their relationship to histopathological findings in the bowhead whale (*Balaena mysticetus*). *Science of the Total Environment* 399:165-178. DOI: 10.1016/j.scitotenv.2008.01.062.
- Sardari RRR, Zarchi SR, Talebi A, Nasri S, Imani S, Khoradmehr A, Sheshde SAR. 2012. Toxicological effects of silver nanoparticles in rats. *African Journal of Microbiology Research* 6:5587-5593. DOI: 10.5897/Ajmr11.1070.
- Segawa T, Karatani N, Itou T, Suzuki M, Sakai T. 2013. Cloning and characterization of bottlenose dolphin (*Tursiops truncatus*) interleukin-10. *Veterinary Immunology and Immunopathology* 154:62-67. DOI: 10.1016/j.vetimm.2013.04.009.
- Seixas TG, Kehrig HA, Di Benedetto AP, Souza CM, Malm O, Moreira I. 2009. Essential (Se, Cu) and non-essential (Ag, Hg, Cd) elements: what are their relationships in liver of *Sotalia guianensis* (Cetacea, Delphinidae)? *Marine Pollution Bulletin* 58:629-634. DOI: 10.1016/j.marpolbul.2008.12.005.

- 
- Shahare B, Yashpal M. 2013. Toxic effects of repeated oral exposure of silver nanoparticles on small intestine mucosa of mice. *Toxicology Mechanisms and Methods* 23:161-167. DOI: 10.3109/15376516.2013.764950.
- Shin SH, Ye MK, Kim HS, Kang HS. 2007. The effects of nano-silver on the proliferation and cytokine expression by peripheral blood mononuclear cells. *International Immunopharmacology* 7:1813-1818. DOI: 10.1016/j.intimp.2007.08.025.
- Sitt T, Bowen L, Blanchard MT, Smith BR, Gershwin LJ, Byrne BA, Stott JL. 2008. Quantitation of leukocyte gene expression in cetaceans. *Developmental and Comparative Immunology* 32:1253-1259. DOI: 10.1016/j.dci.2008.05.001.
- Soares T, Ribeiro D, Proenca C, Chiste RC, Fernandes E, Freitas M. 2016. Size-dependent cytotoxicity of silver nanoparticles in human neutrophils assessed by multiple analytical approaches. *Life Sciences* 145:247-254. DOI: 10.1016/j.lfs.2015.12.046.
- Svec D, Tichopad A, Novosadova V, Pfaffl MW, Kubista M. 2015. How good is a PCR efficiency estimate: recommendations for precise and robust qPCR efficiency assessments. *Biomolecular Detection and Quantification* 3:9-16. DOI: 10.1016/j.bdq.2015.01.005.
- Taylor SC, Mrkusich EM. 2014. The state of RT-quantitative PCR: firsthand observations of implementation of minimum information for the publication of quantitative real-time PCR experiments (MIQE). *Journal of Molecular Microbiology and Biotechnology* 24:46-52. DOI: 10.1159/000356189.
- Thummabancha K, Onparn N, Srisapoome P. 2016. Analysis of hematologic alterations, immune responses and metallothionein gene expression in Nile tilapia (*Oreochromis niloticus*) exposed to silver nanoparticles. *Journal of Immunotoxicology* 3:909-917. DOI: 10.1080/1547691X.2016.1242673
- Tizard IR. 2013a. Cell signaling: cytokines and their receptors. In: Tizard IR, ed. *Veterinary Immunology*. 9 ed. St. Louis: Saunders, 75-83.
- Tizard IR. 2013b. Helper T cells and their response to antigen. In: Tizard IR, ed. *Veterinary Immunology*. 9 ed. St. Louis: Saunders, 137-149.
- van der Zande M, Vandebriel RJ, Van Doren E, Kramer E, Herrera Rivera Z, Serrano-Rojero CS, Gremmer ER, Mast J, Peters RJ, Hollman PC, Hendriksen PJ, Marvin HJ, Peijnenburg AA, Bouwmeester H. 2012. Distribution, elimination, and

- toxicity of silver nanoparticles and silver ions in rats after 28-day oral exposure. ACS Nano 6:7427-7442. DOI: 10.1021/nm302649p.
- Vandesompele J, De Preter K, Pattyn F, Poppe B, Van Roy N, De Paepe A, Speleman F. 2002. Accurate normalization of real-time quantitative RT-PCR data by geometric averaging of multiple internal control genes. Genome Biology 3:research0034.1–research0034.11.
- Veiopoulou C, Kogopoulou O, Tzakos E, Mavrothalassitis G, Mitsias D, Karafoulidou A, Paliogianni F, Moutsopoulos HM, Thyphronitis G. 2004. IL-2 and IL-10 production by human CD4+T cells is differentially regulated by p38: mode of stimulation-dependent regulation of IL-2. Neuroimmunomodulation 11:199-208. DOI: 10.1159/000078437.
- Walters CR, Pool EJ, Somerset VS. 2014. Ecotoxicity of silver nanomaterials in the aquatic environment: a review of literature and gaps in nano-toxicological research. Journal of Environmental Science and Health. Part A, Toxic/hazardous Substances and Environmental Engineering 49:1588-1601. DOI: 10.1080/10934529.2014.938536.
- Wang H, Ho KT, Scheckel KG, Wu F, Cantwell MG, Katz DR, Horowitz DB, Boothman WS, Burgess RM. 2014. Toxicity, bioaccumulation, and biotransformation of silver nanoparticles in marine organisms. Environmental Science and Technology 48:13711-13717. DOI: 10.1021/es502976y.
- Wang Z, Liu S, Ma J, Qu G, Wang X, Yu S, He J, Liu J, Xia T, Jiang GB. 2013. Silver nanoparticles induced RNA polymerase-silver binding and RNA transcription inhibition in erythroid progenitor cells. ACS Nano 7:4171-4186. DOI: 10.1021/nm400594s.
- Woshner VM, O'Hara TM, Bratton GR, Suydam RS, Beasley VR. 2001. Concentrations and interactions of selected essential and non-essential elements in bowhead and beluga whales of arctic Alaska. Journal of Wildlife Diseases 37:693-710. DOI: 10.7589/0090-3558-37.4.693

Table 1. The size distribution and zeta potential of the 20 nm citrate-AgNPs (C-AgNP₂₀)

Concentration (µg/ml)	100	500
Z-Average (nm)	26.62 ± 0.15	26.54 ± 0.08
Size (nm) (intensity)	30.27 ± 0.18 (100%)	29.64 ± 0.30 (100%)
Zeta potential (mV)	-38.97 ± 1.33	-44.2 ± 1.35
PdI	0.12 ± 0.00	0.11 ± 0.01

Results shown are means ± SD from three different lectures.

NP were suspended in 2nM citrate buffer and measurements performed at room temperature.

PdI, Poly-dispersity Index.

Table 2. Primer sets used in this study and their efficiencies

Gene	Accession number	Primer sequence(5'-3')	Efficiency (%)	R ²	Reference
GAPDH	DQ404538.1	CACCTCAAGATCGTCAGCAA	100.97	0.9949	Chen et al. 2015
		GCCGAAGTGGTCATGGAT			
B2M	DQ404542.1	GGTGGAGCAATCAGACCTGT	93.32	0.9984	Chen et al. 2015
		GCGTTGGGAGTGAACCTAG			
IL-2	EU638316	CATGCCCAAGAAGGCTACAGAATTG	91.92	0.999	Sitt et al. 2008
		GTGAATCTTGTTTCAGATCCCTTTAG			
IL-4	EU-638315,	GGAGCTGCCTGTAGAAGACGTCTTTGC	99.25	0.9982	Sitt et al. 2008
		CTTCATTCACAGAACAGGTCATGTTTGCC			
IL-10	AB775207	TGCTGGAGGACTTTAAGGGTTA	93.14	0.9986	Segawa et al. 2013
		ATGAAGATGTCAAATCACTCATG			
IL-12	EU638319	CAGACCAGAGCGATGAGGTCTTG	91.08	0.9999	Sitt et al. 2008
		GGGCTCTTTCTGGTCCTTAAGATA			
IFN-γ	EU638318	CAGAGCCAAATAGTCTCCTTCTACTTC	92.42	0.9976	Sitt et al. 2008
		CTGGATCTGCAGATCATCTACCGAATTTG			
TNF-α	EU638323	GAGGGAAGAGTTCCCAACTGGCTA	101.48	0.9934	Sitt et al. 2008
		CTGAGTACTGAGGTTGGCTACAAC			

Figure legends

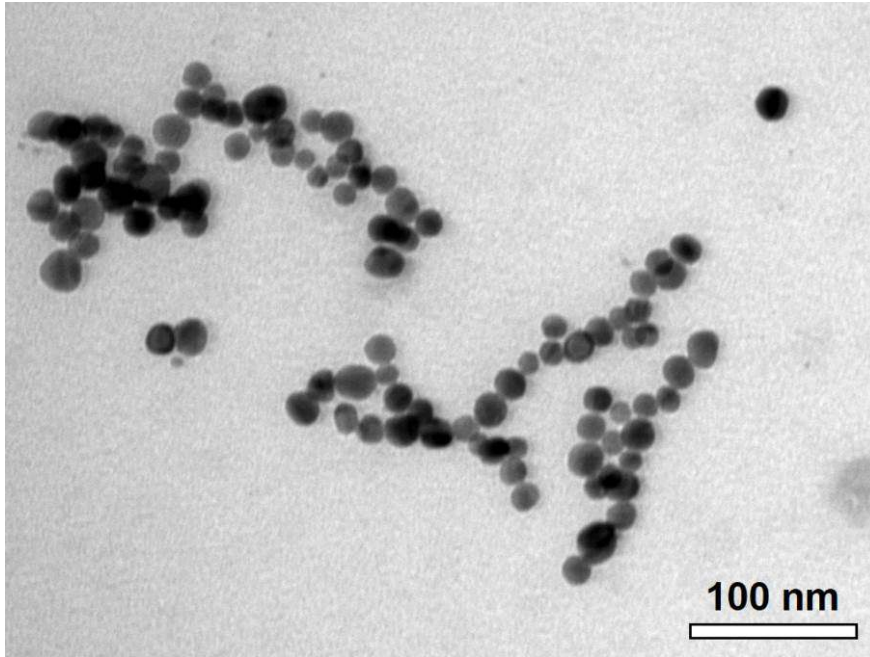


Figure 1. Characterization of C-AgNP₂₀. Representative TEM image of C-AgNP₂₀ in complete RPMI-1640.

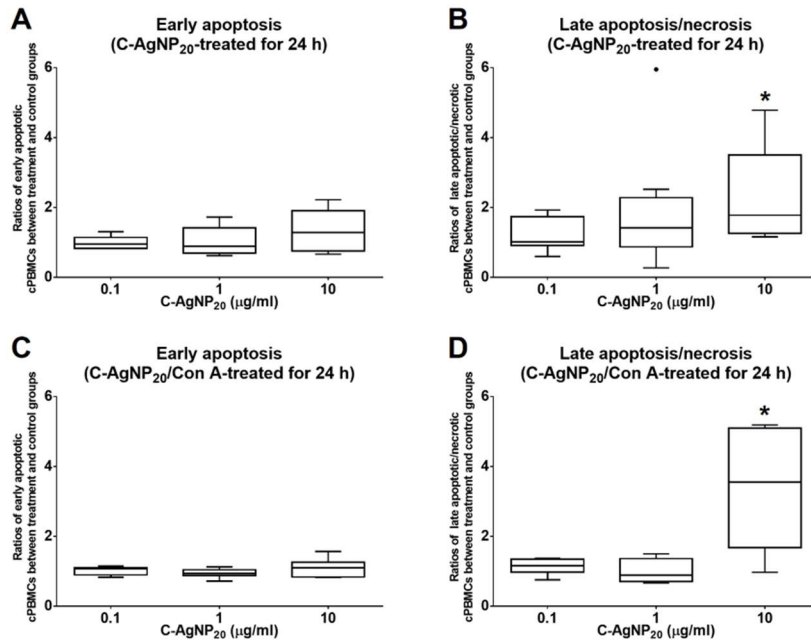


Figure 2. Cytotoxicity of C-AgNP₂₀ on cPBMCs after 24 h of culture with or without ConA. (A) Ratio of apoptotic cPBMCs in percentage between treatment and control without ConA. (B) Ratio of late apoptotic/necrotic cPBMCs in percentage between treatment and control without ConA. (C) Ratio of apoptotic cPBMCs in percentage between treatment and control with ConA. (D) Ratio of late apoptotic/necrotic cPBMCs

in percentage between treatment and control with ConA. The bar in the middle of the box represents the median, and the bottom and top of the box describe the first and third quartiles. The whiskers show the 75th percentile plus 1.5 times IQR and 25th percentile minus 1.5 times IQR of all data, and any values that are greater than these are defined as outliers and plotted as individual points. Asterisks indicate a statistically significant difference from the control ($p < 0.05$, Kruskal-Wallis Test).

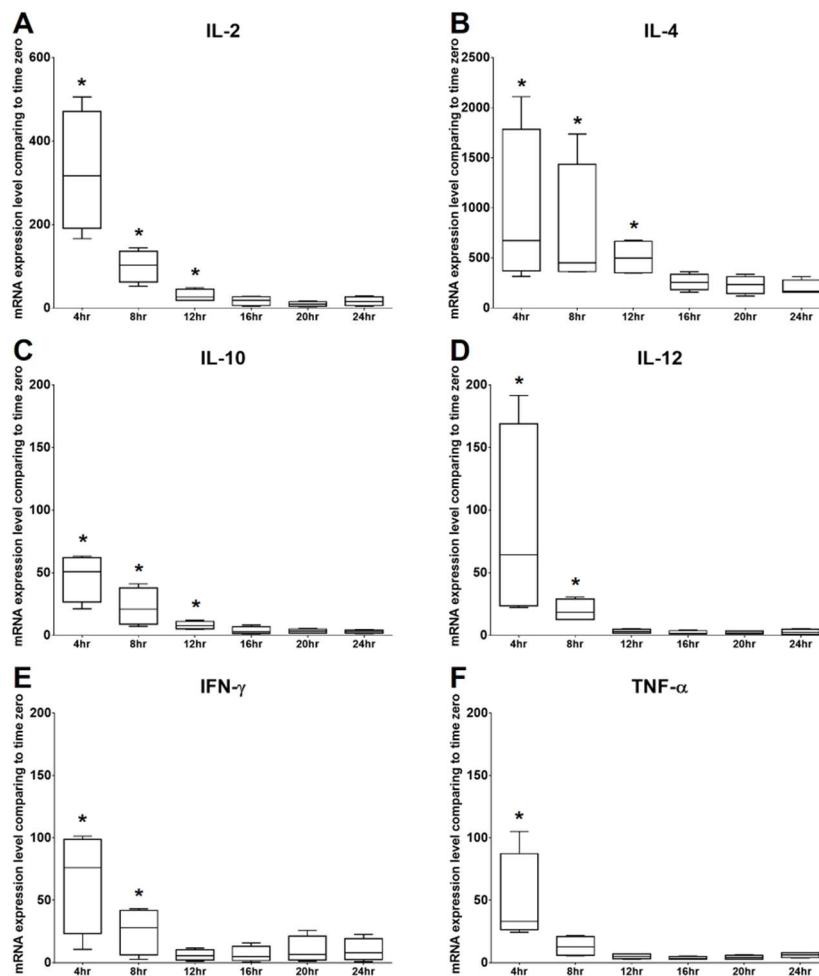


Figure 3. Time kinetics of mRNA expression levels of (A) IL-2, (B) IL-4, (C) IL-10, (D) IL-12, (E) IFN- γ and (F) TNF- α of cPBMCs with ConA. The bar in the middle of the box represents the median, and the bottom and top of the box describe the first and third quartiles. The whiskers show the 75th percentile plus 1.5 times IQR and 25th percentile minus 1.5 times IQR of all data, and any values that are greater than these are defined as outliers and plotted as individual points. Asterisks indicate a statistically significant difference from the control ($p < 0.05$, Kruskal-Wallis Test).

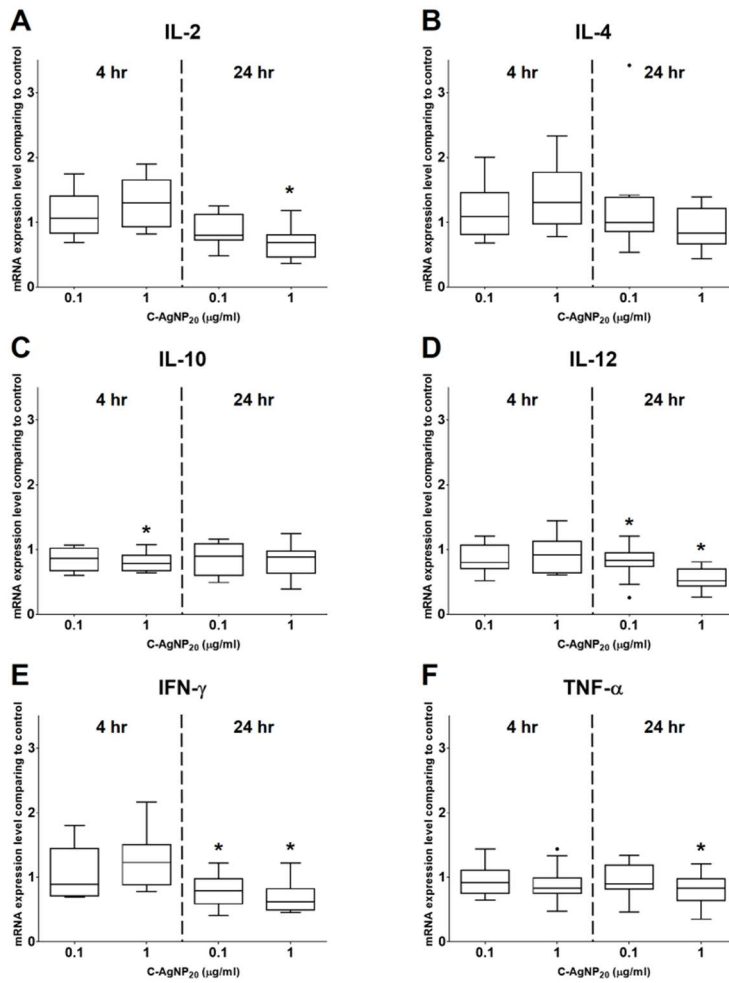


Figure 4. Effects of C-AgNP₂₀ on mRNA expression levels of (A) IL-2, (B) IL-4, (C) IL-10, (D) IL-12, (E) IFN- γ and (F) TNF- α of cPBMCs with ConA. The bar in the middle of the box represents the median, and the bottom and top of the box describe the first and third quartiles. The whiskers show the 75th percentile plus 1.5 times IQR and 25th percentile minus 1.5 times IQR of all data, and any values that are greater than these are defined as outliers and plotted as individual points. Asterisks indicate a statistically significant difference from the control ($p < 0.05$, Kruskal-Wallis Test).

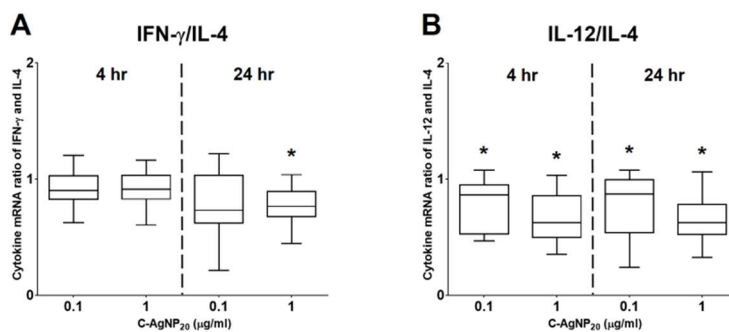


Figure 5. The ratios of Th1 (IFN- γ and IL-12) and Th2 (IL-4) polarizing cytokines at

4 and 24 h of culture. (A) Ratio of IFN- γ and IL-4; (B) Ratio of IL-12 and IL-4. The bar in the middle of the box represents the median, and the bottom and top of the box describe the first and third quartiles. The whiskers show the 75th percentile plus 1.5 times IQR and 25th percentile minus 1.5 times IQR of all data, and any values that are greater than these are defined as outliers and plotted as individual points. Asterisks indicate a statistically significant difference from the control ($p < 0.05$, Kruskal-Wallis Test).

Chapter VI: General Discussion



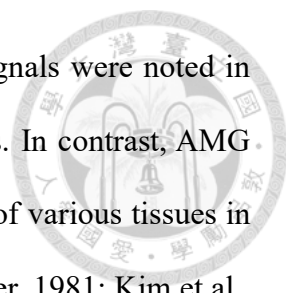
6.1 Ag concentrations of cetacean liver and kidney tissues estimated by cetacean histological Ag assay (CHAA)

The CHAA was developed based on the autometallography (AMG) positivity values and regression model, which is statistically validated by the extra sum-of-squares F test and Akaike's information criterion. The adjusted R^2 of the CHAA for livers (0.74) and kidneys (0.69) indicates that most of the response is attributed to Ag concentration, but some undetermined factors still influence the CHAA for the liver and kidney tissues of cetaceans. Possible factors influencing the accuracy and precision of CHAA for the liver and kidney tissues of cetaceans are animal species (i.e. different animal species have different habitats, prey, and physiological characteristics) and relatively small sample size with known Ag concentrations determined by ICP-MS. If the sample sizes for each animal species and samples with known Ag concentrations are large enough, a more accurate model for estimating the Ag concentration can be developed for each cetacean species.

The tissues of cetaceans in this study were from 7 different species that have different habitats and prey, but no significant difference in Ag concentrations between different cetacean species was found, suggesting that the Ag contamination may have existed in all aspects of the marine ecosystem. Furthermore, our results suggest that Ag contamination is more severe in cetaceans living in the North-western Pacific Ocean than in cetaceans living in other marine regions of the world and may have caused detrimental effects on their health condition. Therefore, it is necessary to raise the public awareness and encourage more studies on the issue of Ag contamination.

6.2 Metabolic pathway of Ag in cetaceans

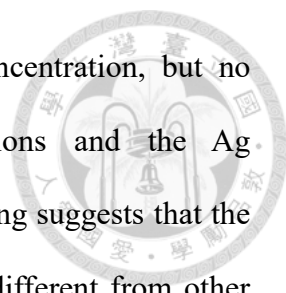
The AMG positive signals were variably sized brown to black granules in the cytoplasm of proximal renal tubular epithelium, hepatocytes, and Kupffer cells.



Occasionally, amorphous golden yellow to brown AMG positive signals were noted in the lumen and basement membrane of some proximal renal tubules. In contrast, AMG positive signals were commonly found in the basement membranes of various tissues in rats exposed to AgNPs (60 nm in diameter) or silver lactate (Danscher, 1981; Kim et al., 2009b), suggesting that the metabolic profile of Ag in cetaceans may be different from that in laboratory rats. The underlying mechanisms that cause the different metabolic profile of Ag in cetaceans are still undetermined, but several possibilities should be considered, including 1) cetaceans may have different physiological characteristics, such as different composition of the basement membrane, 2) cetaceans may be exposed to different types/concentration/time period of Ag/Ag compounds, 3) cetaceans may be exposed to varieties of contaminants; thus, the interactions between Ag and other contaminants may affect the process of Ag deposition. The current study has found a significant age-dependent increase in the Ag concentration of cetacean liver and kidney tissue, and it is suggested that the Ag deposition in cetaceans aggravates with time, and thus the source of Ag deposition is most likely from their prey. Considering the relatively high Ag concentrations in the liver rather than kidney, it is presumed that the liver is the main storage organ for Ag/Ag compounds, but the kidneys may be a transit station for the metabolism of Ag/Ag compounds in cetaceans (or just means that majority of the uptaken Ag/Ag compounds will store in the liver while only a small proportion will excrete from kidney prior to reaching the limit of liver storage capacity). The presumptive metabolic pathway of Ag in cetaceans is illustrated in Chapter 2, figure 5. However, a more comprehensive investigation by AMG method to determine the Ag distribution in cetaceans is warranted.

6.3 Histopathological lesions possibly caused by the Ag in cetaceans

In our study, Ag concentrations of the liver (kidney) tissues in approximate 50%

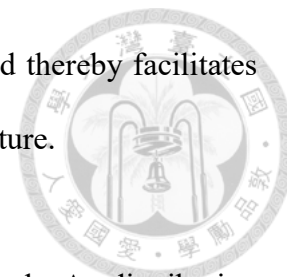


(30%) of the individuals were higher than the unhealthy Ag concentration, but no statistically significant correlation between the observed lesions and the Ag concentrations were noted in the liver and kidney tissues. This finding suggests that the toxicity caused by Ag, as non-essential/non-toxic metals, may be different from other non-essential toxic metals, which are usually organ targeting, such as the neurotoxicity caused by mercury and renal toxicity caused by cadmium. In other words, the negative health effects caused by Ag in cetaceans may be systemic rather than organ targeting. Therefore, the negative health effects caused by Ag in cetaceans should be further investigated.

6.4 The immunotoxicity of AgNPs on the leukocytes of cetaceans

Only one study on the functional activity of human leukocytes exposed to AgNPs was reported, and it revealed that functional activity was not affected by AgNPs (Haase et al., 2014). However, our study demonstrated that AgNPs at the sub-lethal doses (0.1 and 1 $\mu\text{g/ml}$) could negatively affect the functional activities of cPMNs (phagocytosis and respiratory burst) and cPBMCs (proliferative activity) and induce Th2 cytokine bias of cPBMCs. Comparing to previous human studies, our results suggest that the leukocytes of cetaceans are more vulnerable than those of humans to the negative effects of AgNPs. This result also reminds us of “when we constantly generate new substances for our convenience as humans, these new substances may have negative health impacts on the environment and wildlife”. Furthermore, the immunotoxicity caused by AgNPs found in the present study is an important warning signal for human medicine. There are many studies on the application of AgNPs (as adjuvant for chemotherapy and target therapy) for the cancer therapy. Therefore, our study not only benefits the environmental medicine/conservation but also reminds human medicine of the possible negative health effects of AgNPs. The *in vitro* toxicity test by using cetacean leukocytes can be applied

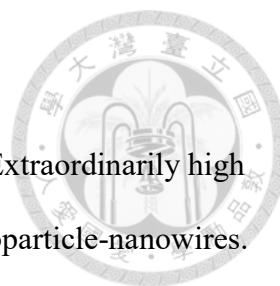
to investigate the toxicity mechanism of emerging contaminants and thereby facilitates the establishment of regulations for emerging contaminants in the future.



6.5 Summary and suggestions of future study

The current study has developed an adjuvant method to localize the Ag distribution at suborgan levels (Chapter II), has estimated the Ag concentrations of cetacean tissues by CHAA (Chapters II and III), has provided a presumptive metabolic pathway of Ag in cetaceans (Chapter III), has demonstrated the possible systemic rather than organ-targeting negative health effects caused by Ag in cetaceans (Chapter III), and has revealed the cytotoxicity and immunotoxicity caused by AgNPs on the leukocytes of cetaceans (Chapters IV and V). All the data have demonstrated the negative impacts of Ag/Ag compounds and AgNPs on the health of cetaceans and its potential ecotoxicity in marine environment.

There are several suggestions for the future studies, including 1) investigations on the systemic Ag distribution is warranted, which may provide a more comprehensive Ag metabolic pathway in cetaceans; 2) the causes of death/stranding, pathological findings, and infectious diseases in stranded cetaceans with different Ag concentrations are worth to be investigated for evaluating the negative health effects caused by Ag in cetaceans; 3) experiments on the molecular mechanism of phagocytosis of cPMNs is necessary to expand the knowledge on the phagocytosis of cPMNs as well as to determine the interactions between AgNPs and phagocytosis of cPMNs; and 4) the differences of AgNP-induced toxicity in different cells/animals may be associated with the different state (such as coating, sizes, and the intracellular Ag ions release) of the AgNPs; thus, investigations on the underlying cytotoxic/immunotoxic mechanisms of AgNPs in the leukocytes of cetaceans with comprehensive AgNPs characterization and a suitable reference of Ag ions are warranted.

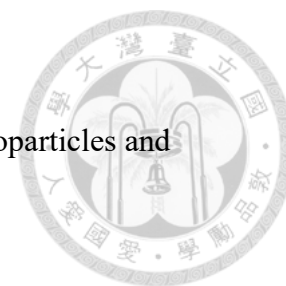



References

- Ajmal, C.M., Menamparambath, M.M., Choi, H.R., Baik, S., 2016. Extraordinarily high conductivity of flexible adhesive films by hybrids of silver nanoparticle-nanowires. *Nanotechnology* 27, 225603. 10.1088/0957-4484/27/22/225603
- Akaighe, N., Maccuspie, R.I., Navarro, D.A., Aga, D.S., Banerjee, S., Sohn, M., Sharma, V.K., 2011. Humic acid-induced silver nanoparticle formation under environmentally relevant conditions. *Environ Sci Technol* 45, 3895-3901. 10.1021/es103946g
- Buffet, P.E., Zalouk-Vergnoux, A., Chatel, A., Berthet, B., Metais, I., Perrein-Ettajani, H., Poirier, L., Luna-Acosta, A., Thomas-Guyon, H., Risso-de Faverney, C., Guibbolini, M., Gilliland, D., Valsami-Jones, E., Mouneyrac, C., 2014. A marine mesocosm study on the environmental fate of silver nanoparticles and toxicity effects on two endobenthic species: the ragworm *Hediste diversicolor* and the bivalve mollusc *Scrobicularia plana*. *Sci Total Environ* 470-471, 1151-1159. 10.1016/j.scitotenv.2013.10.114
- Danscher, G., 1981. Light and electron microscopic localization of silver in biological tissue. *Histochemistry* 71, 177-186.
- Degger, N., Tse, A.C., Wu, R.S., 2015. Silver nanoparticles disrupt regulation of steroidogenesis in fish ovarian cells. *Aquat Toxicol* 169, 143-151. 10.1016/j.aquatox.2015.10.015
- Farkas, J., Christian, P., Urrea, J.A., Roos, N., Hasselov, M., Tollefsen, K.E., Thomas, K.V., 2010. Effects of silver and gold nanoparticles on rainbow trout (*Oncorhynchus mykiss*) hepatocytes. *Aquat Toxicol* 96, 44-52. 10.1016/j.aquatox.2009.09.016
- Farre, M., Gajda-Schranz, K., Kantiani, L., Barcelo, D., 2009. Ecotoxicity and analysis

- of nanomaterials in the aquatic environment. *Anal Bioanal Chem* 393, 81-95.
10.1007/s00216-008-2458-1
- Gagne, F., Auclair, J., Fortier, M., Bruneau, A., Fournier, M., Turcotte, P., Pilote, M., Gagnon, C., 2013. Bioavailability and immunotoxicity of silver nanoparticles to the freshwater mussel *Elliptio complanata*. *J Toxicol Environ Health A* 76, 767-777. 10.1080/15287394.2013.818602
- Gambardella, C., Costa, E., Piazza, V., Fabbrocini, A., Magi, E., Faimali, M., Garaventa, F., 2015. Effect of silver nanoparticles on marine organisms belonging to different trophic levels. *Mar Environ Res* 111, 41-49. 10.1016/j.marenvres.2015.06.001
- Garcia-Alonso, J., Rodriguez-Sanchez, N., Misra, S.K., Valsami-Jones, E., Croteau, M.N., Luoma, S.N., Rainbow, P.S., 2014. Toxicity and accumulation of silver nanoparticles during development of the marine polychaete *Platynereis dumerilii*. *Sci Total Environ* 476-477, 688-695. 10.1016/j.scitotenv.2014.01.039
- Ge, L., Li, Q., Wang, M., Ouyang, J., Li, X., Xing, M.M., 2014. Nanosilver particles in medical applications: synthesis, performance, and toxicity. *Int J Nanomedicine* 9, 2399-2407. 10.2147/IJN.S55015
- Glover, R.D., Miller, J.M., Hutchison, J.E., 2011. Generation of metal nanoparticles from silver and copper objects: nanoparticle dynamics on surfaces and potential sources of nanoparticles in the environment. *ACS Nano* 5, 8950-8957.
10.1021/nn2031319
- Gomez-Caballero, J.A., Villasenor-Cabral, M.G., Santiago-Jacinto, P., Ponce-Abad, F., 2010. Hypogene ba-rich todorokite and associated nanometric native silver in the san miguel tenango mining area, Zacatlan, Puebla, Mexico. *Canadian Mineralogist* 48, 1237-1253. 10.3749/canmin.48.5.1237
- Haase, H., Fahmi, A., Mahltig, B., 2014. Impact of silver nanoparticles and silver ions

- on innate immune cells. *J Biomed Nanotechnol* 10, 1146-1156.
- Hadrup, N., Lam, H.R., 2014. Oral toxicity of silver ions, silver nanoparticles and colloidal silver--a review. *Regul Toxicol Pharmacol* 68, 1-7.
10.1016/j.yrtph.2013.11.002
- Handy, R.D., Owen, R., Valsami-Jones, E., 2008. The ecotoxicology of nanoparticles and nanomaterials: current status, knowledge gaps, challenges, and future needs. *Ecotoxicology* 17, 315-325. 10.1007/s10646-008-0206-0
- Hawkins, A.D., Thornton, C., Kennedy, A.J., Bu, K., Cizdziel, J., Jones, B.W., Steevens, J.A., Willett, K.L., 2015. Gill histopathologies following exposure to nanosilver or silver nitrate. *J Toxicol Environ Health A* 78, 301-315.
10.1080/15287394.2014.971386
- Huang, H., Lai, W., Cui, M., Liang, L., Lin, Y., Fang, Q., Liu, Y., Xie, L., 2016a. An Evaluation of Blood Compatibility of Silver Nanoparticles. *Sci Rep* 6, 25518.
10.1038/srep25518
- Huang, J., Cheng, J., Yi, J., 2016b. Impact of silver nanoparticles on marine diatom *Skeletonema costatum*. *J Appl Toxicol* 36, 1343-1354. 10.1002/jat.3325
- Hyun, J.S., Lee, B.S., Ryu, H.Y., Sung, J.H., Chung, K.H., Yu, I.J., 2008. Effects of repeated silver nanoparticles exposure on the histological structure and mucins of nasal respiratory mucosa in rats. *Toxicol Lett* 182, 24-28.
10.1016/j.toxlet.2008.08.003
- Jeevanandam, J., Barhoum, A., Chan, Y.S., Dufresne, A., Danquah, M.K., 2018. Review on nanoparticles and nanostructured materials: history, sources, toxicity and regulations. *Beilstein J Nanotechnol* 9, 1050-1074. 10.3762/bjnano.9.98
- Ji, J.H., Jung, J.H., Kim, S.S., Yoon, J.U., Park, J.D., Choi, B.S., Chung, Y.H., Kwon, I.H., Jeong, J., Han, B.S., Shin, J.H., Sung, J.H., Song, K.S., Yu, I.J., 2007.



- 
- Twenty-eight-day inhalation toxicity study of silver nanoparticles in Sprague-Dawley rats. *Inhal Toxicol* 19, 857-871. 10.1080/08958370701432108
- Jung, Y.J., Kim, K.T., Kim, J.Y., Yang, S.Y., Lee, B.G., Kim, S.D., 2014. Bioconcentration and distribution of silver nanoparticles in Japanese medaka (*Oryzias latipes*). *J Hazard Mater* 267, 206-213. 10.1016/j.jhazmat.2013.12.061
- Kim, S., Choi, J.E., Choi, J., Chung, K.H., Park, K., Yi, J., Ryu, D.Y., 2009a. Oxidative stress-dependent toxicity of silver nanoparticles in human hepatoma cells. *Toxicol In Vitro* 23, 1076-1084. 10.1016/j.tiv.2009.06.001
- Kim, S., Ryu, D.Y., 2013. Silver nanoparticle-induced oxidative stress, genotoxicity and apoptosis in cultured cells and animal tissues. *J Appl Toxicol* 33, 78-89. 10.1002/jat.2792
- Kim, W.Y., Kim, J., Park, J.D., Ryu, H.Y., Yu, I.J., 2009b. Histological study of gender differences in accumulation of silver nanoparticles in kidneys of Fischer 344 rats. *J Toxicol Environ Health A* 72, 1279-1284. 10.1080/15287390903212287
- Kim, Y.S., Kim, J.S., Cho, H.S., Rha, D.S., Kim, J.M., Park, J.D., Choi, B.S., Lim, R., Chang, H.K., Chung, Y.H., Kwon, I.H., Jeong, J., Han, B.S., Yu, I.J., 2008. Twenty-eight-day oral toxicity, genotoxicity, and gender-related tissue distribution of silver nanoparticles in Sprague-Dawley rats. *Inhal Toxicol* 20, 575-583. 10.1080/08958370701874663
- Kim, Y.S., Song, M.Y., Park, J.D., Song, K.S., Ryu, H.R., Chung, Y.H., Chang, H.K., Lee, J.H., Oh, K.H., Kelman, B.J., Hwang, I.K., Yu, I.J., 2010. Subchronic oral toxicity of silver nanoparticles. *Part Fibre Toxicol* 7, 20. 10.1186/1743-8977-7-20
- Kwok, K.W., Dong, W., Marinakos, S.M., Liu, J., Chilkoti, A., Wiesner, M.R., Chernick, M., Hinton, D.E., 2016. Silver nanoparticle toxicity is related to coating materials and disruption of sodium concentration regulation. *Nanotoxicology* 10,

1306-1317. 10.1080/17435390.2016.1206150

Lee, H.Y., Choi, Y.J., Jung, E.J., Yin, H.Q., Kwon, J.T., Kim, J.E., Im, H.T., Cho, M.H., Kim, J.H., Kim, H.Y., Lee, B.H., 2010. Genomics-based screening of differentially expressed genes in the brains of mice exposed to silver nanoparticles via inhalation. *Journal of Nanoparticle Research* 12, 1567-1578. DOI 10.1007/s11051-009-9666-2

Lee, J.H., Kim, Y.S., Song, K.S., Ryu, H.R., Sung, J.H., Park, J.D., Park, H.M., Song, N.W., Shin, B.S., Marshak, D., Ahn, K., Lee, J.E., Yu, I.J., 2013. Biopersistence of silver nanoparticles in tissues from Sprague-Dawley rats. *Part Fibre Toxicol* 10, 36. 10.1186/1743-8977-10-36

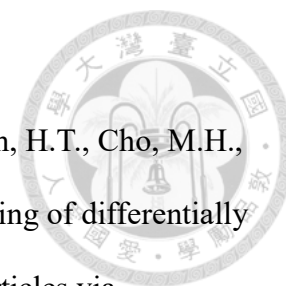
Liz, R., Simard, J.C., Leonardi, L.B., Girard, D., 2015. Silver nanoparticles rapidly induce atypical human neutrophil cell death by a process involving inflammatory caspases and reactive oxygen species and induce neutrophil extracellular traps release upon cell adhesion. *Int Immunopharmacol* 28, 616-625. 10.1016/j.intimp.2015.06.030

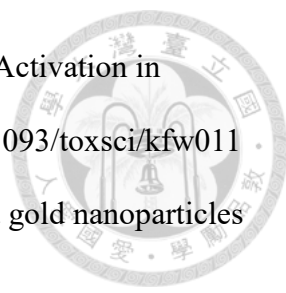
Lubick, N., 2008. Nanosilver toxicity: ions, nanoparticles--or both? *Environ Sci Technol* 42, 8617.

Mao, B.H., Tsai, J.C., Chen, C.W., Yan, S.J., Wang, Y.J., 2016. Mechanisms of silver nanoparticle-induced toxicity and important role of autophagy. *Nanotoxicology* 10, 1021-1040. 10.1080/17435390.2016.1189614

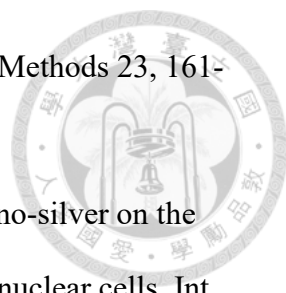
McGillicuddy, E., Murray, I., Kavanagh, S., Morrison, L., Fogarty, A., Cormican, M., Dockery, P., Prendergast, M., Rowan, N., Morris, D., 2017. Silver nanoparticles in the environment: Sources, detection and ecotoxicology. *Sci Total Environ* 575, 231-246. 10.1016/j.scitotenv.2016.10.041

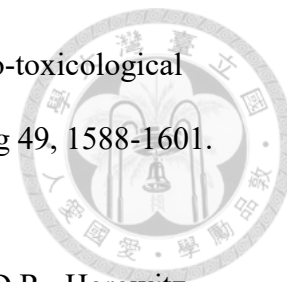
Mishra, A.R., Zheng, J., Tang, X., Goering, P.L., 2016. Silver Nanoparticle-Induced



- 
- Autophagic-Lysosomal Disruption and NLRP3-Inflammasome Activation in HepG2 Cells Is Size-Dependent. *Toxicol Sci* 150, 473-487. 10.1093/toxsci/kfw011
- Moreno-Garrido, I., Perez, S., Blasco, J., 2015. Toxicity of silver and gold nanoparticles on marine microalgae. *Mar Environ Res* 111, 60-73.
10.1016/j.marenvres.2015.05.008
- Mukunthan, K.S., Elumalai, E.K., Patel, T.N., Murty, V.R., 2011. *Catharanthus roseus*: a natural source for the synthesis of silver nanoparticles. *Asian Pac J Trop Biomed* 1, 270-274. 10.1016/S2221-1691(11)60041-5
- Myrzakhanova, M., Gambardella, C., Falugi, C., Gatti, A.M., Tagliafierro, G., Ramoino, P., Bianchini, P., Diaspro, A., 2013. Effects of nanosilver exposure on cholinesterase activities, CD41, and CDF/LIF-like expression in zebrafish (*Danio rerio*) larvae. *Biomed Res Int* 2013, 205183. 10.1155/2013/205183
- Oberdorster, G., Sharp, Z., Atudorei, V., Elder, A., Gelein, R., Kreyling, W., Cox, C., 2004. Translocation of inhaled ultrafine particles to the brain. *Inhal Toxicol* 16, 437-445. 10.1080/08958370490439597
- Park, E.J., Bae, E., Yi, J., Kim, Y., Choi, K., Lee, S.H., Yoon, J., Lee, B.C., Park, K., 2010a. Repeated-dose toxicity and inflammatory responses in mice by oral administration of silver nanoparticles. *Environ Toxicol Pharmacol* 30, 162-168.
10.1016/j.etap.2010.05.004
- Park, E.J., Yi, J., Kim, Y., Choi, K., Park, K., 2010b. Silver nanoparticles induce cytotoxicity by a Trojan-horse type mechanism. *Toxicol In Vitro* 24, 872-878.
10.1016/j.tiv.2009.12.001
- Piao, M.J., Kang, K.A., Lee, I.K., Kim, H.S., Kim, S., Choi, J.Y., Choi, J., Hyun, J.W., 2011. Silver nanoparticles induce oxidative cell damage in human liver cells through inhibition of reduced glutathione and induction of mitochondria-involved

- apoptosis. *Toxicol Lett* 201, 92-100. DOI 10.1016/j.toxlet.2010.12.010
- Poirier, M., Simard, J.C., Antoine, F., Girard, D., 2014. Interaction between silver nanoparticles of 20 nm (AgNP20) and human neutrophils: induction of apoptosis and inhibition of de novo protein synthesis by AgNP20 aggregates. *J Appl Toxicol* 34, 404-412. 10.1002/jat.2956
- Poirier, M., Simard, J.C., Girard, D., 2016. Silver nanoparticles of 70 nm and 20 nm affect differently the biology of human neutrophils. *J Immunotoxicol* 13, 375-385. 10.3109/1547691X.2015.1106622
- Riaz Ahmed, K.B., Nagy, A.M., Brown, R.P., Zhang, Q., Malghan, S.G., Goering, P.L., 2017. Silver nanoparticles: Significance of physicochemical properties and assay interference on the interpretation of in vitro cytotoxicity studies. *Toxicol In Vitro* 38, 179-192. 10.1016/j.tiv.2016.10.012
- Ringwood, A.H., McCarthy, M., Bates, T.C., Carroll, D.L., 2010. The effects of silver nanoparticles on oyster embryos. *Mar Environ Res* 69 Suppl, S49-51. 10.1016/j.marenvres.2009.10.011
- Sahu, S.C., Zheng, J., Graham, L., Chen, L., Ihrie, J., Yourick, J.J., Sprando, R.L., 2014. Comparative cytotoxicity of nanosilver in human liver HepG2 and colon Caco2 cells in culture. *J Appl Toxicol* 34, 1155-1166. 10.1002/jat.2994
- Sal'nikov, D.S., Pogorelova, A.S., Makarov, S.V., Vashurina, I.Y., 2009. Silver ion reduction with peat fulvic acids. *Russian Journal of Applied Chemistry* 82, 545-548. 10.1134/S107042720904003x
- Sardari, R.R.R., Zarchi, S.R., Talebi, A., Nasri, S., Imani, S., Khoradmehr, A., Sheshde, S.A.R., 2012. Toxicological effects of silver nanoparticles in rats. *African Journal of Microbiology Research* 6, 5587-5593. Doi 10.5897/Ajmr11.1070
- Shahare, B., Yashpal, M., 2013. Toxic effects of repeated oral exposure of silver

- 
- nanoparticles on small intestine mucosa of mice. *Toxicol Mech Methods* 23, 161-167. 10.3109/15376516.2013.764950
- Shin, S.H., Ye, M.K., Kim, H.S., Kang, H.S., 2007. The effects of nano-silver on the proliferation and cytokine expression by peripheral blood mononuclear cells. *Int Immunopharmacol* 7, 1813-1818. 10.1016/j.intimp.2007.08.025
- Soares, T., Ribeiro, D., Proenca, C., Chiste, R.C., Fernandes, E., Freitas, M., 2016. Size-dependent cytotoxicity of silver nanoparticles in human neutrophils assessed by multiple analytical approaches. *Life Sci* 145, 247-254. 10.1016/j.lfs.2015.12.046
- Sung, J.H., Ji, J.H., Park, J.D., Yoon, J.U., Kim, D.S., Jeon, K.S., Song, M.Y., Jeong, J., Han, B.S., Han, J.H., Chung, Y.H., Chang, H.K., Lee, J.H., Cho, M.H., Kelman, B.J., Yu, I.J., 2009. Subchronic inhalation toxicity of silver nanoparticles. *Toxicol Sci* 108, 452-461. 10.1093/toxsci/kfn246
- Takenaka, S., Karg, E., Roth, C., Schulz, H., Ziesenis, A., Heinzmann, U., Schramel, P., Heyder, J., 2001. Pulmonary and systemic distribution of inhaled ultrafine silver particles in rats. *Environ Health Perspect* 109 Suppl 4, 547-551.
- Thummabancha, K., Onparn, N., Srisapoome, P., 2016. Analysis of hematologic alterations, immune responses and metallothionein gene expression in Nile tilapia (*Oreochromis niloticus*) exposed to silver nanoparticles. *J Immunotoxicol* 13, 909-917. 10.1080/1547691X.2016.1242673
- van der Zande, M., Vandebriel, R.J., Van Doren, E., Kramer, E., Herrera Rivera, Z., Serrano-Rojero, C.S., Gremmer, E.R., Mast, J., Peters, R.J., Hollman, P.C., Hendriksen, P.J., Marvin, H.J., Peijnenburg, A.A., Bouwmeester, H., 2012. Distribution, elimination, and toxicity of silver nanoparticles and silver ions in rats after 28-day oral exposure. *ACS Nano* 6, 7427-7442. 10.1021/nn302649p
- Walters, C.R., Pool, E.J., Somerset, V.S., 2014. Ecotoxicity of silver nanomaterials in



- the aquatic environment: a review of literature and gaps in nano-toxicological research. *J Environ Sci Health A Tox Hazard Subst Environ Eng* 49, 1588-1601. 10.1080/10934529.2014.938536
- Wang, H., Ho, K.T., Scheckel, K.G., Wu, F., Cantwell, M.G., Katz, D.R., Horowitz, D.B., Boothman, W.S., Burgess, R.M., 2014. Toxicity, bioaccumulation, and biotransformation of silver nanoparticles in marine organisms. *Environ Sci Technol* 48, 13711-13717. 10.1021/es502976y
- Wen, L.S., Santschi, P.H., Gill, G.A., Paternostro, C.L., Lehman, R.D., 1997. Colloidal and particulate silver in river and estuarine waters of Texas. *Environmental Science & Technology* 31, 723-731. DOI 10.1021/es9603057
- Wu, Y., Zhou, Q., 2013. Silver nanoparticles cause oxidative damage and histological changes in medaka (*Oryzias latipes*) after 14 days of exposure. *Environ Toxicol Chem* 32, 165-173. 10.1002/etc.2038
- Yang, D.P., Chen, S.H., Huang, P., Wang, X.S., Jiang, W.Q., Pandoli, O., Cui, D.X., 2010. Bacteria-template synthesized silver microspheres with hollow and porous structures as excellent SERS substrate. *Green Chemistry* 12, 2038-2042. 10.1039/c0gc00431f
- Yu, S.J., Yin, Y.G., Liu, J.F., 2013. Silver nanoparticles in the environment. *Environ Sci Process Impacts* 15, 78-92.
- Zhang, T., Wang, L., Chen, Q., Chen, C., 2014. Cytotoxic potential of silver nanoparticles. *Yonsei Med J* 55, 283-291. 10.3349/ymj.2014.55.2.283
- Zhang, X.F., Shen, W., Gurunathan, S., 2016. Silver Nanoparticle-Mediated Cellular Responses in Various Cell Lines: An in Vitro Model. *Int J Mol Sci* 17. 10.3390/ijms17101603